The Shape of Damping:

Optimizing Damping Coefficients to Improve Transparency on Bilateral Telemanipulation

By

OLMO ALONSO MORENO FRANCO

PhD Program In Bioengineering and Robotics
UNIVERSITÀ DEGLI STUDI DI GENOVA

A dissertation submitted to Università degli Studi di Genova in accordance with the requirements of the degree of DOCTOR OF PHILOSOPHY (XXXI Cycle) in the Department of Informatics, Bioengineering, Robotics and Systems Engineering in affiliation to Istituto Italiano di Tecnologia.

Prof. Domenico Prattichizzo (Supervisor)

Dr. João Bimbo (Co-supervisor)

FEBRUARY 2019

Supervisor:
Prof. Domenico Prattichizzo. Full Professor, University of Siena,
Department of Information Engineering, Siena, Italy.

Co-supervisor:
Dr. João Bimbo. Post Doc, Istituto Italiano di Tecnologia,
Advanced Robotics Department, Genova, Italy.

Head of the PhD program:
Prof. Giorgio Cannata. Associate Professor, University of Genova,
Mechatronics and Automatic Control Laboratory, Genova, Italy.

Thesis Reviewers:
Prof. Fabio Morbidi. Associate Professor, Picardie Jules Verne University,
Information and Systems Laboratory, Amiens, France.

Prof. Lucia Pallottino. Associate Professor, University of Pisa,
Department of Information Engineering, Pisa, Italy.

Prof. Francesco Chinello. Assistant Professor, Aarhus University,
Department of Business and Technology Development, Herning, Denmark.

Abstract

This thesis presents a novel optimization-based passivity control algorithm for haptic-enabled bilateral teleoperation systems involving multiple degrees of freedom. In particular, in the context of energy-bounding control, the contribution focuses on the implementation of a passivity layer for an existing time-domain scheme, ensuring optimal transparency of the interaction along subsets of the environment space which are preponderant for the given task, while preserving the energy bounds required for passivity. The involved optimization problem is convex and amenable to real-time implementation. The effectiveness of the proposed design is validated via an experiment performed on a virtual teleoperated environment.

The interplay between transparency and stability is a critical aspect in haptic-enabled bilateral teleoperation control. While it is important to present the user with the true impedance of the environment, destabilizing factors such as time delays, stiff environments, and a relaxed grasp on the master device may compromise the stability and safety of the system. Passivity has been exploited as one of the the main tools for providing sufficient conditions for stable teleoperation in several controller design approaches, such as the scattering algorithm, time-domain passivity control, energy bounding algorithm, and passive set position modulation.

In this work it is presented an innovative energy-based approach, which builds upon existing time-domain passivity controllers, improving and extending their effectiveness and functionality. The set of damping coefficients are prioritized in each degree of freedom, the resulting transparency presents a realistic force feedback in comparison to the other directions. Thus, the prioritization takes effect using a quadratic programming algorithm to find the optimal values for the damping.

Finally, the energy tanks approach on passivity control is a solution used to ensure stability in a system for robotics bilateral manipulation. The bilateral telemanipulation must maintain the principle of passivity in all moments to preserve the system's stability. This work presents a brief introduction to haptic devices as a master component on the telemanipulation chain; the end effector in the slave side is a representation of an interactive object within an environment having a force sensor as feedback signal. The whole interface is designed into a cross-platform framework named ROS, where the user interacts with the system. Experimental results are presented.

Dedication

To Libia and Prudenciano.

Acknowledgements

Since I first arrived to this country, I was immediately fascinated by its people, landscapes and flavours. I always wanted to experience living on a city with big cargo ships, cruise ships, and trains; Genova has it, including the most weirdest elevators in the world. But no doubt, the best experience was to collaborate with a group of the most intelligent worldwide persons in IIT. I consider my self lucky. I would like to thank my friend João Bimbo for being next to me in this journey and push a lot to make things happen, thanks for your wisdom and patience, I learned a lot. Also, to Claudio Pacchierotti who I had the chance to learn, interact and participate in haptics matters; Francesco Chinello my desk neighbour and accomplice in all technology gags; and Leonardo Meli for the adventures here and in Siena. My gratitude goes to my friend and co-author Gianni Bianchini, you put this work on the right track. To Mahdi Ghazaei, thanks a lot for sharing your experience and holding the rookie trophy of crossfit with me.

On my first weeks in IIT I had the chance to interact with amazing people, thanks Anaïs, Dina, Stefka, Nawid, Sasha, Bilal, and Ioannis, you made me feel integrated. I would never forget the great adventures in Lago di Brayes, Cinqueterre, Lago di Como, Camogli and Lago Iseo, I miss all of you. To my two inspirational friends Jorge and beautiful Lorenzo (Lolo), thanks so much for the stories either here or Malaga, or Madrid (or maybe Pisa in the future); I hope we can have more. This experience would not have been the same without the Brescians Marta and Maria, thanks a lot for the cakes and concerts, you are exceptional. And in round six at IIT's arena I would like to thank Lucia, great times in Australia and Raggiolo. To Jesus and Veronica, thanks so much for joining me to the trip to Mexico, great conference, great people in an awesome place. To my dear country fellows at Genova: Esau, Edith, Paquito, Maggi, Gabri, Edwin and Octavio, thank so much, you made me feel at home. Alperen and Haoqi, thanks for the tales at Vico della Cittadella, that place was something; and for the social activities at San Nicola thanks to Anthony, I hope you can sleep this year brother. Once in a while you have the opportunity to meet incredible people, thanks Federica, Giulia M., Ana, Federica C., Giulia S., Maria Elena, Roberto, Soraya, Marco and Lia; you people are awesome!

My friends of the XXXI cycle, Ali, Marie, Michela, Kourosh, Josephus, Amira, Domingo, Davide, Romeo, Jessica, Zeyu, Barbara, Rajesh, Yeshavi, Giulia, Qinqi, and Nuno (adopted cycle friend), we started something three years ago and I was fortunate to see you grow and reach success, I'm really proud of you. When we have a social meeting among IIT's colleagues, we use to introduce ourself by name and the floor where we work, most of non IIT's colaborators do not understand, but it is our distinctive mark; thanks to my floor-mates Mehrdad, Giandomenico, Enrico, Marco, Emiliano, Edoardo, Fernando, Vassia, Stefanos, Matteo, Christian, Tommaso, Stefano, Francesca, Lorenza, Lara, Cheng, Leonardo, Nikhil, Nabeel, Yonas, Dario, Mo, Giacinto, Jacopo, Louis, Fanny, Andre, Sara, Abdeldjallil, Roodra, Andrea, and Arfu; 4th floor rocks! To bad for Vignesh, Dimitris, Diego and Shamel you belong to another dimension (thank you guys).

My good friends in Advanced Robotics, Dynamic Interaction Control, Dynamic Legged Systems, Graphene Labs, Human-Robot Interfaces and Physical Interaction, Humanoids and Human Centered Mechatronics, Soft Robotics for Human Cooperation and Rehabilitation, Nanotechnology for Precision Medicine, and Smart Materials thank you all.

I would like to thank Andreea Radulescu and Virginia Ruiz who contributed in the presentation session to review this work. Thanks to Andie for the good times in Athens and Berenice for your support. Special thanks to Laura Morano who did all the effort to make me learn Italian (in the first year of the PhD) and she was so close to get it. In ADVR special thanks to Silvia, Valentina, Simona, Giulia, Laura and Floriana, patience is a virtue; at UNIGE I would like to thank Roberta Usari and Valentina Scanarotti. To my friend Clara at the gym, thanks a lot for the cheering. Thanks so much to my friend Stefano De Simone, all the paper work at the questura paid off.

I am thankful with my parents, my brothers, grandparents, aunts, uncles, cousins, nieces and nephews along Mexico and abroad, some of you had the chance to come and visit me, some others I did it back there, I love you so much. Kely, Kiko, Luyo, Pakun, Luis, Sofia and Mel thanks so much for coming here, it is nice to see you again. To my good friend Luis Alberto, you were absolutely right about living an academic experience abroad. My dear friend Carlos Sauri at UniModelo, thanks so much for the chances, attentions and support back in Merida, it was a great adventure what we build there. Finally but not least, my best friend Vanessa, who is aware of all details happening here, congratulations on your new life stage with Andrea, you make a beautiful team. To all, who some how are/were involved through this adventure, thanks so much, you have a special place here. Thanks Morego, thanks Genova, thanks Italy.


Michela
Eduardo
Emilio
Edoardo
Edisa
Kelly
Alicia
Anaïs
Vignesh
Qinqi
Edgar
Roberta
Frank
Ioannis
Paty
Simona
Bertha
Alberto
Yaneli
Matteo
Roma
Magnolia
Torino
Pedro
Yamil
Rafa
Prudenciano
Puerto-Morelos
Stefan
Jorge
Ruben
Raymundo
Zeuoqui
Chakz
Roodra
Lorenza
Domingo
Ney
Eder
Leonel
Luis-Alberto
Vicky
Rosalía
Federica
Elisa
Lucia
Fernando
Denis
Isidra
Diego
Luz
Umair
Alonso
Raul
Arash
Itzel
Libia
Reyna
Máximo
Sara
Paramesvari
Sinaloa
Gianni
Rajesh
Guilherme
Yadira
Stefano
Daniel
Villa-Bassa
Bilal
Italuvi
Edwin
Fermín
Citlati
Pablo
Queta
Manuel
Haoqi
Rigoberto
Andreea
Kely
Agnni
Omar
Corerepe
Alexia
André
Jesus
Genova
Rolonia
Roy
Alice
Chata
Marisela
Italia
Romeo
Amaya
Leelou
Pépe
Zeyu
Tijuana
Emiliano
Jörn
Rossy
Fabiola
Rafel
Wansoo
Quela
Firenze
Yukitoshi
Dimitris
Cuquis
Pinto
Alejandro
Axell
Leonardo
Ali
Carlos
Floriana
Marianna
Maggie
Mizael
Isabel
Asier
Lizett
Andie
Samara
Octavio
David
Valeria
Laura
Soda
Silvia
Evie
Tencha
Don-Carlos
Bronico
Tenochtitlán
Mayté
Tommaso
Marco
João
Melina
Jonathan
Margarita
Mahdi
Valentina
Paquito
Roxana
Olivia
Miguel
Napoli
Giacinto
Virginia
Andrea
Pietro
Esmeralda
Jovany
Dina
Berenice
Sofía
Vanessa
Sasha
Nikol
Raggiolo
Ana-Kelly
Cansunor
Jorgito
Ivan
Bahía-Kino
Salvador
Aldo
José-Enrique
Cinquetierre
Dave
Lago-Ixco
Amira
Morego
Ellie
Soraia
Renan
Rubí
Juan-Alejandro
Ieva
Aaron
Nuno
Kenneth
Anthony
Haydeé
Cancún
Teresita
Lia
México
Vassia
Brescia
Luisillo
Mehrdad
Paul
Juana
Armando
Freddy
Moe
Trinidad
Angelina
Shamel
Tanis
Adán
Marta
Nikhil
Clara
Mérida
Arman
Mario
Quiané
Veronica
Gerardo
Benjamin
Yonas
Griselda
Rafael
Luka
Ligia
Katy
Nabeel
Ramon
Joan
Betillo
Querétaro
Cigdem
Lolo
Pakun
Claudio
Arezzo
Giulia
Alperen
Enrico
Nawid
Roberto
Barolo
Topo
Pamela
Esau
Diana
Javier
Aleksandrina
Remedios
Lago-de-Yeguas
Corta
Marie
Belén
Marina
Enfermo
Francesco
Livorno
Elvis
Mauro
Giandomenico
Sergio
Edith
Ernesto
Siena
Lunga
Arfu
Maria
Elco
Cunegli
Lara
Julieta
Iker
Shey
Josephus
Pisa
Barbara
IIT
Jair
Stefka
Jessica
Emily
Gilberto
San-Gimignano
Gemela
Elena
Milano

Author's declaration

I declare that the work in this dissertation was carried out in accordance with the requirements of the University's Regulations and Code of Practice for Research Degree Programmes and that it has not been submitted for any other academic award. Except where indicated by specific reference in the text, the work is the candidate's own work. Work done in collaboration with, or with the assistance of, others, is indicated as such. Any views expressed in the dissertation are those of the author.

Olmo Alonso Moreno Franco.

February, 2019.

Table of Contents

List of Tables

List of Figures

CHAPTER 1

INTRODUCTION

It was in 1954 when the first telemanipulation system was developed by Raymond Goertz [1–3]. The aim was to manipulate hazardous nuclear materials in a remote environment. Following that, the first problem related to time delay in teleoperation appeared as described in the work of Ferrel [4]. There, a statistical prediction model for the movement and position of the manipulator was developed in an open-loop system. In the experiments conducted by Ferrel, the user had to create a strategy waiting for the response of movement sensation from the manipulator's feedback signal. Time delays on telemanipulated systems will take an important part of the multiple instability issues encountered on bilateral teleoperation. As mentioned by Siciliano [5], at the end of the '70s, researchers understood the motion problem for rigid bodies, but when manipulators started interacting with environments, a new control problem appeared: force control. When the user interacts with the remote location through an electromechanical device, it was needed the kinesthetic information of the environment to report the user about the current position of the grasper, but that information came with delay, creating a threshold of unknown information on a time slot. That threshold increased the error of the user desired positions and velocities to the manipulator, making the teleoperation performance almost not achievable. The lack of information on time slots resulted into operation failures with potential damage to the user and environment, making unsafe or risky the remote manipulation.

In order to kinaesthetically couple the master with the slave robots a new control law was developed, as reported by Anderson in [6]. This law used passivity and scattering theory to maintain stability in bilateral manipulation within any environment and with any time delay. Using a scattering variable in the communication channel, the system was able to transfer energy across the telemanipulation chain, but there was the presence of negative factors such as virtual energy, making the system unstable and creating difficulties to the user performance. If in the

interaction with the remote location is not possible to display the environment forces at the master side, the transparency of the system is severely affected. Anderson's work represented the motivation for Franken, Stramigioli, Reilink, Secchi and Macchelli in [7] to develop a new control method based on different approaches such as Passivity Observer-Passivity Controller (PO/PC) by Ryu in [8], Energy Bounding Algorithm (EBA) by Kim in [9], and the framework proposed by Lee using PD control [10]. Franken *et al.* successfully implemented a solution into a one degree of freedom (DoF) system, presenting the energy tank concept to ensure stability, but with a high cost on transparency. Currently, the energy tank approach is a reliable tool for bilateral telemanipulation systems, it gives a solution to maintain stability into the system.

1.1 Motivation

The concepts and experiments presented in this thesis on bilateral telemanipulation are the intellectual development of more than sixty five years of research by a large scientific group. Nowadays, there is an important infrastructure in place in terms of telecommunication. This represents an opportunity to exploit the data networks for telerobotics applications. As presented in [11], current technology could provide the bandwidths needed to do telepresence and achieve performances on telerobotics that were not possible in the past; medical applications such as remote echography are possible by seizing the advantages of communication networks. A significant application for telerobotics is hazardous materials manipulation. For example, the European Organization for Nuclear Research (CERN) has the necessity to provide maintenance to the 22 km loop tunnel of the Large Hadron Collider (LHC), where it has been developed a complex mechatronic system that consists of a series of wagons with a manipulator to perform remote surveillance inside the tunnel, as described in [12, 13]. Also, bilateral telemanipulation plays an important role in industry, by providing an interactive element (manipulator) to perform a remote task in a production line or another specific area. Research on industrial prototype applications for teleoperation is presented in [14] and [15].

Another problem is that systems need real time communication protocols to ensure safety on the area and in the task execution; DexROV [16] is a project that involves a vessel on the sea to control an Underwater Vehicle-Manipulator System (UVMS) from an onshore operation center; here, a human operator using an exoskeleton will command the remote vehicles for exploring purposes under the sea, sending all data information via satellite. As an industrial application for oil extraction, Garcia [17] presents a remote manipulator for inspection and maintenance tasks in a drilling rig.

From people who suffered accidents to congenital malformation, there is the field for robotics in medicine, where the use of manipulators (in the form of exoskeletons) can help people to interact with a virtual environment (or real depending on the training). MARSE-4 [18] is a 7 DoF upper limb exoskeleton for physical therapy, where the user must track some desired trajectories

in order to force the upper-limbs for muscle rehabilitation.

But challenges arise when system complexity increases. As mentioned by Panzirsch in [19], the future in teleoperation will be defined by the task, and with this, new methodologies and strategies will be required, improving sensor accuracy, transparency, sample rate and control stability.

1.1.1 Historical Perspective

Bilateral telemanipulation represents the link of the closed-loop circuit between a human operator (as a master interface) and a robot manipulator (as a slave interface) [20]. The importance of robotics teleoperation is present when the risk of the operator is reduced by distance, remote and unmanned task [21]. In addition, bilateral manipulation applications should optimize the task performance, as mentioned by Lawrence [22]; the term telepresence describes the idea of "being there" in a high fidelity aspect that it seems the person was in site [23]; where the user experiences the intuitiveness, speed and accuracy of the system [24]. That means enhancing the experience over the system performance with haptic force feedback [25]. The applications tend to extend human capabilities in areas such surgical robotics [26, 27], space robotics [28], remote mining and others [29]. As mentioned before, the first telemanipulation experiment was developed in the 1950s, and the main problem began when time delays appeared in the telemanipulation chain, complicating the performance of tasks.

Tasks with remote manipulation present destabilizing factors that affects performance, these factors present a control problem to solve regards transparency and stability. The telemanipulation chain is destabilized by several factors, such as (i) hard contacts, (ii) high stiffness of the environment, and (iii) time delays. Various studies on control methods have been developed to provide a solution to this problem, where the different approaches are studied as the supervisory control method based on hybrid systems [30], the non-linear adaptive control [31], and passivity control theory. Moreover, the solutions in passivity control rely on algorithms that guarantee passivity over the system through the scattering variables [6] in order to exchange fractions of energy between the elements of the telemanipulation chain.

In the work of Lee [10], it is presented a passive controller to obtain real haptic position feedback. Their framework enforces the position synchronization between the master and the slave when time delays occur. In terms of transparency, Lawrence [22] substantiates the importance of transmitting four data types (forces and positions) bidirectionally in the telemanipulation chain, achieving stability using passivity. Sanchez [32] developed an application based on surgical robotics, the goal is to provide a more realistic environment using a visco-elastic model; the interaction between the robot and the patient should be totally safe. Furthermore, solutions based on passivity have been discussed by Ryu [8] using time domain passivity control. This approach exchanges energy packages between the master and slave interfaces; the terms "passivity-observer" and "passivity -controller" are introduced to define a two-port system that connects with diverse

environments and speeds. Kim et al. [33] proposed an interaction with virtual environments where the passivity control limits the virtual energy generated applying an effective damping element to the teleoperation devices; disregarding the system sampling frequency, this method guarantees stability and a transparency. The research presented by Lee [34] shows an approach based in a tank to store energy from a spring-damper controller; it is described as a passive set-position modulation where the energy is injected by the user, the stored energy is used to limit the robot's movements in the slave side, preserving passivity and stability.

Finally, the work of Franken et al. [35] illustrates an elegant solution for dealing with destabilizing factors. A two-layer approach algorithm for bilateral telemanipulation control is presented. The work is related to varying factors with time delays, where the first layer processes the transparency of the system, and the second layer determines the passivity. In fact, the solution incorporates the use of energy tanks in order to regulate and maintain passivity on the telemanipulation chain.

1.1.2 State of the Art

The core of the research presented in this thesis is based on the work by Franken *et al*. [7], where the concept of Energy Tanks and the Two-Layer Approach is introduced as a solution to preserve passivity in a bilateral telemanipulated system that presents varying time delays. The concept was first presented in [36], and implemented in [37–43] among others.

Since bilateral telemanipulation schemes are mostly affected by time delays, different solutions have been developed to tackle this problem. Panzirsch [19] presents an extended predictive model-mediated teleoperation using multilateral control. This model tends to compensate the effects caused by high time delays in the system, by providing instantaneous force feedback to the user from a local virtual model of the slave robot; this is called fictitious local force feedback. Despite the system presenting low transparency, the remote haptic feedback seems to be accurate and to provide an exact state to the user about the remote environment. A similar research on fictitious force feedback is presented by Pitakwatchara in [44].

Another approach is adaptive control. In [45], an adaptive sliding-mode controller is tested for bilateral telemanipulation system of 2 DoF under symmetric time delay conditions, using Lyapunov-Krasovskii functions and Linear Matrix Inequalities (LMIs), where closed-loop stability is the main objective. In systems where wave variables are used (energy variables as $\dot{x}$ and force F are convert in wave variables u and v in the communication channel), negative aspects are presented, such as wave reflection and position drift among the master and the slave; for Zheng Chen [46], a novel proposal is to introduce weighted coefficients into the wave variables to command the slaves into a four-channel architecture. The purpose is to optimize the signal transmission in the communication channel and guarantee stability, providing an ideal transparency and good performance.

Another method proposed to compensate time delays is Internal Model Control (IMC). This

technique was presented in [47] and consists in designing a controller based on the inverse model of the system. In this work, mobile robots are used as master and slave, and the inverse model of the robot is compared with the plant (in the control system) to compensate disturbances. A proportional controller is extended with a damping injection algorithm to saturate the torque at the master side when large time delays occur. This strategy seeks to maintain a stable system, guaranteeing a strong performance on the task.

In Heck [48], an implementation resembling [35] of 1 DoF set up is presented, being an extension of [49]. In contrast with the two-layer approach, they present two tank level controllers (one for the master and one for the slave), which in [35] is only one in the master side. The novelty relies on having a second Tank Level Controller (TLC) on the slave side, which means that in order to preserve passivity, not only the operator injects energy to the system, but this process is duplicated because the remote environment can also transfer energy into the second tank. The results show a bilateral teleoperated interaction with stiff contacts, which remains stable even with notable increases in the time delay. The Time-domain Passivity Control Approach (TDPC) is commonly used in bilateral teleoperation architectures with time delay as a reliable approach to ensure stability. Ahmad [50] proposed an extension for TDPC architectures from bilateral to multilateral structures, where the communication channel is redesigned in order to exchange information with multiple masters and slaves. In the field of optimization, Ferraguti [39] exposes a solution to solve the problem for energy on wave variables, where the objective is to reach a desired level on the forces and velocities displayed at the master's side. The wave variables describe commands that contain information related to energy exchange in both sides of the telemanipulation chain. The general scope is to obtain the maximum amount of power contained in the wave variable by minimizing the incoming power variable in function of force and velocity.

1.1.3 Technological Impact

According to [51], there are four main features on telemanipulation: *a) operability*, *b) remote access*, *c) communication infrastructure*, and *d) synchronization*. Also the system must present communication capabilities such as bandwidth, bit error rate and management of lost packages. The teleoperation task should be able to backup, analyse, and reproduce data; as well as present real time processing capabilities. One of the challenges is to reduce the effect of time delay in the operation, even to include a prediction error estimator. Mechanically, a teleoperation system should satisfy ergonomics, electromechanical and electrical performance requirements. The system also allows task configuration and gives autonomy and intelligence features such as task co-operation, telemetry and security protection.

The immersion of the human being inside virtual and augmented realities has created alternative scenarios to interact and perform activities, from training simulations to real operations. In each of these, there is a strong need of information to enhance the experience. Studies on multi-contact point haptic interfaces reveal that the interaction with remote environments seems

more transparent if the number of actuated parts on the master side is higher. Thus, it is possible to manage more information to the user about the remote location and increase telepresence [52–56].

Another relevant technological aspect is the number of operators on a telemanipulated system. In [57], an interesting concept of two asymmetric slave manipulators is presented. For this approach, a single operator can telemanipulate two different robots that perform single tasks individually (subtasks). These research aims to prove that when controlling two asymmetric slaves, a couple of operators (co-operating pair) will improve the task performance when these are compared to a single operator. On this field, Shahbazi in [58] presents a comparison of the classical Single-Master/Single-Slave (SM/SS) teleoperation systems and the multilateral teleoperation framework. A minimum of three agents are involved to perform a remote task, four architectures are presented to facilitate the review: *a) Multi-Master/Single-Slave (MM/SS)*, *b) Single-Master/Multi-Slave (SM/MS)*, *c) Multi-Master/Multi-Slave (MM/MS)*, and *d) trilateral architecture*. The importance of this study lies in the categorization of all topologies for telemanipulated systems with their respective application.

Finally, a topic that is growing interest in bilateral telemanipulation systems is shared control. Defined as the combination of a human user and an autonomous agent, shared-control takes advantage of the human intelligence and the agent capabilities to aid each other [59, 60]. In Islam [61, 62], a shared-control project is presented where an operator uses a haptic device to command Miniature Aerial Vehicles (MAV). A force-reflection algorithm provides situational awareness about the environment, guiding the operator to control and navigate the MAV safety.

1.2 Objectives and Approach

The Two-layer Approach with energy tanks is a method that provides a solution to maintain stability on a telemanipulated system while preserving passivity. This thesis presents a strategy that prioritizes damping coefficients to achieve higher transparency along a number of desired directions. One of the main goals of haptic systems is to convey realistic forces (transparency) to the user. In bilateral telemanipulation control, factors such as relaxed grasp of the user, time delays and stiff environments may compromise the stability of the system. Ensuring passivity in the system, i.e. not generating energy by itself, can prevent unstable behaviour. To preserve passivity, a 3 DoF two-layer approach based on energy tanks is implemented; the energy provided to the slave side is limited by the energy obtained from the user at the master side. This energy is generated by a damping-like element that is activated when destabilizing factors occur. The method consists of solving a quadratic optimization problem that minimizes the projection of the damping force on different directions while maintaining passivity.

The aim of this work is to present an optimization-based design of the passivity layer which guarantees the maximum possible degree of transparency along subsets of the environment space

that are preponderant for the given task at a given time, while preserving the energy bounds that are required to guarantee passivity. The optimal rendered force is computed via the solution of a convex quadratic program that is characterized by modest computational complexity and amenable to implementation in real time.

As seen in Fig. 1.1, the typical telemanipulated system is generally divided in a master and a slave side. The two-layer approach is implemented to compute (by the transparency layer) and limit torques (by the passivity layer).

In the master side, the user commands the haptic device to send the positions of the haptic grasp to the other side, simultaneously the haptic device is receiving the force feedback coming from the slave side. At the slave side, the manipulator receives the commands as forces to perform the movements that the user defines; on the same way it is sending the positions of the end-effector to the master side. Both sides master and slave have an energy tank, with this approach it is possible to maintain passivity inside the system and make it stable.

Assuming that an initial condition is zero energy inside the system, the only way to put energy in the tank is through a viscous damper on the master side, this algorithm is called Tank Level Controller. Thus, the user is obliged to exert some force in all directions at the haptic device until the energy reaches a desired level, the TLC produces the damping forces according to the difference of the current energy level and the desired level, making the damping *feeling* dynamic.

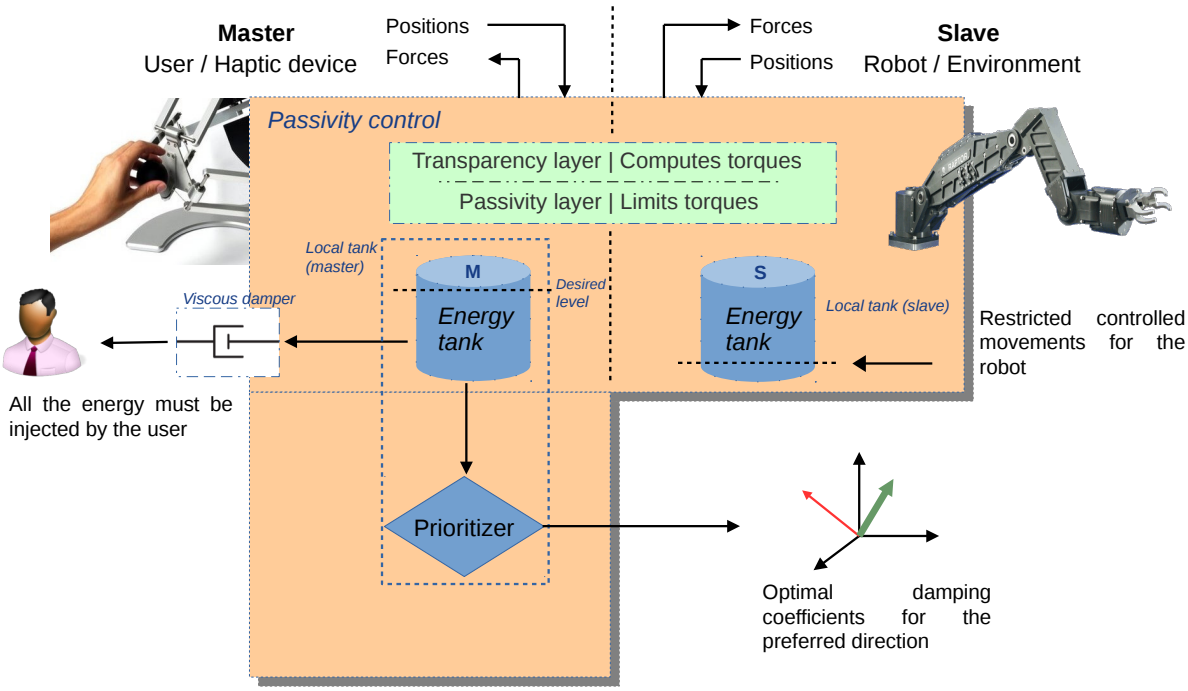

FIGURE 1.1. Bilateral telemanipulation system based on the two-layer approach and the damping coefficients optimizer.

This desired level is the energy budget necessary to reproduce movements in the slave side. As the manipulator in the slave side consumes the energy, the energy level will drop down the desired level, displaying the damping force in all directions at the haptic device and making the user introduce energy again. This process reduces the perception of transparency to the user, and when the energy tanks drop to the lowest level (zero) the forces are cut off, making impossible to manipulate the remote environment.

To improve the transparency when performing a defined task, an optimization method is implemented in the master side. The objective is to obtain the damping coefficients that minimizes the damping forces on a preferred direction, with this, the transparency will be higher. The cost function to minimize is detailed in equation (3.15) in Sec. 3.3, and the implementation of it in Section 4.2.1.

1.3 Research Context

The work developed in this thesis was sponsored by the project "Soft-Bodied Intelligence for Manipulation (SOMA)"[1]. The objective of SOMA is to develop a disruptive and innovative path for the development of a simple, compliant, strong, robust, and easy-to-program manipulation system. The results achieved on this thesis fit on the Human/Robot Collaboration impact of SOMA by improving the human capabilities to interact with environments in remote locations using a manipulation system that ensures stability.

This work is also related to the research line conducted by Prof. Domenico Prattichizzo at Siena Robotics and Systems Lab (SIRSLAB)[2] at University of Siena; the topics on haptics and passivity control have been studied since 2002 with the project described in [63], where a PHANTOM ^{TM} [3] haptic interface is used for rendering deformable objects and also calculating the correct interaction force of interactive virtual elements. This project derived into a research project for ultrasound 3D reconstruction called *The FeTouch Project* [66, 67], where the aim is to obtain physical interaction with a 3D scanned fetus model through a haptic device. The first developments in teleoperation research within the group were carried out in [68]. In this project the objective was to insert a linear-stage rigid endoscope into the patient with a remote manipulator on the slave side, using a haptic device on the master side.

More related to the main topic of this thesis, work on transparency for bilateral telemanipulation were conducted by Dr. Claudio Pacchierotti in [69], who was member of the SIRSLAB

[1] SOMA is funded by the Horizon 2020 European Framework Programme, where the following institutions are participating: Technische Universität Berlin (Germany), University of Pisa (Italy), Italian Institute of Technology (Italy), German Aerospace Center (Germany), Institute of Science and Technology Austria (Austria), Ocado Ltd. (United Kingdom), and Disney Research (Switzerland). Website: *https://cordis.europa.eu/project/rcn/194335_es.html*

[2] Siena Robotics and Systems Lab: *http://sirslab.dii.unisi.it/*

[3] The introductory literature to haptics is referenced in [64]. Haptic applications with the Phantom interface can be consulted in [65].

group and acted as fellow at Instituto Italiano di Tecnologia. The research literature on improved transparency for bilateral telemanipulation can be consulted in [70–72].

1.4 Contributions

The contribution of this Ph.D. thesis is an extension of the work presented by Franken *et al.* in [35], this extension is divided in: *a) 3 DoF extension*, *b) optimization of the damping coefficient parameters*, *c) dynamic desired level*, *d) simple energy tank simulator*, and *e) ROS package for bilateral telemanipulation*.

- 3 DoF extension. The original work presented in [35] has an implementation of a 1 DoF robot in both master and slave sides. In this thesis an extension of 3 DoF with a haptic device (in the master side) and a virtual environment (in the slave side) is presented. Since in the original version the force injected into the system was gathered for only one direction, in the extension the viscous damping effect is felt in 3 DoF.

- Optimization of the damping coefficient parameters. One of the problems to solve is how to increase transparency on a bilateral telemanipulated system, while maintaining passivity and a stable system. In [35], the viscous damper is rendered in the haptic device to introduce energy in the tank. The viscous damper (dynamic damper) depends on the difference of the current amount of energy and the desired level, this creates the effect of highly damped movements when the tank is almost empty, and undamped movements when the tank is full (total transparency). To improve the overall transparency, a preferred direction is chosen depending on the task; thus, the prioritizer in the TLC at the master side will optimize the damping coefficients to be displayed at the haptic device, reducing the damping forces in the preferred direction, and resulting in higher transparency.

- Dynamic desired level. One of the constraints used in the optimizer is designed to ensure a minimum amount of energy in the system, the desired level should change constantly according to the energy demand while the task is performed. In the work of Franken, the desired level was selected by the user to create a minimal energy budget to the system. In this thesis, the approach relies on a dynamic desired level that uses a parametrizable gain and an energy consumption estimator.

- Simple energy tank simulator. The energy tank simulator is a piece of software created in *Processing*[4] that simulates the energy tank behaviour for the two-layer approach implementation. The purpose is to understand how the system behaves when an energy exchange process occur, the software provides a graphical and interactive interface for the bilateral telemanipulation system.

[4]Processing is a programming language and framework to code within the context of engineering and visual arts. Website: *https://processing.org/*

- ROS package for bilateral telemanipulation. The whole system was designed and implemented following the structure of the Robotic Operative System (ROS)[5] and the nodes are written in C++. The system aims to be a *plug and play* package, the inputs are positions and the outputs are forces in both master and slave sides.

1.5 Outline

Chapter 2 provides the background theory of the thesis. It begins with the definitions of teleoperator, telemanipulator and telepresence. Then, an overview on bilateral telemanipulation is provided, with the topics about master side, slave side, and two-port network. Second, the section on haptics is divided by devices, applications, rendering and interfaces. Third, the problem of transparency on bilateral telemanipulation is described including its limitations. Fourth, there is a brief definition on passivity control theory, and how the proposed approach is a solution to stabilize teleoperated systems. Finally, the background of the energy-tank based two-layer approach proposed by Franken *et al.* [35] is covered.

Chapter 3 presents the definition of the 1 DoF Two-layer Approach. In addition, the 3 DoF extension and optimizer is detailed; the theoretical approach on the optimization process is explained in order to improve the transparency on a preferred direction with the proposed TOPL controller. Then, the description of the control architecture of the method is provided. The chapter ends with the correction method of the desired level to enhance the performance of the TOPL approach.

Chapter 4 presents the implementation and results of the TOPL approach. Second, an experimental set up of this optimization is provided as an early experiment of the solution, the name is Poke/Drag Experiment (PODREX). This last presents the validation of an experimental set up with the haptic device and the virtual environment, different scenarios are evaluated to prove the TOPL approach. Next, a complex designed task to evaluate the performance of the controller as the core of the contribution is developed, this is called Palpation Experiment (PE). This implementation consists of an optimal design of the passivity layer where the damping coefficients of the TLC controller are shaped according to a preferred direction, and so achieve a more transparent system. Besides, the task is evaluated to prove the TOPL approach, here, the user must find a stiffer area by exploring a surface with a fix stiffness value on different time-delay conditions and using three diverse controllers.

Chapter 5 introduces the energy tank simulator as part of the contributions of this thesis and the description of the software used to develop the system for the presented experiments. Beginning with a brief introduction on bilateral telemanipulation, this chapters gives an overview of how energy is taken from the physical environment and is exchanged from the master to the slave side and vice versa. Later on, the description of the simulator functionality is provided as

[5]Robot Operating System (ROS) is a software framework for robotics development. Website: *http://www.ros.org/*

well as the features. A system run is shown to describe the operation of the interactive simulator. Finally, the description of a teleoperated architecture developed for this thesis is given; all the software components were designed in ROS.

Chapter 6 summarizes the outcome of this thesis highlighting the important insights and contributions of the presented work. It is also discussed the relevance regarding innovation on the theoretical aspects to extend and optimize previous work. Also, the technological aspects about telemanipulation are analysed and impact, future work and challenges are presented.

CHAPTER 2

BACKGROUND

As Siciliano states in [5], the most relevant issue is to identify the challenges on solutions for robotics according to the demands of the sectors, either academic or industrial. At the beginning of the 1970s, researchers considered the problem of motion control for industrial manipulators (rigid bodies) as solved, but in practice, force control issues started to arise [73]. In the field of teleoperation, transparency is the main objective to achieve, thus, the master device ideally must emulate the environment where it is interacting. To perform teleoperation tasks a haptic interface is required, but some physical constraints should be considered such as peak acceleration, isotropy and dynamic range of impedances [5]. Facing those constraints, an elegant solution to bilateral telemanipulation control resides on the passivity theory, where the aim is to maintain stability reaching the highest transparency and using virtual energy contained in virtual reservoirs; these topics will be discussed along this chapter.

2.1 Telemanipulation

In the book by Sheridan in [74], the term *teleoperator* describes a machine that extends the user's capabilities to manipulate or sense a remote environment. Also, it is mentioned the necessity of sensors to measure the remote location. These are adapted into electro-mechanical devices, which apply forces and produce mechanical work on the site. On the other hand, a *telerobot* is an advanced form of a teleoperator. This device performs tasks based on the information received from the human operator in addition of the sensory data. For Hayward *et al*. [75], teleoperation represents the mother discipline for telerobotics and telemanipulation, where the haptic interface plays an important role to the human, giving the sensation of "touch" in the telemanipulation chain (See Fig. 2.1). To Goodrich [76], teleoperation belongs to a branch of Human Robot Interaction (HRI) which represents a paradigm on an emerging work on

FIGURE 2.1. Block diagram of a simple telemanipulation chain.

robotics invoking a sense of presence when tasks are performed. An accurate definition for telemanipulation is the act of handling a remote object by a human operator with a Human-Machine-Interface (HMI) [20]. Similarly, [23] the word *telepresence* is defined as the experience of a person of "being there" in high fidelity form.

The developments on teleoperation are the results of the need to interact in hazardous environments, to avoid the risk of operating with dangerous materials, or to displace objects remotely. To perform a task, the operator uses an electromechanical device and receives information feedback about the conditions of the remote environment. This information gives the user a better perspective of telepresence, enhancing his experience. A telerobotics system is commonly a hybrid system which contains both continuous-time and discrete event dynamics [77]. The main objective in teleoperation is to improve task performance when the user is interacting with the environment. In the process, some challenges may appear, such as time delays due to the distance to the environment, limited communication bandwidth, and lack of information at the remote location. As seen in figure 2.1, a typical telemanipulation chain is composed by the user operating the master device, a communication channel to exchange information between sides, and a robot interacting with the environment on the slave side [78]. Bilateral telemanipulation could be seen as an end application of Augmented Reality (AR), where the user interacts with the real world manipulating virtual objects superimposed upon or composited on it (a supplementation of reality). In contrast with Virtual Environment (VE), the user is immersed into a synthetic and artificial location, real objects do not coexist in the same space; AR lies between VE (completely synthetic) and telepresence (completely real) [79].

There is a wide range of applications for robotic telemanipulators (See Fig. 2.2). In the field of surgical robotics [80, 81] there are several examples of applications. In [82] telemanipulation is applied to provide assistance guidance for surgery, a teleoperated laparoscopic system is set in [83], Papachristos [84] presents a telemedicine implementation for surgeon's training, in [85] a telesurgery system is shown, a robotic endoscopic microsurgery procedure is performed [86], and in Su [87] a teleoperated minimally invasive surgery method is presented. Another applications are focused on hazardous materials manipulation [88], like nuclear plants waste or harsh environments [12, 89]. Also remote vehicle manipulation is having an impact on telerobotics [90**?** –95], as well flying telepresence [96]. Similarly, experiments in the field of telepresence are

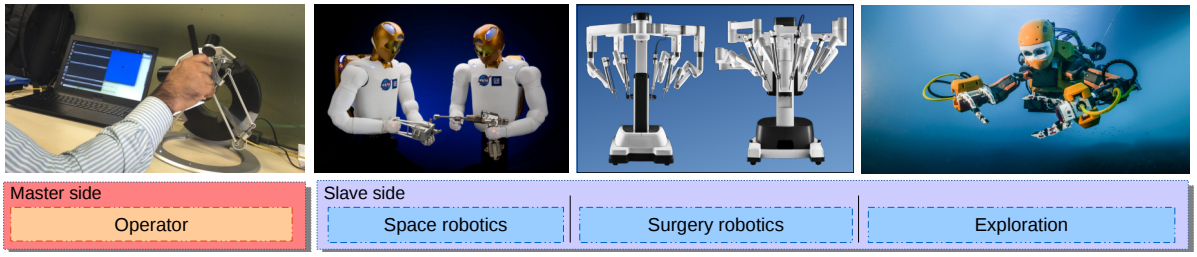

FIGURE 2.2. Telemanipulation applications. Master side: operator[1]. Slave side: Space robotics[2]; Surgical robotics[3]; Vehicle telemanipulation[4].

mentioned in [97–99]. Moreover, one of the most critical telemanipulated tasks are space robotics, since the long distances between the interfaces could affect synchronization. There are several cases for robotic space telemanipulation, such as telerobotics assembly line [100], reassignment of satellite orbit mission [101], on orbit hardware verification [102], the experiments on teleoperation with the hybrid robotic model METERON SUPVIS Justin Space-Robotics Experiment [103, 104], and space exploration [105–109]. Another example is the space robot experiment (ROTEX), a fully teleoperated system launched on 1993 by NASA in the flight STS 55, in which the capabilities of human operator at the ground station were able to send grasping commands to a manipulator [110]. Lastly, [111] presents a taxonomy about tasks and subtasks that telemanipulators could perform for heavy duty teleoperation actions. This study includes a set of movements according to the contact or no-contact operation, which indicate the path/action to follow.

Bilateral telemanipulation research relies over the closed-loop system (feedback information) that exists between the human operator and the manipulation of the environment [20], where the manipulator (slave) can also control the input device (master) [112]. As presented in [113], there are plenty technical challenges to achieve bilateral manipulation and the first one is detecting collisions in real time. Colgate and Kim [114, 115] state that the sensation between the operator and the environment gets affected by time delays, and as the distance between user and manipulator increases, so does the time delay, reflecting this issue on the task performance.

Therefore, the lag between the extreme components of the telemanipulation chain, destabilizes the system [115]; due to the time variation of the force feedback, the user experiences the force reaction moments later than when he/she performed the movement, this situation tends to cause oscillations in the haptic and manipulator forces. In a closed-loop system is possible to rename the master and slave sides in terms of impedances (Zm and Zs respectively) and be modelled as a damper-spring system. The behaviour of the chain is affected by the stiffness of the environment

[1]Haptic device Omega 6 ^{TM} by Force Dimension: *http://www.forcedimension.com/products/omega-6/overview*
[2]NASA and GM Robonaut2: *https://www.nasa.gov/images/content/421731main_jsc2009e155295.jpg*
[3]Intuitive Surgical Da Vinci ^{TM} : *https://www.intuitive.com/products-and-services/da-vinci/surgical-systems*
[4]Stanford Robotics, the Red Sea Robotic Exploratorium: *https://news.stanford.edu/2016/04/27/robotic-diver-recovers-treasures/* Image credit: Frederic Osada and Teddy Seguin/DRASSM

(Zs). If it is too high, the user applies a rigid grasp to the haptic device (Zm) to stabilize the system [116]. A proposal to solve the time delay issue was done by developing a passivity and scattering theory by Anderson in [6]. The formula for time delay in the master side is defined as:

$$F_m(t) = F_s(t-T)\,, \tag{2.1}$$

where F_m is the force on the master, F_s represents the force on the slave side and T the time delay of the communication channel.

In an ideal system, the user will interact with the environment without noticing the presence of the teleoperator. However, in practice, the teleoperator will not provide a perfect transparent kinesthetic coupling to the user due to the inertia and friction of the robots and time delays in the communication channel. The information exchanged by a bilateral telemanipulation system distorts the perception of the user about the environment. Dealing with this internal dynamics issue is common to abstract the information used to operate the robot. For a low level of abstraction, the teleoperator uses raw information such as position and force measurements to command executions. On the other hand, a high level of abstraction (classification of the raw information) indicates conceptual information from the measurements and generates a complex task (such as an objective). Regardless of the level of abstraction, the information along the system must be processed by a control technique, and achieve a stable performance. This means that a high level of abstraction could represent a concept as a task to perform by the robot, this level of abstraction creates a high level of data, which could be decomposed by the robot into low level instructions. The control technique allows to do equitable predictions and to adjust the behaviour of the teleoperator according to the expected performance [78].

2.1.1 Bilateral Telemanipulation: Models

In bilateral telemanipulation, the distant interaction occurs when the operator manipulates a remote location using mechanical devices on both sides (master and slave). The system exchanges information such as position and force from one side to the other. This section discusses the model of the controller. For the model of the master see Section 2.1.1-(A) and for the model of the slave see Section 2.1.1-(B). The force feedback could be generated from the information of the positions (see position control in Sec. 2.1.2-(A)), the information of the forces (see force control in Sec. 2.1.2-(B)) or a higher level of abstraction such as impedance control (see Sec. 2.1.2-(C)).

A) Model of the Master Controller

The model of the master controller is implemented on the base of the haptic device location. A proxy is a representative object that substitutes the physical contact point, end-effector or probe in the virtual environment [117–119]. It represents the ideal location in the environment. The

master controller generates a force feedback to match the distances between the master and proxy every time it is necessary [85].

Mitra and Niemeyer present in [120], a model in free space assuming there is no contact between the proxy and the environment, from which the behaviour of the proxy follows:

$$x_p = x_m, \tag{2.2}$$

where x_p indicates the positions of the proxy and x_m for the positions of the master.

When a contact with the environment occurs, the proxy increases its distance from the master generating a force feedback according to this mismatch. If the proxy has no velocity and force feedback is based only on deflection, the model is:

$$F_m = -k(x_m - x_p). \tag{2.3}$$

In this equation, F_m is the force displayed at the master robot and k is a constant that represents the stiffness of the spring. After the contact is lost, the proxy goes immediately to the master position as in (2.2).

In a second order dynamic model, assuming that the proxy has a mass m, a spring with stiffness k and a damper ratio b, the proxy motion is defined by:

$$m\ddot{x}_p = b(\dot{x}_m - \dot{x}_p) - k(x_m - x_p) + F_{virtual}. \tag{2.4}$$

As seen in equation (2.4), $F_{virtual}$ describes the forces coming out from collisions in the virtual environment. Also Mitra in [120] states that the feedback forces displayed at the master robot f_m are computed using the spring-damper elements:

$$F_m = -b(\dot{x}_m - \dot{x}_p) - k(x_m - x_p). \tag{2.5}$$

Finally, Fig. 2.3 depicts the connection of the master-proxy model with a spring-damper configuration [120]. It is important to remark that the model considers a virtual element to study the relationship of the force feedback with the master side. On a real scenario there might be a force sensor attached to the robot's end-effector that provides force feedback of the environment to the master side (haptic device). The equation displayed in Fig. 2.3 defines the power P as the product of the velocities of the proxy v_p multiplied by the force reflection $-F_m$.

B) Model of the Slave Controller

The model of the slave controller is task dependent. It could be designed as a position, force or a hybrid controller or both. In the case of a force controller, the following equation implements a simple PD control strategy [78]:

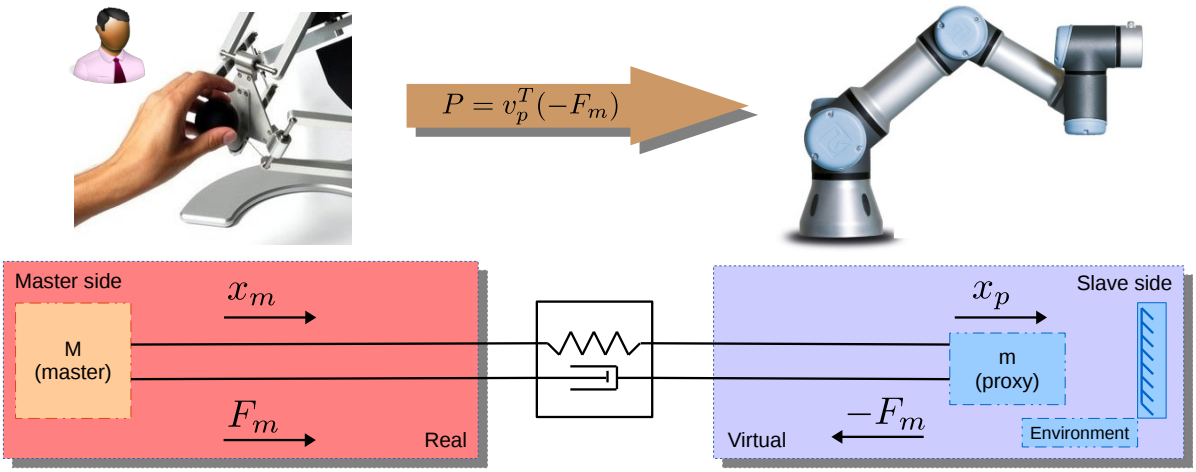

FIGURE 2.3. Model of the master-proxy connector through a spring-damper configuration.

$$F_s = k_s(x_{Td} - x_s) + d_s(\dot{x}_{Td} - \dot{x}_s). \tag{2.6}$$

F_s is the force of the slave, there is a stiffness component k_s and a damping ratio d_s, Td stands for a desired task and x_s and $\dot{x}_s$ are position and velocities of the slave side respectively.

If velocity is not part of the task, the parameter could be set to zero and the controller will track only position. The damping coefficient plays the role of a stabilizer, since it breaks the motion of the robot. When the user exerts a force in the haptic device on free space, the controller strives to have a good steady-state tracking performance. Nonetheless, this is not a critical problem in the model because the controller is only used for interacting with stiff environments, where motion is relatively small.

C) Two-Port Network Model

An important aspect of bilateral telemanipulation is stability. A considerable amount of research on the topic places the two-port network model on experimental set up as a reliable approach [121–123]. For a better understanding of the closed-loop teleoperation behaviour, the two-port network model presents a perspective to study the connection between user and environment as a series of energy exchanges [124–126]. The interpretation of this model describes an electrical circuit with two-port impedance elements [124, 127, 128], and it is the link to the passivity approach, where energy dissipation can be used to solve stability.

The performance of the two-port network model has been proven to be robust when destabilizing factors occurs, such as time delays (more factors described in Section 2.3.1) [22]. In that work it is stated that in order to increase transparency on the system, positions and forces must be

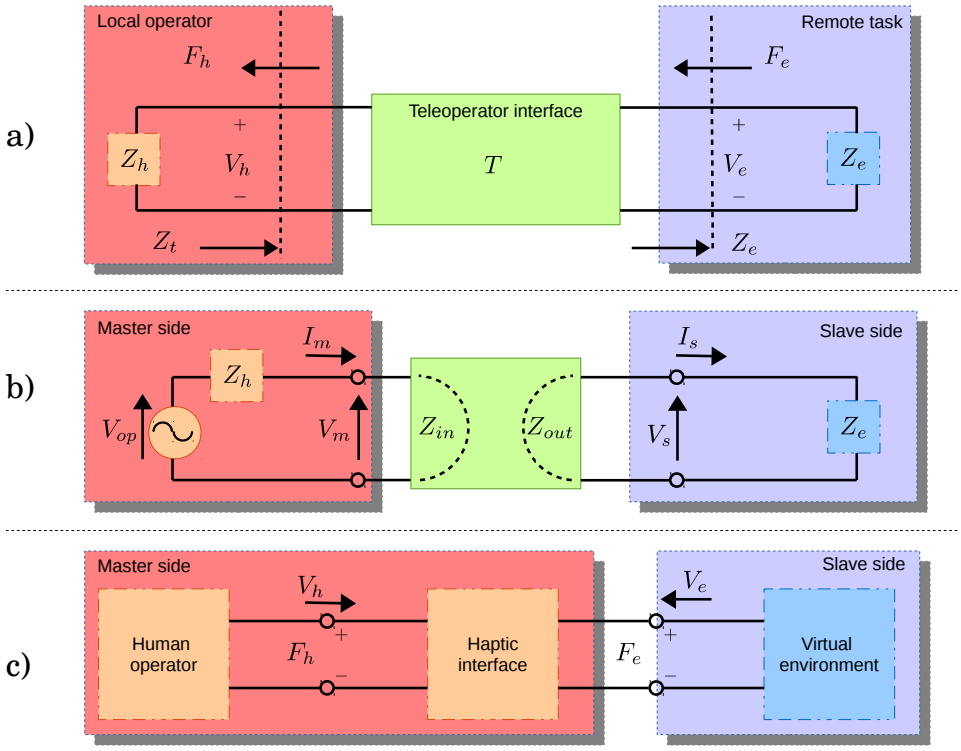

FIGURE 2.4. Two-port Network Model: a) Model by Lawrence [22], b) Model by Yokokohji [130], c) Model by Adams [121].

included as a set of information to exchange. This control architecture is named as four-channel network [129], and it considers the bilateral teleoperation without the telecommunication delays [40]. In Fig. 2.4-a, the two-port model depicted belongs to Lawrence [22], where the impedances Z_h (human) and Z_e (environment) are coupled by a teleoperator interface T. The electrical analogy presented by Yokokohji [130] (see Fig. 2.4-b) shows the currents I_m and I_s as the velocities of master and slave ($\dot{x}_m$ and $\dot{x}_s$ respectively); the voltages V_{op}, V_m and V_s correspond to the forces of the operator τ_{op}, master f_m and slave f_s respectively. Due to the "cost" of data-processing, this thesis is centred on the two-port network approach.

A typical Two-port model is a "black-box" which transfers *efforts* (forces) and *flows* (velocities). The relationship between efforts and flows could be sorted on a *immittance matrix* (which contains information of the impedance and admittance matrices) as described in [121]. The haptic device could be depicted as a two-port system which exchanges energy between a human operator (F_h, v_h) and a virtual environment (F_e, v_e) as shown in Fig. 2.4-c. The stability of the two-port network relies on its terminal immittances. A teleoperation system is said to be stable if all of its elements are passive and the system does not generate energy by itself [121]. Time delays on the communication channel violate the passivity condition, as demonstrated in [127] and [6]. Later on, passivity will be discussed in Section 2.3.2, which shows a general overview of the two-port

approach.

Despite some studies indicating that passive networks reduce the stiffness sensation of the user about the environment [131], a proper passive based design could improve the transparency of such systems as in [35] when destabilizing factors appear. Different approaches present experiments on stability for the two-port model as the Projection-Based Force-Reflection (PBFR), where the algorithm splits the bandwidth of the system to improve force convergence against negative influences such as time delays [132].

2.1.2 Bilateral Telemanipulation: Control Techniques

Goertz [1] identified the problem of stability and the need to improve performance when interacting with a remote location. As explained by Okamura [133], the aim of bilateral telemanipulation relies in providing the user (at the master side) the highest level of control over the slave. Techniques such as virtual fixtures partially remove the user's control over the slave. The operator achieves a better performance when he receives more information from the environment as haptic feedback. There is a large set of previous research on bilateral telemanipulation control, but regarding contacts in the environment, a wider investigation must be performed.

Several control laws are applied to the teleoperator task, according to the desired capability such as position, force, and environment impedance [133]. Among the control methods, impedance control is the most common. In this method (described in Sec. 2.1.2-(C)), virtual impedance forces are used to couple the master and slave robots, this cause them to track each other. Also, in this method force sensors are not required, this becomes in position exchange control.

When force sensors on the remote robot (slave) are used to track the forces displayed at the master, it is called position/force feedback control (see Section 2.1.2-(B)). This control method turns chaotic if there is a large number of DoFs to track. If the master and slave differ on the number of DoFs, the telemanipulation chain is called sensor/actuator asymmetry control. In this last approach, the information displayed at the master feels strange to the operator; the system creates its own energy, making it non-passive and potentially unstable [134].

Due to the limitations in the basic types of impedance control, providing realistic haptic feedback is a challenging task. There exist many methods to improve the performance with and without sensing. An adaptive controller can estimate mechanical properties of the environment such as mass, stiffness, and damping [135]; in [136] an implementation of adaptive control is shown. But one of the negative sides is that this type of model considers a linear environment; meaning the adapted remote location properties will be constantly changing to reflect the new *local* linear environment properties. It has been proved that some environment properties are non-linear to very small deformations [137]. Another method to improve stability in a bilateral manipulation system is passivity control, which will be discussed in Section 2.3.2.

A) Position-Position Control

In position-position control (PPC) (see Fig. 2.5), the errors of the position and velocity are measured and the controller produces a virtual spring-damper to couple the devices (master and slave); this action activates the motors together in order to emulate the direct mechanical connection of the systems (master and slave) [138]. This architecture [116, 124] is one of the oldest used in telerobotics because of simplicity and stability [1]. An implementation of position-position control is presented in [139], the goal of their experiment is to achieve zero steady-state position error in contact free movement.

As mentioned in [140], the path X_m of the master robot is used as a reference trajectory for the slave robot. The proportional-derivative (PD) position controller means that the slave will try to follow the master, acting as a spring of stiffness P_s and a damper of constant D_s. Force reflection is achieved due to the actuation of a PD_m controller when tracking the error. It is important to remark that these robots are represented by impedances (Z_m, Z_s) in terms of positions and not velocities. The operator exerts a force to move his own arm and also the robot Z_{op}, so the total force τ_{op} applied to the master f_m follows equation (2.7):

$$\tau_{op} = f_m + Z_{op} X_m. \tag{2.7}$$

On the same way, the force displayed on the slave robot f_s is the interaction result of the external sources τ_e, the environment impedance Z_e and the positions of the slave robot X_s as defined in :

$$-f_s = \tau_e + (-Z_e X_s). \tag{2.8}$$

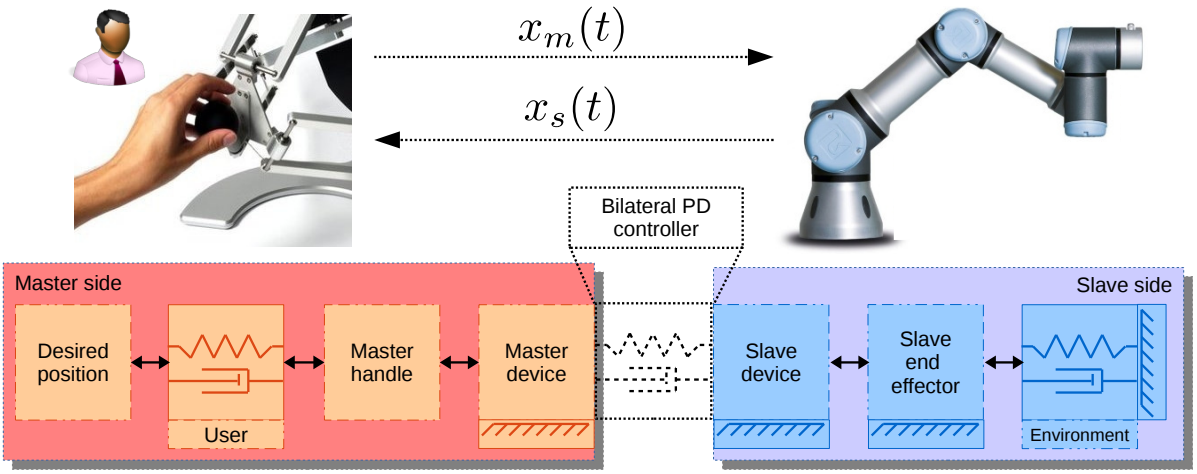

FIGURE 2.5. Block diagram of a Position-position control telemanipulation system.

To choose a strategy of control is necessary to identify the objective of the application, such as high positioning accuracy, tracking precision and motion dynamics [141]. Fig. 2.7 displays the diagram of a symmetric position-position controller proposed by Aliaga in [140].

B) Position-Force Control

As presented in [138], position-force control (PFC) is an alternative strategy to provide accurate feedback by only measuring the force of contact between the slave and the remote location. In this strategy, the slave robot follows the positions of the master using a PD controller, and in some cases an integral feedback. The forces measured with a sensor at the end-effector in the slave robot (see Fig. 2.6 [138, 142]) are displayed at the master robot motor almost simultaneously. When a contact of the slave robot at the remote location occurs, the user experiences the interaction at the master side. Although the system is more direct for the user's interaction with the environment, this architecture presents contact instability. Typically, all forces must be attenuated by the user to prevent closed-loop feedback instability. Moreover, all high-frequency force feedback is distorted by the dynamic features between the haptic device motor and the user's hand.

Also in this controller (see Fig. 2.7), the slave robot is dedicated to follow the master. When a collision is located in the slave, the master must display this event to the user. The force of the collision must be sensed at the end-effector of the slave robot and scaled with a constant K at the master side. As stated in [143], this controller shows that the system is stable for any environment if the constant K is less than a critical value. This value is roughly the quotient of the masses of the master and the slave robots [140].

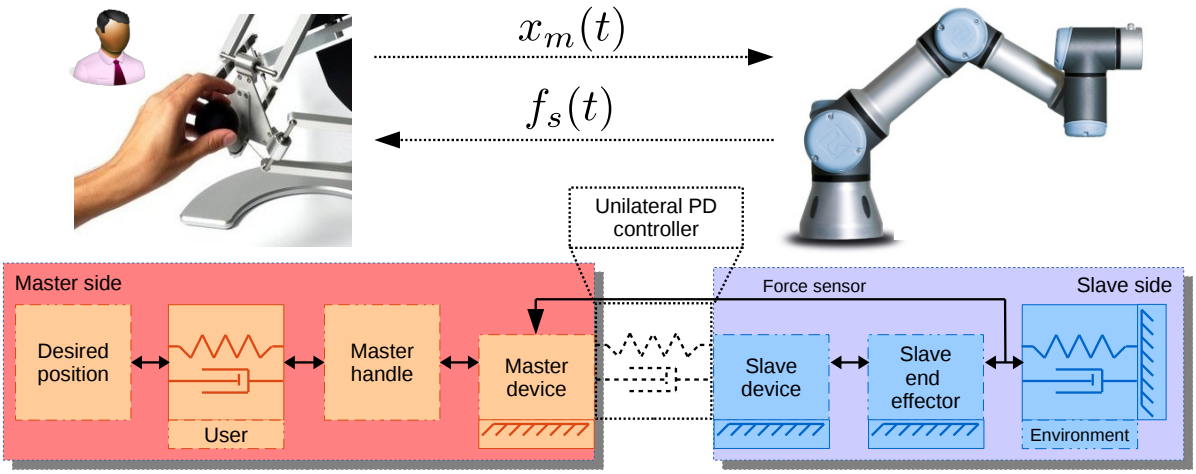

FIGURE 2.6. Block diagram of a Position-force control telemanipulation system.

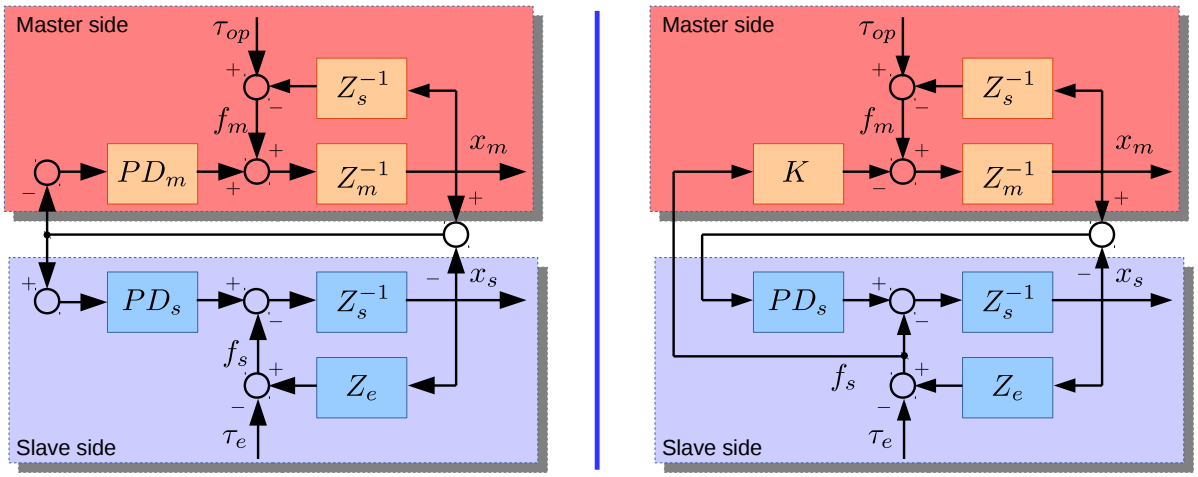

FIGURE 2.7. Architecture of Position-position control (left) and Position-force control (right).

C) Bilateral Impedance Control

So far, two strategies for bilateral telemanipulation control have been presented (PPC and PFC), and it has been said that one of the greatest issues for bilateral telemanipulation tasks are time delays. For that, bilateral impedance control theory has shown to reach a high level of fidelity for teleoperation, specially under time delays [124]. Another approach to solve instability problems is admittance control [144] for bilateral telemanipulation systems, as presented in the work of Osa [145], but this thesis is focused on impedance control type due to the characteristics of the implementation set up.

As discussed by Van der Linde *et. al* [146], the control paradigm of impedance control relies on the force applied by the user to the haptic device, generating a force executed by the slave robot in the environment. Using the haptic device as an observer, a displacement is introduced to the haptic and a force is the haptics outcome. In contrast, admittance control implies that the user exerts a force into the haptic device, and the slave robot reacts with a displacement. Again, if the haptic device is used as an observer, the force exerted by the user represents an input, and the outcome is a displacement. The literature covered by [147] provides the comparison of admittance control and impedance control types for bilateral telemanipulation.

Previous researches [148, 149] show that the simplest two-port architecture (described in Section 2.1.1) is not able to handle the minimal time-delay due to the transmission of impedance information being iterated around the complete control loop including the time delay. To solve it, Hannaford [124] presented an architecture (see Fig. 2.8) in which a local servo loop displays a commanded impedance force. In his model, the information transferred across time delays can be filtered to stabilize the telemanipulation chain. When filtering, the frequency compensation of

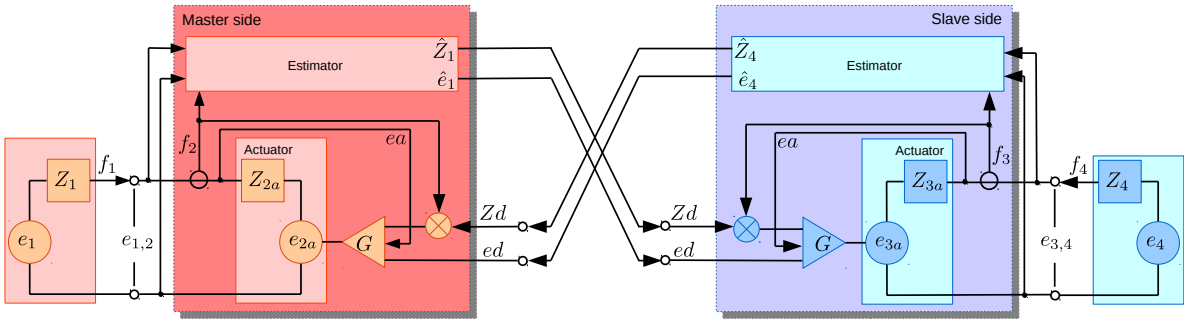

FIGURE 2.8. Architecture of Bilateral impedance control.

the signal information will degrade the fidelity. The high frequencies represent force information of the environment, while the low frequencies the force feedback to the user. Bilateral impedance control depends on the existence of an estimator which is capable of identifying the impedance of the environment and the human operator. This task is arduous because of numerical conditioning problems and noise. A solution is creating assumptions about the environment through the use of estimators [124].

A study of open-loop and closed-loop impedance controllers architectures is presented in the work of Carignan [150], where force feedback control improves the performance quality for haptic applications.

As seen in Fig. 2.8, the estimators could be used to reduce the impedance vectors Z_i that makes the system unstable [124]. Those estimators read sensor data to classify the flow of information from both sides (master and slave). In case the remote environment is pre-designed, Z_i could be part of common objects with well known properties. If Z_i belongs to the human estimator, this vector may correspond to predefined telemanipulation states, such as fine position control (high level of mechanical impedance), free motion (medium level), and force control (low level).

2.2 Haptic Devices

Smart mechatronic devices are the result of development of haptics technology for the past decades. This technology allows the user to interact with remote environments (virtual or real) and provides a sense of touch [151], a haptic interface functions as a force display device in your hand [152]. According to Benali-Khoudja [153], the human haptic sense is formed by the kinesthethic (motion, force) and tactile (tact, touch) senses. Touch sensations and haptic perception literature can be consulted in [154–158]

A haptic device is an electro-mechanical system that allows the user to experience the sensation of movement and dexterity when it is interacting with real or virtual environments.

a) b) c) d) e)

FIGURE 2.9. Haptic devices: a) Delta configuration: Omega 6 ^{TM} [5], b)Exoskeleton hand type: Dexmo ^{TM} [6], c) 6 DoF type: PHANToM ^{TM} [7], d) Exoskeleton type: HUG[8]and e) Exoskeleton hand type: Wolverine[9].

A haptic interface permits to apply tactile and kinaesthetic information to the user from a remote environment [151]. Fig. 2.9 shows some commercial and experimental haptic devices. The kinaesthetic and tactile information are reflected on the system through feedback forces and positions from the environment [151]. As reported by Colgate and Brown [159], haptic devices should generate mechanical impedances within a dynamic range of a stiff viscoelastic body; the main goal is to ensure a robust interactive behaviour. These devices, also known as force reflecting interfaces, manipulanda or hand controllers [159], have several applications in areas such as robotic surgery [26] and space training missions [113].

For Totorkulov and Ryu [160] there is a categorization for haptic devices corresponding to their rendering mode: a) *impedance type mode* and b) *admittance type mode*; further discussed in Sections 2.2.3 and 2.2.3. In the first one, the force rendered by the device depends on the velocity entered by the user; in the second one instead, the force presented in the device is related to the position of the operator's input force. This categorization is important for application purposes, admittance type devices have greater performance in terms of wall stiffness display over the impedance type ones, but also, these devices present a huge risk of instability operation when moving on free spaces.

Haptic devices work under impedance reflection algorithms, the most prominent author on this is Hogan [161–163] who describes the Impedance Control Approach for manipulation. Documentation related to mechanical impedance can be seen in [164–166]. Displaying a realistic sensation to the user when the an interaction in the environment occurs is a challenging task. One of the main issues on this topic is the way in which the user grasps the haptic interface. In this context, the work of Kuchenbecker [138, 167] presents a characterization of the human wrist

[5]Haptic device Omega 6 ^{TM} by Force Dimension: *http://www.forcedimension.com/products/omega-6/overview*

[6]Dexmo ^{TM} by Dexta Robotics: *https://www.dextarobotics.com/*

[7]Phantom ^{TM} by 3D Systems: *https://www.3dsystems.com/*

[8]HUG by DLR/Institute of Robotics and Mechatronics: *https://www.dlr.de/rm/en/desktopdefault.aspx/tabid-11704/#gallery/28737*

[9]Wolverine by Stanford University: *http://techfinder.stanford.edu/technologies/41529*

to improve haptic interaction. In haptics it is important to achieve accurate models of stability, Fu in [168] studied the dynamics model and variability of kinaesthetics haptic interfaces. Another scheme to achieve realistic haptic performance is proposed by Hwang [169], where they increase the bandwidth of the frequencies on a open-loop model. This characterization creates stiffer contacts in the environment interaction, displaying a more realistic scenario.

2.2.1 Haptics Applications

Haptic devices have a wide range of applications such as: medicine, gaming and robotics, communication, mobile devices, 3D simulation, data visualization, multi-user environments [170, 171], education, industry and graphical arts [172]. Fig. 2.10 presents some of the haptics applications mentioned in this section. Haptic devices play an important role in medicine, Fetch in [173] presents a highly dependent guidance rehabilitation method designed to improve the mutual adaptation of therapist and patient.

The medical applications of haptics cover a wide field: rehabilitation [174], tissue palpations experiments for surgical procedures [175], assisted surgery with haptic force feedback [176], laparoscopic surgery systems [83, 177], needle insertion with haptic force feedback [178, 179], teleoperated surgery [32, 133, 145, 180], endoscopy with haptic playback [181, 182], arthoplasty planning [183], a virtual environment to train veterinarians in palpation [184], and image examination with haptic force feedback [185]. For an extensive study on medical telerobotics the work of Avgoutsi [186] presents relevant cases of surgical teleoperation.

An interesting approach of haptics research comes from [187], who presents the use of the interface for interaction designs, relying on the simplicity of the device operation with the haptic interface. To Moussette in [187], the haptic experience in terms of manipulation is based on how the user affects the world, what are "sensory qualities" that forms the objects, and finally what does the user learn from it (interaction). Some works present the research and advances in haptics oriented to the technological and aesthetical aspects of the designs [188–190]. An example of modern haptics technology is the work of Bonanni in[191], a wearable haptic system that allows to record, broadcast and play sensations for emotional therapy is presented. In [192], an experiment of pseudo-haptics is presented, where visual and force feedback are introduced to the user as an augmentation of the haptic sensation leading to a non-veridical perception of virtual objects and their properties; this effect creates a different feel in the user's perception of friction.

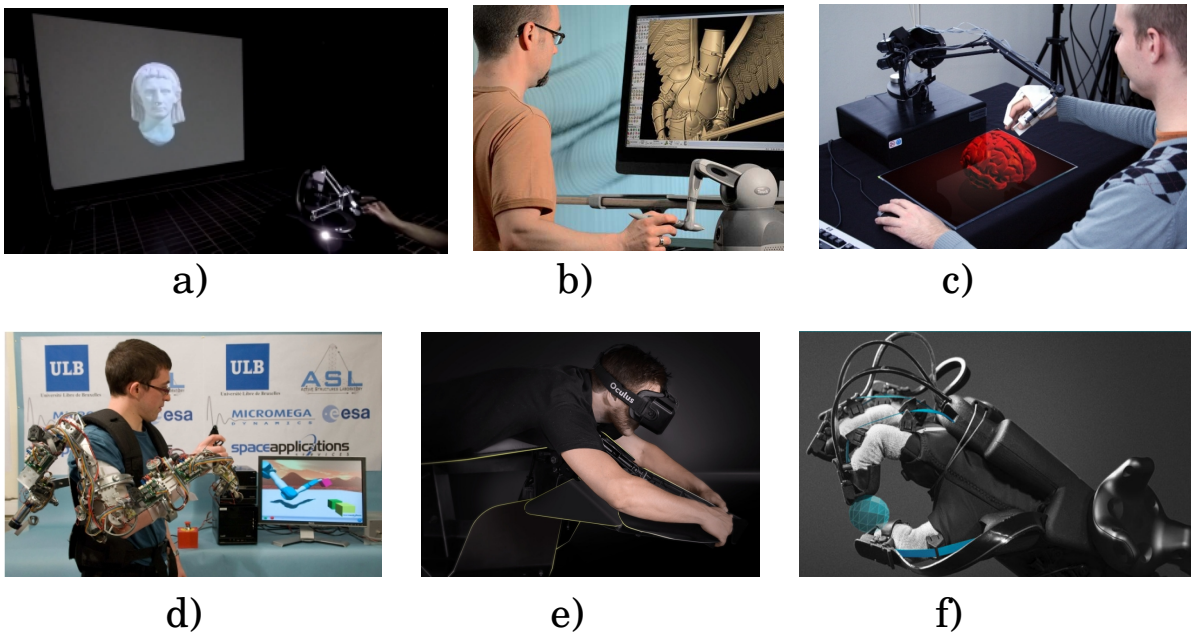

FIGURE 2.10. Haptic applications: a) Augmented reality with haptic[10], b) Geomagic Sculpt ^{TM} [11], c) Simulated haptic telerobotics brain surgery[12], d) Haptic exoskeleton for training [193], e) Haptics for gaming: Hypersuit ^{TM} [13]and f) Haptics for virtual reality interaction: Haptx ^{TM} gloves[14].

Nowadays, shared control in haptics is a growing topic. The highlights on this field rely on the user guidance or assistance by the haptic device to perform tasks. The aim is to improve the user performance and enhance the outcome of the task [194]. A complete study about haptic performance and measurements such as DoF, device-body interface, motion range, peak force and acceleration, energy flux, inertia and damping among other features, can be found in [152]. Haptic technology is also applied to wearable haptics as the exoskeleton of 7 DoF presented in [195], which interacts with a virtual environment. In [150], an exoskeleton haptic interface is presented to train subjects in virtual environments for specific tasks. A similar study conducted by Letier in [193], presents an articulated arm exoskeleton with configurable scenarios in the remote environment.

Haptic rendering is an extensive area of applications. A deeper discussion on this topic is

[11]Percorsi Didattici Interattivi, Multisensoriali e Multiutenti Attraverso Tecnologie di Virtual Reality: il Museo Archeologico Nazionale delle Marche: *https://www.archeomatica.it/musei/nuove-installazioni-di-realta-virtuale-per-il-museo-archeologico-nazionale-delle-marche*

[12]Geomagic Sculpt software with the Phantom haptic from 3D Systems and OR3D: *https://www.or3d.co.uk/wp-content/uploads/2017/10/Geomagic-Haptic-Devices-2016-Brochure-by-OR3D.pdf*

[13]Center for Image Analysis, Swedish University of Agricultural Sciences, Uppsala University: *http://www.cb.uu.se/research/whh/index.html*

[14]Hypersuit ^{TM} system: *https://www.hypersuit.fr/*

[15]Haptx ^{TM} device: *https://haptx.com/*

provided in Section 2.2.2. Examples of haptic rendering can be found in [196] and [197]. For haptic rendering applications, modelling friction represents an important task to perform a realistic manipulation of the environment. A friction model implementation for impedance and admittance haptic types is presented in [198]. A complete study on haptic rendering with time delays and Coulomb friction model is shown in [199].

2.2.2 Haptic Rendering

In the work of Colgate *et al.* [113], the issues with regards to interaction behaviours such as collision, sliding, penetration and cutting are discussed. Such behaviours point to haptics rendering, the process to compute generated forces of two separated elements (a master device and a robot in the remote location) as the result of the user interaction with an environment. To achieve these sensations on the device, it is necessary to render the forces and positions based on a spring-damper model where the stiffest sensation is represented as a *wall*. After rendering the model, it is possible to have touching sensations for free-space moving, contact transients, persistence and impedance force, surface friction, curvature and texture feeling [200, 201].

In the early days of haptics, these technologies allowed the user to interact with virtual environments and graphical scenarios with simulated objects. Those objects were able to be palpated with haptic devices using geometrical models, collision techniques and cost-effective processes. The result was a sophisticated sensation of object displayed behaviour. Haptic-rendering algorithms are the appropriate interaction forces generated between the haptic device and all the elements presented in the virtual environment [200].

As shown in Fig. 2.11 [201], the first block of the scheme consists of the physics engine. This engine contains the collision detector, the force response and the control algorithms. When the positions x_{haptic} of the haptic device overlap a contact S in the collision detector, the force response block generates the desired forces f_d according to the contact. These forces could be modelled as a typical spring-mass element as discussed in Section 2.1.1. In [202] an effective realistic render of three basic elements is compared: a spring, a damper and a spring-damper. A control algorithm will display the rendered force f_r in the haptic device. The simulation engine block establishes the limits of free space and the position of the objects, in order to have a map of the interactive virtual environment. Once the interaction is performed the simulation engine repositions the virtual objects according to the information provided by the collision detector and the force response block. Lastly, a graphics engine unit will generate the visual interface to be displayed on a monitor from the information provided by the simulation engine.

An example of haptic rendering is *The Penn Haptic Texture Tool Kit* by Cultbertson [203], it is a collection of a hundred haptic textures and friction models that display rendered realistic sensations. In [204], a set of haptic textures are rendered through rapid variations of viscous-damping, to achieve accurate dynamics of the displayed forces in the haptic device. Yim [205], presents a rendering model of frictional sliding contact designed for medical training, similar to

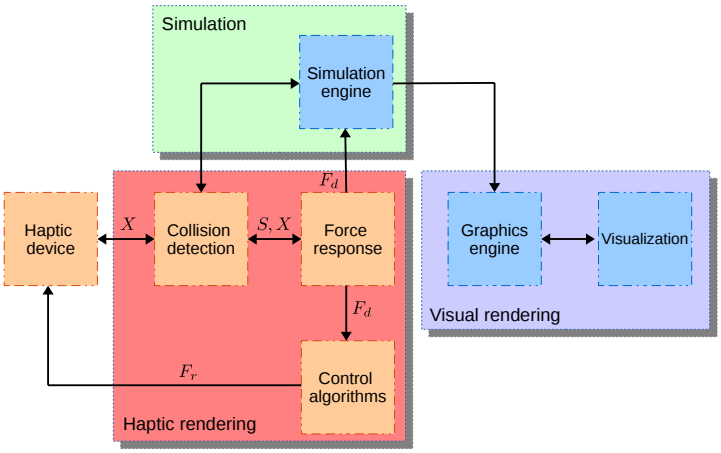

FIGURE 2.11. Block diagram of the haptic rendering algorithm.

[206]. A rendering approach capable of capturing and displaying visco-elastic material effects is presented in [207].

With regards to 3D reconstruction, an algorithm of geometry-based haptic texture modelling and rendering to provide higher texture resolution is described [208]. For medical robotics, a model for respiratory studies of patients in motion is presented in [209]. Here, techniques of computed tomography images and direct visuo-haptic 4D volume rendering are combined. This method reaches a frame rate of 2 kHz on the haptic rendering. To explore ultrasonic images with a haptic device, a model of friction is developed for fingertip rendered dynamics in [210].

In the work of Klingbeil [211], a human-robot interaction is performed with a 6 DoF robot, the task consists of placing a box and different shaped rendered objects on their corresponding hole in a virtual environment. A similar approach is presented in [212]. In this project [213], a 6 DoF haptic simulation renders sharp geometric contact objects, and the forces generated create the sensation of sharp objects in multi-region contact scenarios. Another haptic render experiment is shown in [214], where an algorithm to display feedback from volumetric datasets is proposed as an aid to regular visualization. Susa *et. al* [215] presents a haptic rendering algorithm based on finite element simulation of vibration to study different materials. A haptic rendering method for depth penetration is presented by Li in [216], in this work a 3 DoF end-effector interacts with an optimized environment that performs an approximation method of depth penetration among rigid objects.

A challenge in haptics is to generate realistic haptic textures. In [217], a method using random fractal surface to texturize irregular surfaces is presented. The project *HapticDrone* was developed to create kinaesthetic information about the stiffness and weight of an object, displaying the information in the drone, acting as a haptic device [218]. Haptic rendering with virtual reality objects is shown in [118]. Finally in [219], a realistic model of interactive clay for

pottery is presented. The deformation algorithm maintains the volume of clay to provide a study model about the incompressible nature of semi-solid clay.

As presented in this thesis, the robust interactive behaviour, rendering process and categorization of the haptic devices are related with real time, passivity and transparency issues. For bilateral manipulation purposes the keystone is stability. As presented by Ferrel in [4] when teleoperation is performed at long or short distances a time delay will invade the system, creating an unstable behaviour to the user sensation. Finally, according to Franken *et al.* [35], in addition to time delays there are causes such as a relaxed grasp of the user, stiff position, force control settings, and hard contacts in the remote environment that affects stability in the devices.

2.2.3 Haptic Interfaces Types

As described before, a haptic interface must provide the most realistic force display to the user about the environment where the interaction is happening. Force rendering algorithms come together with visual feedback as depicted in Fig. 2.11, and it is possible to include auditory feedback. The force rendering capabilities of the haptic interface depend on the device type. There are two principal types of haptic devices: a) *admittance type* and b) *impedance type*. Their differences are related to the motion of the device, the manner that the user grasps the device and how it is mechanically coupled [220]. Another type of device (not the admittance or impedance type), permits to the user to move freely without force feedback, having as response thermal feedback, vibration or sound [138]. A two-port network [121] is the simple way to couple admittance and impedance types to the environment (virtual or real) as described in Section 2.1.1.

A) Admittance Type

The admittance type haptic device measures the force exerted by the user on the grasp and measures the resulting amount of motion. The resulting force of this type is:

$$v_h = Y_e F_u, \tag{2.9}$$

where v_h is the velocity of the haptic, Y_e is the admittance of the environment and F_u is the input force from the user. In free motion, the system produces almost no inertia and low friction. The user experiences an admittance that may be deviated from the target (in the remote environment), due to the non-ideal force sensors and velocity output. The admittance type presents problems of displaying high stiffness environments [138].

In Adams [221], the control law for the admittance type generates displacements in response of measured forces:

$$F_d(z) = K_d(z)(v_d(z) - v_{com}(z)), \tag{2.10}$$

where F_d stands for the desired force to be displayed in the device, K_d is the controller gain, and v_d and v_{com} the desired and commanded velocities respectively (the desired velocity is the targeted velocity, and the commanded velocity is the current velocity). A coupling implementation that guarantees a stable system could be provided by the two-port architecture. In contrast to impedance type, an admittance type is an alternative configuration to avoid impractical implementations due to the presence of high levels of inertia [222].

B) Impedance Type

A second type of haptics interface is the impedance type. This interface measures the motion exerted by the user on the grasp and alters the amount of the resulting force. The force equation for this type follows:

$$F_r = Z_e v_h, \tag{2.11}$$

in this case, F_r represents the force rendered in the haptic device, Z_e is the impedance of the remote location and v_h the velocity of the user (human). Impedance type devices present better performance on haptic free-space motion, are safer to use around users and more widespread commercially [138].

According to Adams [222], impedance type is the most common implementation for haptic devices. It is composed by optical encoders or potentiometers to measure the positions at the points of actuation. The impedance type presents as a disadvantage a lack of impedance compensation in open-loop configuration. This displays the sensation of inertia and friction from the manipulator when the user moves on free-space. Impedance type implementation is desirable when the robot manipulating the remote location presents low friction and inertia.

C) Haptic Device: Omega^{TM} 6

The Omega 6 is a haptic interface, this device represents the master side on the telemanipulation chain, it consists of a structure of 6 DoF on a delta configuration. It has 3 DoF for translations, which are actuated, and 3 DoF for rotations, which are not actuated.

This impedance type haptic interface measures the positions of the end effector grasped by the human operator as an input, and renders forces on the end effector as an output. The haptic control loop operates at 1 kHz. This haptic interface is depicted in Fig. 2.9 (Master side: Operator). The device is 6 DoF impedance type delta configuration robot, it can provide until 12 N in the translation with resolution < 0.01 mm. The maximum stiffness displayed in closed-loop is 14.5 N/mm. It is gravity compensated and reduces user's fatigue, it includes as safety features velocity monitoring and electromagnetic damping.

This device provides kinesthetic and frictional force feedback, also is capable to produce vibrations among $25-200$ Hz [223]. The dynamic characteristics and kinematics of a delta parallel robot are presented in [224].

The experimental set up described in Sections 4.1.1 and 4.2.1 uses a haptic device by Force Dimension called Omega 6[16]. Other experimental implementations with the Omega 6 can be seen in [41, 42, 69, 70, 179, 194, 225–228].

2.2.4 Haptic Devices and Remote Locations

As defined before, when the haptic device is interacting with a remote location (virtual or real), the rendering algorithm output depends of the environment model. A typical rendering method was described in Section 2.2.2 using a collision detector to detect where the positions of the virtual end-effector commanded by the haptic device overlap, and then, generate the desired forces to be displayed at the haptic interface. In a real environment, a set of sensors attached to the manipulator in the slave side of the teleoperated system could provide information to model the environment where it is interacting.

In Section 2.2.4, a method to render a model of the environment using position feedback is discussed which is mainly used as an input for a collision detector. In Section 2.2.4, a force feedback model for real environments is presented.

A) Virtual Environments: Position Feedback

As mentioned by Kuchenbecker in [138], the geometry of the objects in a virtual environment can be characterized by a mathematical function or the location of the points. When the haptic operator uses a device, its encoders measure the positions of the links, this information could be set in a single position vector mapped by the computer as a virtual end-effector. In Fig. 2.12 the model of a virtual environment is depicted. The green sphere represents the end-effector of a manipulator, while the blue rectangular cuboid is an interactive object.

To execute the interaction between the haptic device and the virtual environment, a computer software must run the collision detection algorithm; in practice, the collision detection algorithm measures the distances of the virtual end-effector and the interactive object by computing the information of its boundaries or limits. Let us define the virtual end-effector as a point on a Cartesian coordinate system P_r with coordinates (x,y,z); and the interactive object with a position in the origin O_v with coordinates (x,y,z), with a geometry dimension of $\sqrt{\|\vec{s_1}\|^2+\|\vec{s_2}\|^2+\|\vec{s_1}\|^2}$, where s_i represents the vectors of the center of the cuboid to the different planes, and width w_v length l_v and height h_v. A simple model of the collision detection is defined in equation (2.12), it states that the center of the virtual end-effector P_r overlaps the limits of the cuboid a contact is done.

[16] Haptic device Omega 6 ^{TM} by Force Dimension specifications: *http://www.forcedimension.com/downloads/specs/specsheet-omega.6.pdf*

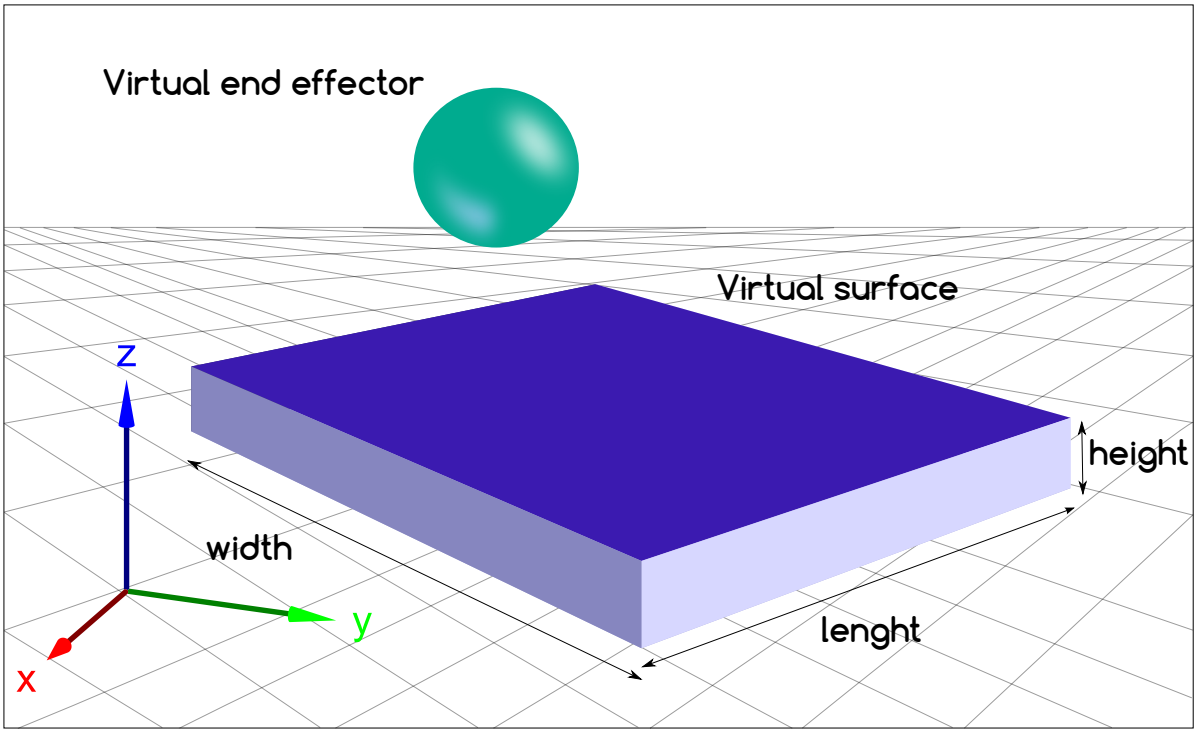

FIGURE 2.12. Interactive virtual environment.

$$P_r(x,y,z) \geq \sqrt{\|\vec{s_1}\|^2 + \|\vec{s_2}\|^2 + \|\vec{s_1}\|^2}. \tag{2.12}$$

B) Real Environments: Force Feedback

The forces coming from the environment must be captured by a sensing device. In Fig. 2.13 a 6 DoF force sensor is mounted in the robotic manipulator, all the forces monitored by the sensor are sent to the computer to be replicated by the haptic device. Ideally, the haptic rendering of those forces must be as much transparent as if the user would be interacting the environment on site. In Section 2.3.1 will be defined the concept of transparency for bilateral telemanipulation; in addition, in Section 2.3.2 will be discussed the technique used in this work to provide stability to a telemanipulation chain.

2.3 Transparency and Passivity

In haptic-enabled teleoperation, the primary concern is to provide a *stable* and *transparent* operation of the system. It is well known that haptic feedback can lead to unstable and therefore unsafe behaviour of the overall system due to factors such as communication latency in the loop,

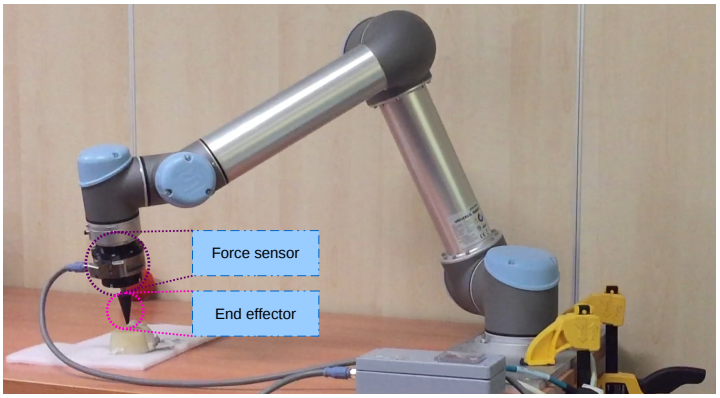

FIGURE 2.13. Interactive real environment.

hard contacts, and relaxed user grasps, as discussed in Section 2.3.1. Such behaviour must be avoided, especially in fields where safety is a paramount and non-negotiable requirement (e.g., medical robotics) [229].

To this purpose, a great variety of control design approaches have been proposed. In this context, passivity theory [230] has been recognized as an effective tool for achieving stable interaction. Hannaford and Ryu in [8, 122] have analysed passivity in the time domain in terms of energy levels of system components. To Niemeyer [231], the problem of making a delayed communication channel passive is addressed. Energy-bounding algorithms to guarantee passivity of the teleoperation loop have been proposed in [33, 232, 233]. Along the same line, in Franken *et al.* [35], a two-layer control scheme is proposed, in which a transparency layer computes the ideal forces to be actuated at both the master and slave sides. While a passivity layer modulates such forces when necessary to avoid violations of the passivity condition, thus guaranteeing stability at the price of a temporary loss of transparency.

2.3.1 A Definition of Transparency

The main goal on applied-haptics with force-feedback is to achieve transparency when the task is performed [234]. Technological limitations as low position and force frequency responses create a poor capability to execute accurate forces on a haptic device. These constraints limit the performance of the devices generating a drawback to achieve transparency in the telemanipulation chain. Filtering out the impedances from the real environment causes a negative rendering in the transparency property [235].

An accurate definition of transparency is given by Secchi *et al*. [236] as the matching of the impedances between the user and the environment, when the user perceives the correspondent forces and positions in time. The experience of manipulating the environment directly as shown in the next equation is given from the forces at the slave side $\tau_s(t)$ to the master side $\tau_m(t)$ and

the velocities as well $\dot{q}_s(t)$ and $\dot{q}_m(t)$ respectively [7].

$$\text{transparency} \begin{cases} \tau_m(t) = \tau_s(t) \\ \dot{q}_m(t) = \dot{q}_s(t). \end{cases} \tag{2.13}$$

Likewise, as mentioned in [7], a reliable transparent system should ensure the condition in the presence of time delay:

$$\text{transparency} \begin{cases} \tau_m(t) = \tau_s(t+T) \\ \dot{q}_m(t) = \dot{q}_s(t+T). \end{cases} \tag{2.14}$$

Fig. 2.14 depicts the scheme of transparency on a telemanipulation system, how the forces and velocities are altered as described in equation (2.13) and (2.14).

A) Transparency Limitations

Pacchierotti [69], presented a novel idea to improve transparency, the method consists of providing the operator a controlled kinesthetic feedback when the interaction with the remote environment is performed. Research developed on transparency can be found in [41, 42, 237, 238].

In Franken *et. al* [35] is mentioned the destabilizing factors that affect the telemanipulation chain are:

- relaxed grasp of the user,
- stiff position and force control set up,
- hard contacts in the remote location,
- time delays in the communication channel.

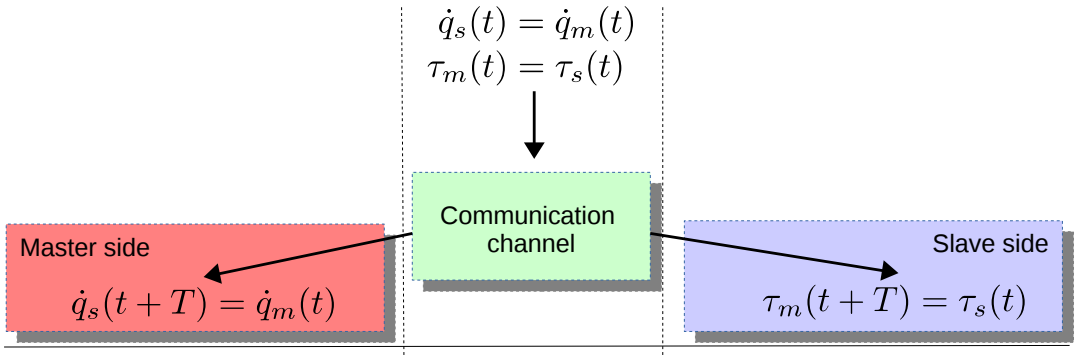

FIGURE 2.14. Block diagram of transparency in the telemanipulation chain.

To understand the problem related to the relaxed grasp of the user, it is important to consider that instabilities occur with low frequencies of the human operator movements. Since the user exerts to the system an impedance force, containing stiffness, damping and mass, the impedance can change with the user's grip; exerting low stiffness and high damping [199]. Hulin [239] presented a stability analysis of the impact/influence of the user as a physical damper when grasping the haptic device. Also, Gersem [240] describes the impact of friction on a bilateral telemanipulation system for soft tissue applications and how it alters haptic transparency for the user's perception.

Rendering hard contacts is one of the most complicated areas on haptics, due to this kind of performance it typically requires a display of high frequencies on the device. The sensation of hard contact is quantified by analysing the high frequency information of acceleration. If the user relies on low frequencies as force feedback, visual or auditive signals as feedback, the sensitivity perceived will reduce during long tasks. This is commonly problematic since the system is closed-loop position/velocity feedback [138].

Regards the problems of stiff position and force control set up, classical controllers can not guarantee passivity (and so, stability) because of extra energy generation by the changing stiffness [241]. A number of authors consider stability problems appear with the display of simple virtual environments. It is a critical balance on frequency rate, stiffness gain, damping-viscosity and the user's performance which are the most notable parameters that affect stability on the telemanipulation chain. The most common strategy for this issue is placing a spring-damper architecture to the haptic rendering, but in a closed-loop system stability is hardly limited [138].

For time delays in the communication channel, the problem is related to the information exchange done from the master side to the slave side and vice versa [39, 242]. The time delay can be induced, created, generated or imposed on the system due to physical characteristics of the communication medium and/or deficiencies of the processing unit on each side.

Despite all the odds, there are solutions to improve haptic transparency to be displayed to the user. Some literature regards transparency improvement can be consulted in [243, 244]. One of these solutions is found on the passivity control theory, which aims to reach stability into the system through the energy balance along the telemanipulation chain.

2.3.2 Passivity Control

Initially, there was not an accurate distinction among the haptic device and the remote environment, in fact, the remote environment represented the control law in the system. The major drawbacks were to guarantee a stabilizing control law for the haptic from a complex dynamic virtual environment, leading into a highly difficult parametrizable system to be tuned for a specific device. The first virtual coupling between the master and the slave side was proposed by Colgate [245]. As mentioned in [222] by Adams, these must be designed for devices with structural flexibility, force sensing, sensors and actuators, and measurement of delay capabilities.

Recalling, haptic devices provides a physical interaction for humans with virtual and real environments through a mechanical system. When the user receives a force feedback signal as a response of the system it is called kinaesthetic information or the sense of touching. Bilateral telemanipulation occurs when the user perceives the information in real time from the slave at the moment to interact with the environment [35]. Reaching the transparency on the contact information, the user could improve the performance of a certain task [6]. The operation of this tasks requires the exchange of virtual energy from the discrete time controller and the physical world, this energy is the result of the forces applied/extracted to the system along the changes on the distance. To avoid virtual energy on the system that could derive in an undesired behaviour of the telemanipulation chain when interacting inside the environment, a methodology with passivity control theory is proposed [7] to preserve the stability and transparency on the system.

Lee *et al.* [34] proposed an approach built around a spring-damper controller, where the energy dissipated by a virtual damper is stored in an energy tank and jumps in spring potential are limited to the available energy in the tank. Colonnese and Okamura [174] introduced the "M-Width" concept, the dynamic range of virtual mass which is able to render in a stable manner. Its definition is inspired by the Z-Width, but it considers BIBO (bounded input, bounded output) stability, it models the human operator as an impedance and not a generic passive element, and the target virtual environment is modelled as a pure mass with motion data filtering. Moreover, the solutions in passivity control rely on algorithms that guarantee passivity over the system through the scattering variables [6] in order to exchange fractions of energy between the elements of the telemanipulation chain.

More recently, in [39] the authors introduced a passivity-based interactive control architecture based on the port-Hamiltonian framework. Most of the cited time-domain approaches employ the concept of energy tanks to enable the use of the (virtual) energy circulating in the controlled system in a flexible and passivity-preserving way.

A simple approach of passivity concept is described by Niknejad [246], where is stated that the passive systems can only store and consume energy, contrary to the active systems which can provide and consume energy. Another condition of passiveness in the system is the lack of gain; in real environments, the amount of energy entered into the passive system is lower than the amount received at the output. As cited in passivity control works [8, 34, 233, 247], it is assumed an initial energy storage condition of $H_T(t)$ equals zero for $t = 0$. Therefore, the values of the forces (f) and velocities ($\dot{q}$) supplied in a passive system must be greater or equal than zero in all moment:

$$\int_0^{\tau} f(\tau)\dot{q}(\tau)d\tau \geq 0, \quad \forall t \geq 0\,. \tag{2.15}$$

In the work of Miller *et al.* [248], it is presented an extended analysis of stability about the energy physical dissipation of the haptic device, in order to achieve passivity on the system. Several studies have been conducted to guarantee stability in a telemanipulation system as adaptive

control [136], adaptive motion/force control [31], the use of *observers* for teleimpedance [249], hybrid parameters on the network [250], scattering operators [6], and series-Shunt approach [251].

In Hannaford [122], two implementations of passivity controllers are presented: a) series (velocity conserving) and b) parallel (force conserving). Some problems are derived from the passivity implementation. As an example, in the case of the series controller, the forces required to dissipate the generated energy may exceed the actuator limits. When the velocity is particularly small, a problem of computation could appear as noise. Due to this, it is important to limit the magnitude of the velocity or force generated by the controller. Thus, the controller may not be able to dissipate all of the energy supplied by a sub-network in one sample time. The excess energy must be stored in the system for the next sample time.

For Ryu *et al.* [8], the interplay between transparency and stability has been an important topic. On his work, it is stated that a bilateral telemanipulation system presents non linear characteristics and the dynamic properties of a human operator are always involved. Summed into this, obtaining the model of a teleoperator system is complicated when it has a high number of DoFs, and not all the parameters of the system could be captured. A solution to this problem is presented in the theory of passivity control. Similar as the one presented by Hogan [161], an stability analysis requires an accurate model of the remote location and the manipulator. To guarantee stability, a key point of the analysis establishes that the environment must be passive. On his definition of passivity, the system will not output more energy at its port of interaction rather than the energy that has been in at the same port in all time periods. According to Shull [252], force reflecting control on bilateral telemanipulation systems is useful when using a large manipulator. One problem on passivity based architectures is the friction and inertia present in the slave robot, since those forces are passed along the user providing information with noise from the environment. To prevent such effect, a force sensor can be placed at the manipulator's end-effector, hence, the user will be informed with force feedback signals and not with inertia and friction from the environment.

A deep study on passivity for time-variant delayed teleoperation systems is presented by Xu [253], on his work it is proposed an energy prediction scheme as a way to maintain a conservative behaviour to the controller when performing bilateral telemanipulation. The study aims to improve transparency and teleoperation quality, it uses the time domain passivity approach (TDPA) which it has also been proved as a stabilizing algorithm for teleoperation. An implementation of the passivity control strategy is presented in [254] where they controlled a group of unnamed aerial vehicles (UAVs). Another implementation to preserve stability with haptic devices and virtual environments using passivity control theory is depicted in [121]. More literature related to the passivity control topic could be checked in [255**?** –261].

To deal with destabilizing factors in the telemanipulation chain, a solution is proposed by Franken *et al.* in [35]. The solution is called the Two-Layer approach, and it provides a method

based on passivity control to achieve stability but with the loss of transparency.

2.3.3 Two-Layer Approach

One of the main goals of haptic systems is to convey realistic forces (transparency) to the user. In bilateral telemanipulation control, factors such as relaxed grasp of the user, time delays and stiff environments may compromise the stability of the system as seen in Fig. 2.15. Ensuring passivity in the system, *i.e.* does not generate energy by itself, it can prevent unstable behaviours. The two-layer approach is a solution proposed by Franken [35], where two energy tanks are introduced in order to control the energy flow between the master and the slave. Also, the two-layer approach is a framework which divides the system in a transparency layer and a passivity layer; this framework provides the flexibility to implement different controllers in the transparency layer being independent of the passivity layer.

Bilateral manipulation can be represented as a closed-loop circuit between a human operator (master interface) and a robot manipulator (slave interface) [20]. This remote operation creates a control problem to solve since the stability of a fully transparent system is affected by destabilizing factors such as time delays, stiff environments, or a soft grasp of the user on the master device as defined previously in Section 2.3.1. Transparency is defined as the full display of the environment impedance to the human operator when this interacts with the robot [262]. As described in [7] by Franken, the transparency of the haptic device acts as an ideal system when the forces (τ_s)

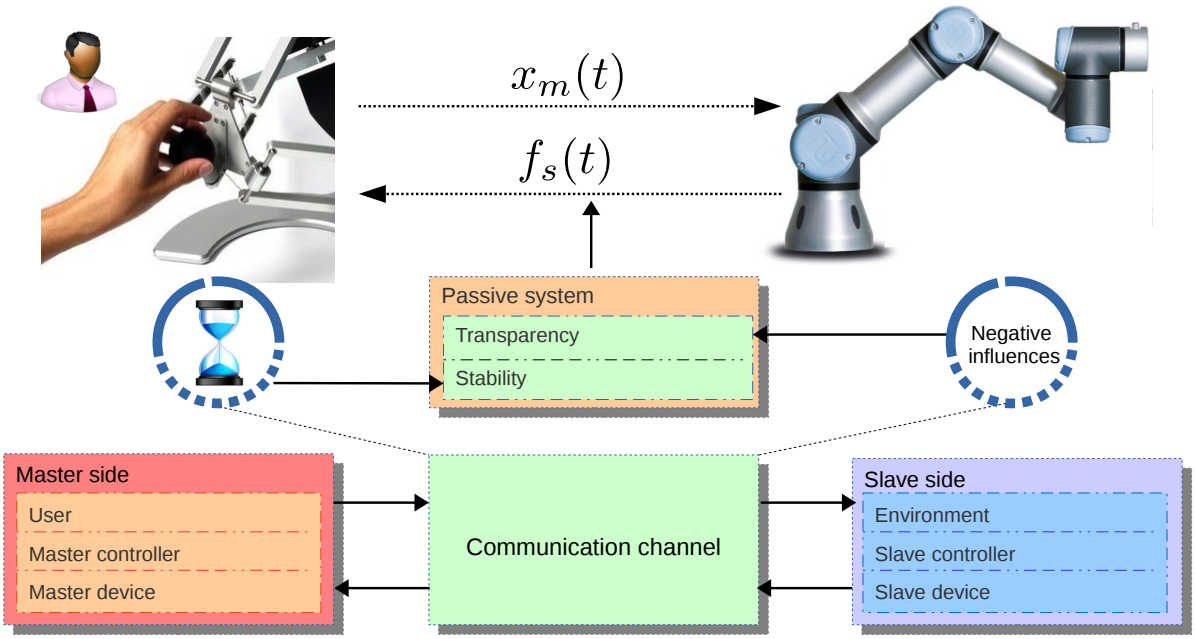

FIGURE 2.15. Block diagram of the problem formulation of a bilateral telemanipulation system.

and velocities ($\dot{q}_s$) of the slave side are equally reflected on the master side ($\tau_m, \dot{q}_m$) as shown in (2.13) in Section 2.3.1.

A major factor that destabilizes a telemanipulation chain is time delay. In the work of Kim [115], is presented the analysis of operating telemanipulators with time delays, and as a part of its results, it is mention that force reflection control can not be performed at time delays above 0.5 to 1 s. Also on this topic, Velanas *et al.* [263] presented an effective way of alleviating the consequences of time-delays, in this work they proposed the use of an adaptive impedance reflection teleoperation scheme, reconstructing a local model of the slave's impedance at the master side. In the work of Li [264], is shown a mode-based approach which uses a passivity observer that modifies the slave force feedback inside a virtual environment, this technique increases the stability of the system when time delays appear. Various studies based on passivity control have been developed to provide a solution to such a problem [6, 8, 42, 174]. Passive systems are capable to store and consume energy, in contrast with active systems that can provide energy [246].

As shown in Fig. 2.16, the transparency layer exchanges the information of positions and forces between the master and the slave side. In the passivity layer, the energy is balanced according to the algorithm described in Section 3.2. As defined by Franken [35], there is a reason about why the two layers must be separated. This is an optimization strategy in order to ensure optimal transparency, where the techniques used in the transparency layer do not affect the desired passivity layer and the other way around. The separation makes the layers non dependent one from the other, permitting to apply a great range of control techniques. Besides, the separation between layers is reflected in the communication channel; there are two ports, one to exchange energy information among sides and the second to transmit information related to the desired display information (forces). An application of the approach can be found in [179].

A full study on teleoperation control algorithms is presented by Muradore in [27], on his work the control models for non communication delay strategies and communication delay strategies are divided. The study covers the approaches on: a) wave variables and scattering transformation, b) PD and passivity terms, c) adaptive algorithm, d) Time Domain Passivity Approach (TDPA), e)

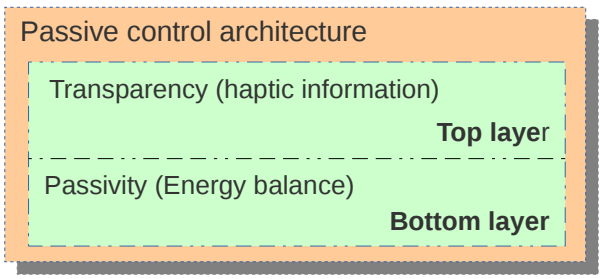

FIGURE 2.16. Block diagram of the Two-layer approach.

Passive Set-Position Modulation (PSPM) and f) two-layer approach. The two-layer approach is related to four main works on passivity control.

First, *Scattering / Wave-Variable-Based Approach* presented by Anderson in [6]. In this work, the concept of wave variables is introduced as described in Section 1.1.2, one of the negative aspects is the generation of "virtual energy" in when time delays are present in the communication channel. For Niemeyer [231], the importance of the wave variables relies in the system stability when using passivity control in time-delayed systems (see Fig. 2.17-a). The wave variables are depicted as "move/push" commands that contain information related to energy exchange in both sides of the telemanipulation chain. But some problems occurs when the user sends the information to the robot, the force feedback returning from the robot is not transparent due to the nonidealities of the system, like time-varying delayed and package loss; this situation is performed when coding or decoding information at the communication channel.

Second, *Time Domain Passivity Control (TDPC)* introduced by Ryu *et al.* in [8]. This algorithm discards the communication channel as seen in Fig. 2.17-b. The method consists of two elements in the telemanipulation chain, a Passivity Observer (PO) and a Passivity Controller (PC); these elements perform simultaneous exchange information between sides on the form of incoming (E_{in}) and outgoing (E_{out}) energy flows, this implementation is robust facing time delays. The method presents a problem regarding impedance reflection forces; since those are predicted locally according to the model of the virtual environment, also the system is designed to guarantee stability and not improve transparency. Hannaford and Ryu proposed a Time Domain Passivity Control (TDPC) [142]. This approach does not require the power variables to be transformed into wave variables. Instead, a straight-forward notion of energy is used to define passivity of the system. An implementation of TDPC of 1 DoF robot can be seen in [264].

Third, *Energy Bounding Algorithm (EBA)* proposed by Kim in [33] and shown in Fig. 2.17-c. The EBA is a strategy that limits the virtual energy generated on the system by dissipation. This dissipation occurs as a viscous friction at the master and slave robots. The problem with the dissipated friction is the decomposition of transparency, because the dissipation is also transferred to the user's arm. With this methodology the stability of the system is jeopardize, it is necessary to select a conservative bound limit on the friction parameter.

Lastly, *Passive Set-Position Modulation (PSPM)* introduced by Lee in [34] and depicted in Fig. 2.17-d. The PSPM strategy is the closest methodology to the two-layer approach because it involves a spring-damper controller, where the energy dissipated by a virtual damper is stored into an energy tank. Comparing the system with a spring model, the algorithm measures the jump of the position and translates into energy terms depending on the jump direction; the control algorithm is limited to the available energy on the tank, a positive jump will subtract energy from the tank, and a negative jump will add energy to the tank. Any excess of energy will be dissipated or transmitted to the other side of the chain. Despite the algorithm preserves passivity, it presents many complications through the operation. For example, the samples of

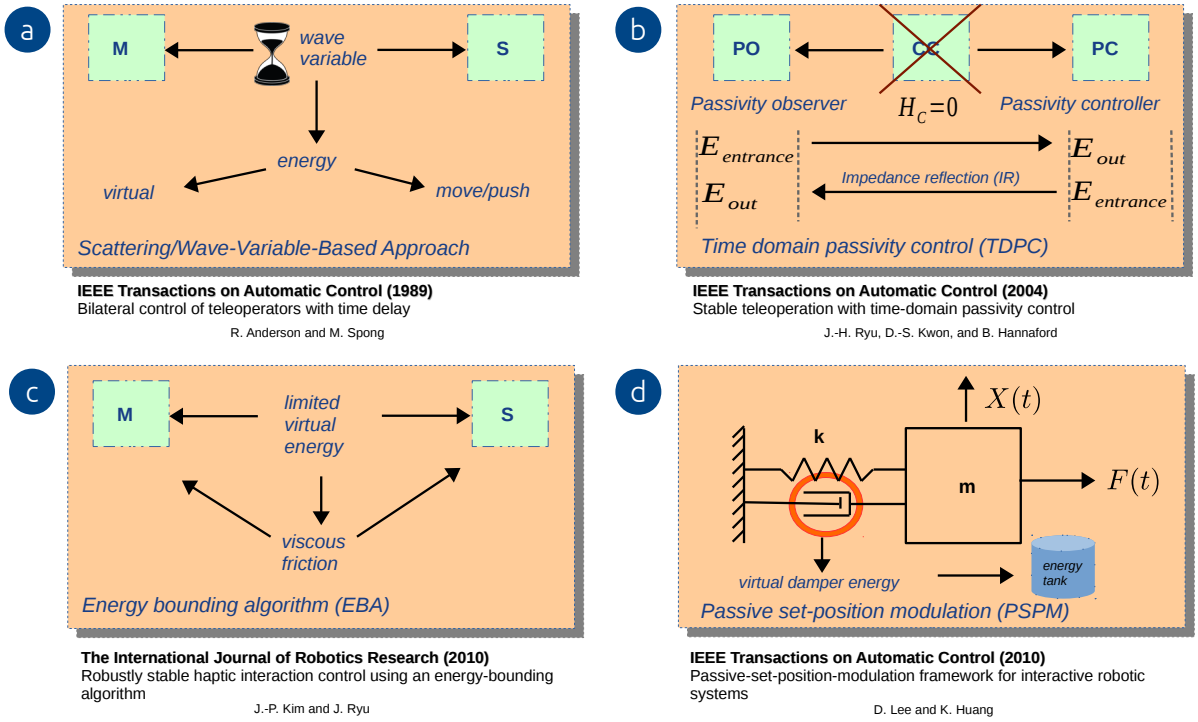

FIGURE 2.17. Block diagram of different passivity methods: *a) Scattering / Wave-Variable-Based Approach* [6], *Time domain passivity control (TDPC)* [8], *c) Energy bounding algorithm (EBA)* [33], and *d) Passive set-position modulation (PSPM)* [34].

the positions are processed as discrete signal, but the computation is considered as a continuous signal system which can create energy on a discrete medium affecting the servo control loop. Also the system is quite sensitive to noise, it uses set position translations to be processed as desired forces and displayed at the device, in this process the estimation of velocity generates the noise because of low sample rate. At the end of the complications is the constant use of damping to extract energy from the user, this situation provokes that despite there is energy on the tanks, the system remains damped all time.

CHAPTER 3

TRANSPARENCY-OPTIMAL PASSIVITY LAYER DESIGN

As described in the previous chapter, in passivity control theory, there is a solution to stabilize the system when it is altered by negative influences. In this chapter, an optimal transparency passivity layer is introduced with the aim of increase transparency. To preserve passivity, a 3 DoF two-layer approach based on energy tanks is implemented. The energy provided to the slave side is limited by the energy obtained from the user at the master side. This energy is generated by a damping-like element that is activated when destabilizing factors occur. This chapter presents a contribution as described in Section 1.4, a strategy to prioritize damping coefficients to achieve higher transparency along a number of desired directions. The method consists of solving a quadratic optimization problem that minimizes the projection of the damping forces on different directions while maintaining passivity, the name of the method is Transparency-optimal Passivity Layer (TOPL).

3.1 TOPL: Introduction

This work builds upon the two-layer architecture proposed in [35]. In that paper, the design of the passivity layer does not explicitly account for the amount of transparency that is lost due to the stabilizing effect. This issue has a fundamental importance specially in complex teleoperation tasks that involve multiple DoF. In bilateral telemanipulation control, factors such as relaxed grasp of the user, time delays and stiff environments may compromise the stability of the system. Indeed, for a particular configuration of a given task, it may be important to conserve transparency in terms of fidelity of the rendered force along some subset of the task space, while other components may be significantly altered in order to preserve passivity without compromising the overall task performance. One of the main goals of haptic systems

is to convey realistic forces (transparency) to the user. Ensuring passivity in the system, i.e. not generating energy by itself, can prevent unstable behaviour. To preserve passivity, a 3 DoF two-layer approach based on energy tanks is implemented. The energy provided to the slave side is limited by the energy obtained from the user at the master side. This energy is generated by a damping-like element that is activated when destabilizing factors occur. The aim of this work is to present an optimization-based design of the passivity layer which guarantees the maximum possible degree of transparency along subsets of the environment space that are preponderant for the given task at a given time, while preserving the energy bounds that are required to guarantee passivity. The optimal rendered force is computed via the solution of a convex quadratic program which is characterized by modest computational complexity and amenable to implementation in real time.

In this chapter an architecture of 3 DoF as a passivity control solution for bilateral telemanipulation is presented . Primarily, the transparency layer process the information of the master and slave side (haptic interface) as a set of forces and positions. A communication channel manages the flow of information that is exchanged in both sides. In addition, the passive layer of the extension is based on the use of an energy tank in the master side. Specifically, the energy tank approach maintains passivity along the system to prevent an incorrect behaviour of the devices. The passive layer has an algorithm that prioritize the damping coefficients on each degree of freedom at the master's side. Therefore, this prioritization is determined to generate a better transparency to the user. To achieve the minimal damping factor for each DoF, a quadratic programming algorithm is used. The work proposed by [35] presents a mechanical model developed in 1 DoF. Another solution for stiff environments presented in [49], shows a 1 DoF system with a control model using flexible spring-damper contacts. In contrast, the solution presented in this work is developed in 3 DoF, using a single energy tank for the master side.

3.2 Two-layer Approach: 1 DoF Implementation

The two-layer approach consists in the division of a methodology to split the impedance control system in two parts: *a) the transparency layer to compute forces* and *b) the passivity layer to compute energy balance*. To define the functionality of the two-layer approach it is necessary to cover concepts of energy transfer in the passivity layer presented by Franken in [267, 268]; in that work is described the operation of an energy monitor. This element comes from the method shown in the TDPC approach previously discussed in Sec. 2.3.3, where a modulated damper is introduced at the master side to preserve passivity in the system. To compute the energy flow from the mechanical system to the impedance controller, an element of energy exchange is:

$$\Delta H(k) = \tau_r(\overline{k})\Delta q_a(k). \tag{3.1}$$

in Eq. (3.1), $\Delta H(k)$ represents the energy exchange in a sample period k, $\tau_r(\overline{k})$ indicates the force displayed by the motors, and $\Delta q_a(k)$ is the difference between positions.

Also in [267], it is stated that to guarantee passivity in the system, an energy balance H must be applied between the master $\Delta H_m(k)$ and the slave $\Delta H_s(k)$ as in:

$$H = \sum_{k=1}^{n} \Delta H_m(k) + \Delta H_s(k) \geq 0. \tag{3.2}$$

The total amount of energy (H_T) in the system is given by the sum of energy of the master tank (H_m), slave tank (H_s) and the flowing energy in the communication channel (H_c) is:

$$H_T(t) = H_m(t) + H_c(t) + H_s(t). \tag{3.3}$$

Fig. 3.1 shows the formulations of energy balance, as defined in Eq. (3.3). The total energy in the system is the sum of the energy amount on each element of the telemanipulation chain. To ensure passivity, an initial condition should be given in which the total amount of energy in the system must be greater or equal to zero $H_T(t) \geq 0$. Finally, the total amount of energy must be less than the power flow in the master and slave sides. This power flow is the passive connection of the entire system and the physical world and it is given by:

$$H_T(t) \leq P_M(t) + P_S(t). \tag{3.4}$$

As proposed by Franken *et al.* in [35], in order to maintain passivity in the system, two energy tanks are presented in the controller section, one for the master (H_m) and another for the slave (H_s). Also, a Tank Level Controller (TLC) is introduced at the master side of the telemanipulation chain. The purpose of this element is to provide a constant monitoring of the energy transfer protocol between the tanks, and so, to avoid the generation of virtual energy when bilateral manipulation occurs. At the beginning, both tanks present an initial condition of zero energy $H_m = H_s = 0$.

As depicted in Fig. 3.1, there is an energy balance described in equation (**??**) to know the total amount of energy, there is a passivity condition detailed in equation (**??**) to ensure passivity is not violated, and there is an energy exchange from the physical world to the impedance controller defined in equation (3.1). The user in the master side is the one who introduces the energy to the system and starts filling the tank up, since there is no energy inside the tanks at the beginning. With this technique, every movement done by the slave will have an energetic cost, and the slave will be extracting energy from the tanks. The master and slave constantly exchange a certain amount of energy through a communication channel H_c, when the slave movements exceed the current energy budget, the master side acts as damping element through the TLC, which can obtain energy from the user, thus, replenishing the tanks with energy.

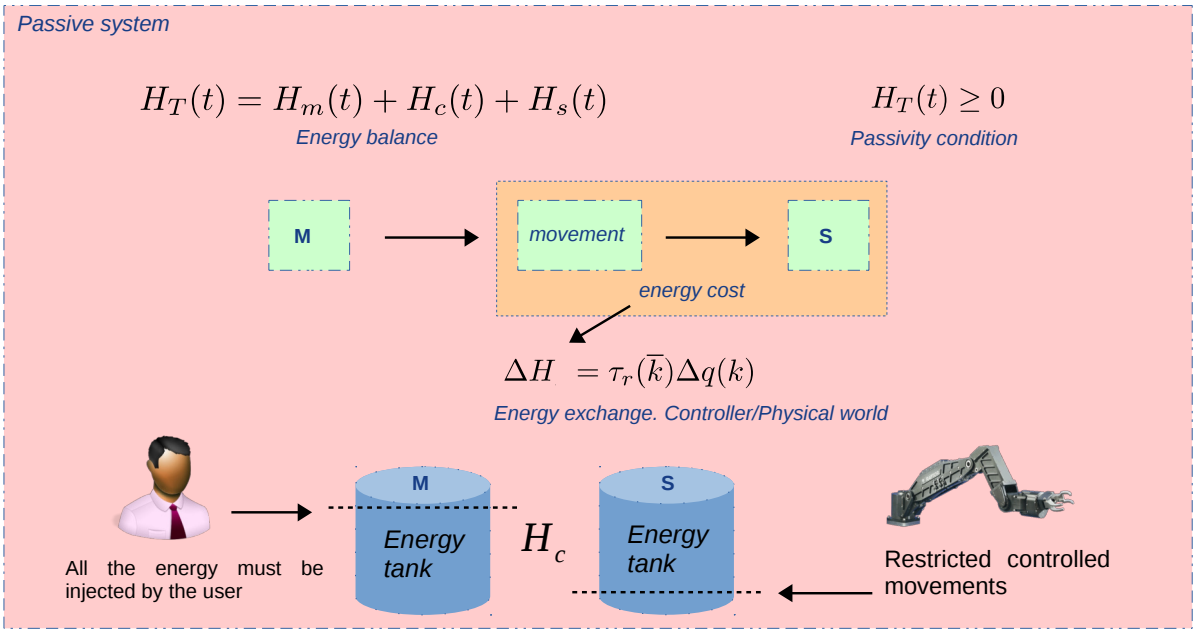

FIGURE 3.1. Block diagram of passivity according to Franken *et al.* [35].

As seen in Fig. 3.2, the TLC element resides in the master side. This is a dynamic viscous damper, the model is described in equation (3.5). The tank of the master side has a limit call the desired level (H_d) that limits the energy budget of the system to perform tasks; when the budget reaches zero, no movements are allowed in the robot side and all the forces are cut off. The user defines a desired level of the tank in the master side, because of the energy exchange between the tanks, the levels of the master and the slave reach the same value. If no activity consumes the energy, the tanks will present the same level $H_d = H_s$. When the master or slave side needs to be actuated, the required force is limited according the amount of energy contained in the tanks.

A second function of the TLC is to check if the master tank level (H_m) has reached the desired level (H_d) which is set by the user. If this condition is negative ($H_m < H_d$), the TLC actives

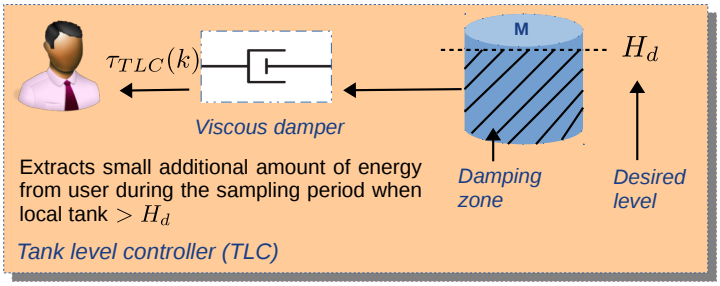

FIGURE 3.2. Block diagram of the tank level controller (TLC).

a virtual damper force (τ_{TLC}) to ensure the user injects energy to the system (and maintains passivity); all the zone below the H_d level is called the virtual damping area. Moreover, this zone is regulated by parameter α, as seen in equation (3.5), is the difference between the desired level (H_d) minus the master level (H_m).

$$\begin{aligned} \tau_{TLC} &= -d(k)\dot{q}_m(k) \\ d(k) &= \begin{cases} \alpha(H_d - H_m(k)) & \text{if } H_m(k) < H_d \\ 0 & \text{otherwise.} \end{cases} \end{aligned} \tag{3.5}$$

As previously described, every movement made by the slave device will have an energetic cost that affects the slave's tank level. If the force and position vectors have the same direction ($\vec{\tau}_s(t) = \vec{q}_s(t)$), the tank's level will decrease; otherwise, the level in the tank will increase. When the tanks are empty, the TLC forces displayed at the master side will be the highest, this means that the damping feeling sensed by the user is the biggest. While the user starts introducing energy, since the tanks are filling up and reaching the desired level, the TLC forces reduce, giving a softer sensation to the user when moving the haptic device.

In addition, the energy exchanged between the master (H_m) and the slave (H_s) tanks is regulated by an energy transfer protocol. The protocol exchanges a fixed fraction of the energy (β) when energy is available in the tanks, this fixed fraction is set by the user. As shown in equation (3.6), the amount of energy transferred depends on the energy equal or above of the desired level (H_d); it is assumed that a constant time delay ($\Delta T_m, \Delta T_s$) occurs in both sides (master and slave), and also that they share the same sample frequency (f_s).

$$\begin{aligned} H_m &= \Delta T_m f_s \beta H_d \\ H_s &= \Delta T_s f_s \beta H_d \ . \end{aligned} \tag{3.6}$$

At this point, it has been remarked the importance of passivity preservation inside the system by not violating this condition (as shown in equation (**??**) and (3.4)). Fig. 3.3 displays the asynchronous quanta moving in the communication channel, these energy packages form queues at the controller's inputs. Thereupon, the energy exchange between the physical world and the impedance controller (see equation (3.1)) is computed by the force and the difference of positions of the end-effectors in the robots. Now, the energy flows from tank to tank at the master and salve side using energy packets. A package of received energy queuing in the input of the controller (incoming package) is defined as:

$$H_+(k) = \sum_{i \in \overline{Q}(k)} \overline{H}(i) \tag{3.7}$$

where H_+ is the total energy received on the queue and i the *ith* energy package. An outgoing package is called energy quantum (H_-), the energy tank level is computed as follows:

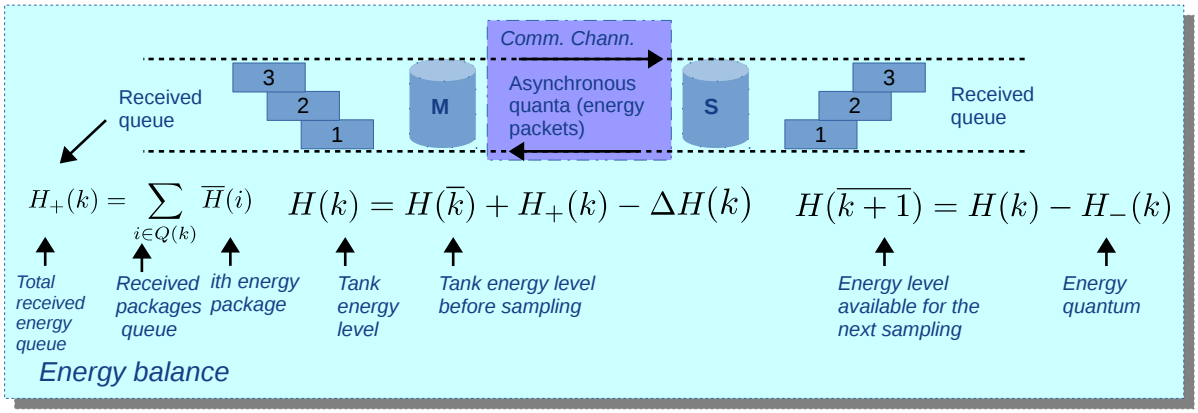

FIGURE 3.3. Block diagram of energy exchange.

$$H(k) = H(\overline{k}) + H_+(k) - \Delta H(k) \tag{3.8}$$

in which $H(k)$ is the energy tank level, $H(\overline{k})$ the level of the tank before sampling, $H_+(k)$ the incoming package, and $\Delta H(k)$ the energy exchange. After sampling the energy, the current level of energy available in the tank is:

$$H(\overline{k+1}) = H(k) - H_-(k). \tag{3.9}$$

The energy transfer along the tanks provides an energy budget to be used every time a movement is performed by the robot. Also it is a safe measure for preventing any damage in the remote environment by the robot, because when the tanks are empty, the forces are cut off.

Finally, the energy accumulated in the tanks limits the maximum force to be displayed by the motors of the robots:

$$H(\overline{k+1}) = 0 \Rightarrow \tau_{max}(k) = 0. \tag{3.10}$$

If after the sampling, the energy tank has no energy, the maximum force applied will be zero. According to Franken [35], more limits could be set to the controller ($\tau_{max2}(k), \tau_{max3}(k)...$) in the passivity layer. The limit of the forces at the transparency layer is:

$$\tau_{PL}(k) = \mathbf{sgn}(\tau_{TL}(k))\mathbf{min}(|\tau_{TL}(k)|), \tau_{max1}(k), \tau_{max2}(k), \tau_{max3}(k)...) \tag{3.11}$$

where τ_{TL} represents the forces of the transparency layer and τ_{PL} the forces of the passivity layer. The forces to be applied at the robot are commanded by the following equation:

$$\tau_r(\overline{k+1}) = \tau_{PL}(k) + \tau_{TLC}(k). \tag{3.12}$$

The applied forces τ_r depend on the passivity layer τ_{PL} and on the TLC forces τ_{TLC} which belong only to the master side. Because there is not a TLC in the slave side, the τ_{TLC} are always set to zero.

To summarize, the algorithm presented in Algorithm 1 describes the work-flow of the passivity layer in the two-layer approach.

Algorithm 1 Passivity layer work-flow

function LOOP(k + 1)
  Sum received energy $H_+(k)$ following (3.7)
  Compute energy exchange $\Delta H_I(k)$ according to (3.1)
  Compute energy tank level $H(k)$ as in (3.8)
  Send an energy package $H_-(k)$
  Change energy tank level $H(\overline{k+1}) = H_-(k)$
  if $MC == TRUE$ **then** ▷ MC stands for Master Controller
    if $H(\overline{k+1}) < H_d$ **then**
      Compute $\tau_{TLC} = -d(k)\dot{q}(k)$ following (3.5)
    else
      $\tau_{TLC} = 0$
    end if
  else
    $\tau_{TLC} = 0$
  end if
  Compute maximum available forces $\tau_{max}(k)$ given (3.11)
  Compute transparency layer force limit $\tau_{PL}(k)$ according to (3.11)
  Compute force actuated $\tau_r(k)$ given (3.12)
end function

3.3 Two-layer Approach: 3 DoF Extension and Optimizer

This section presents a two-layer architecture extension of 3 DoF as a passivity control solution for bilateral telemanipulation[1].

The work proposed by [35] represents a mechanical model developed in 1 DoF. Another solution for stiff environments presented in [49], shows a 1 DoF system with a control model using flexible spring-damper contacts. In contrast, the solution presented in this work is developed in 3 DoF, using a single energy tank for the master side.

[1] Parts of this section have been published in: **Moreno, O.,** Bimbo, J., Pacchierotti, C., Bianchini, G., & Prattichizzo, D. (2017, June). Optimizing Damping Factors in a 3 DoF Passive Two-layer Approach for Bilateral Telemanipulation. In *IEEE World Haptics 2017*.

The implementation used on this project follows a similar approach to the work of Franken in [35]; as shown in the next equation the force given by the passivity layer is related to the energy budget contained in the tank.

$$\tau_{PL}(k)\begin{cases} 0, & \text{if} \quad H(\overline{k+1}) \leq 0 \\ \tau_{TL}(k)+\tau_{TLC}(k) & \text{if} \quad 0 < H(\overline{k+1}) < H_d \\ \tau_{TL}(k), & \text{otherwise} \end{cases} \tag{3.13}$$

where $H(\overline{k+1})$ is the energy tank level in the next sample period, τ_{TL} is the transparency layer force, and τ_{TLC} represents the tank level controller force. If the energy tank level predicted at the next instant is lower than zero, all forces will be cut off. When the energy level is under the desired level the force is limited by the passivity layer. Finally, if the tank level is greater than the desired level, the system becomes fully transparent. The aim of this thesis is to find a suitable τ_{TLC} such that the energy levels are kept above the desired level while prioritizing transparency along different directions.

Let $\dot{q}(k)$ be the vector of current velocities, and P_i is a scalar that defines a priority of a given direction A_i, where the columns of A_i are the basis of a subspace S_i. The projection matrices are obtained using (3.14). Later on, equations (3.14) and (3.15) are reshaped in Section 3.4.2 as equations (3.44) and (3.45) respectively.

$$T_i = A_i(A_i^T A_i)^{-1} A_i^T. \tag{3.14}$$

The objective is to minimize the function J:

$$J = \sum_{i=1}^{m} P_i(k) \left\| T_i(k) \tau_{TLC}(k) \right\|^2. \tag{3.15}$$

Using a damping-like correction:

$$\tau_{TLC}(k) = -B(k)\dot{q}(k). \tag{3.16}$$

where B is a symmetric matrix that contains the damping coefficients. The minimization of J using quadratic programming (QP) requires that it is transformed in the standard form:

$$\min_x \quad \frac{1}{2} x^T M x + c^T x \quad s.t. \quad Ax \geq b \tag{3.17}$$

where x is the vector enclosing the minimum damping coefficients. Replacing (3.16) in (3.15):

$$
\begin{aligned}
J(B,P_i,T_i) &= \sum_{i=1}^{m} P_i \tau_{TLC}^T(k) T_i^T(k) T_i(k) \tau_{TLC}(k) \\
&= \sum_{i=1}^{m} P_i \dot{q}^T(k) B^T(k) T_i^T(k) T_i(k) B(k) \dot{q}(k) \\
&= \dot{q}^T(k) B^T(k) \underbrace{[\sum_{i=1}^{m} P_i(k) T_i^T(k) T_i(k)]}_{\text{R(k)}} B(k) \dot{q}(k).
\end{aligned} \tag{3.18}
$$

By placing the elements of the symmetric matrix $B \in \mathbb{R}^{3\times3}$, in a vector $x \in \mathbb{R}^{6\times1}$ one can obtain the next equation:

$$
B(k) \cdot \dot{q} = Q(k) \cdot x. \tag{3.19}
$$

Describing (3.19) in (3.20):

$$
B(k) \cdot \dot{q} = \begin{bmatrix} b_{11} & b_{12} & b_{13} \\ b_{12} & b_{22} & b_{23} \\ b_{13} & b_{23} & b_{33} \end{bmatrix} \cdot \begin{bmatrix} q_1 \\ q_2 \\ q_3 \end{bmatrix} = \begin{bmatrix} b_{11}q_1 + & b_{12}q_2 + & b_{13}q_3 \\ b_{12}q_1 + & b_{22}q_2 + & b_{23}q_3 \\ b_{13}q_1 + & b_{23}q_2 + & b_{33}q_3 \end{bmatrix} \tag{3.20}
$$

Rearranging (3.20) $Q(k)$ and $x(k)$ are obtained:

$$
B(k) \cdot \dot{q} = \underbrace{\begin{bmatrix} q_1 & q_2 & q_3 & 0 & 0 & 0 \\ 0 & q_1 & 0 & q_2 & q_3 & 0 \\ 0 & 0 & q_1 & q_2 & q_3 & 0 \end{bmatrix}}_{Q(k)} \cdot \underbrace{\begin{bmatrix} b_{11} \\ b_{12} \\ b_{13} \\ b_{22} \\ b_{23} \\ b_{33} \end{bmatrix}}_{x(k)} \tag{3.21}
$$

Reaching the desired form:

$$
J = x^T(k) \underbrace{Q^T(k) R(k) Q(k)}_{M} x(k). \tag{3.22}
$$

Now the changes on the tank level depend on the quantity of energy in the tank, the difference of energy exchange with the transparency layer and the damping force:

$$
H(\overline{k+1}) = H(k) - \tau_{TL}^T(k) \dot{q}(k) + \dot{q}^T(k) B(k) \dot{q}(k). \tag{3.23}
$$

A constraint is added to ensure that the tank level does not drop below a given desired level H_d:

$$H(\overline{k+1}) \geq H_d(k). \tag{3.24}$$

Shaping equation (3.24) in (3.25):

$$H(k) - \tau_{TL}^T(k)\dot{q}(k) + \dot{q}^T(k)Q(k)x(k) \geq H_d(k). \tag{3.25}$$

Using the quadratic programming form on (3.17) the terms for the constraints are:

$$\underbrace{\dot{q}^T(k)Q(k)}_{A}x(k) \geq \underbrace{H_d(k) - H(k) + \tau_{TL}^T(k)\dot{q}(k)}_{\text{b}}. \tag{3.26}$$

Finally, the energy exchange flow in the 3 DoF extension is computed as in equation:

$$\Delta H(k) = \sum_{i=x,y,z} \tau_i(\overline{k})\Delta q_i(k) \tag{3.27}$$

3.4 TOPL: Method

The continuous time index is denoted as t and the discrete time index as k. For a continuous-time signal $q(t)$, also is denoted its sampling $q(k - T_s)$ with $q(k)$ without ambiguity, being T_s the sampling period. Furthermore, the interval from time $k-1$ to time k is indicated as $\bar{k}$, and $H(\bar{k})$ denotes a signal H being held constant during $\bar{k}$. For a vector or matrix v, v' indicates its transpose. The notation $v \odot w$ is used to denote the component-by-component product of v and w. $\|v\|$ is the Euclidean norm of v.

As presented in Section 2.3.1, transparency is defined as the full display of the environment impedance to the human operator when he/she interacts with the robot [200, 262]. Described in [7], ideal transparency is achieved when the generalized forces τ_s and velocities $\dot{q}_s$ at the slave side are equally reflected in the forces τ_m and velocities $\dot{q}_m$ at the master side module a suitable scaling and an intrinsic time delay.

Stability of the teleoperation chain is a key requirement in order to ensure a safe interaction on both the master and the slave sides. This property may be compromised by several factors such as relaxed user grasp, stiff contacts in the environment, and communication delays. Passivity represents a viable solution to the problem of preserving stability. Indeed, the interaction between passive systems is guaranteed to be stable, and properly combining passive systems results in a passive system [230]. Moreover,the human operator has been shown to preserve stability when

interacting with a passive system [162]. Hence, ensuring passivity of all components of the telemanipulation system is a convenient sufficient condition for stability of the interaction at all levels.

For a generic component R of a mechanical teleoperation system, let $H_R(t)$ denote its total internal energy. Passivity of R boils down to the condition that $H_R(t)$ never exceeds its initial value $H_R(0)$. Assuming without loss of generality a zero-energy initial condition, R is passive if:

$$H_R(t) = \int_0^t \tau_R'(\sigma)\dot{q_R}(\sigma)d\sigma \geq 0 \quad \forall t \geq 0\,, \tag{3.28}$$

where $\tau_R(t)$ and $\dot{q_R}(t)$ represent the applied external forces and generalized velocities, respectively.

Following [35], the total energy $H_T(t)$ of the system can be decomposed as in equation (3.3) in Section 3.2. From (3.28), passivity of the overall system is therefore achieved if the controller is able to regulate the system in order to preserve the condition:

$$H_T(t) \geq 0 \quad \forall t \geq 0. \tag{3.29}$$

3.4.1 Control Architecture of TOPL

The present work builds upon the energy monitoring control architecture presented in [35]. With reference to Fig. 3.4, the overall system is made of several layers. The *physical layer* represents the user/haptic device and robot/environment interactions. The generalized forces and displacements at the master [slave] side are denoted by $\tau_m(k)$ [$\tau_s(k)$] and $q_m(k)$ [$q_s(k)$], respectively. The two-layer approach is composed by the controller which contains the transparency and passivity layer respectively. The controllers have some restrictions with passivity-based methods to achieve transparency. In order to ensure stability on the system the implemented framework must be able to manage unsynchronized time delays [35]. The *transparency layer* implements a position force controller (PFC) and interacts between the physical and passivity layer exchanging information on forces and positions. As shown in the same figure, the positions of the haptic device in the master side (q_m) and the robot at the slave side (q_s) are processed in separate controllers, calculating the speed of the displacements and computing the resulting velocities into forces. By position-force control (PFC) the transparency layer reflects the impedance forces in both sides F_{TLm} and F_{TLs}, respectively; only in the master side, the force is calculated using the difference in position of the slave device in order to limit the transparency.

A standard implementation of the PFC is as follows:

$$\tau_{TLm}(k) = \tau_e(k-T) \tag{3.30}$$

$$\tau_{TLs}(k) = -K_p(q_m(k-T) - q_s(k)) - K_d\dot{q}_s(k) \tag{3.31}$$

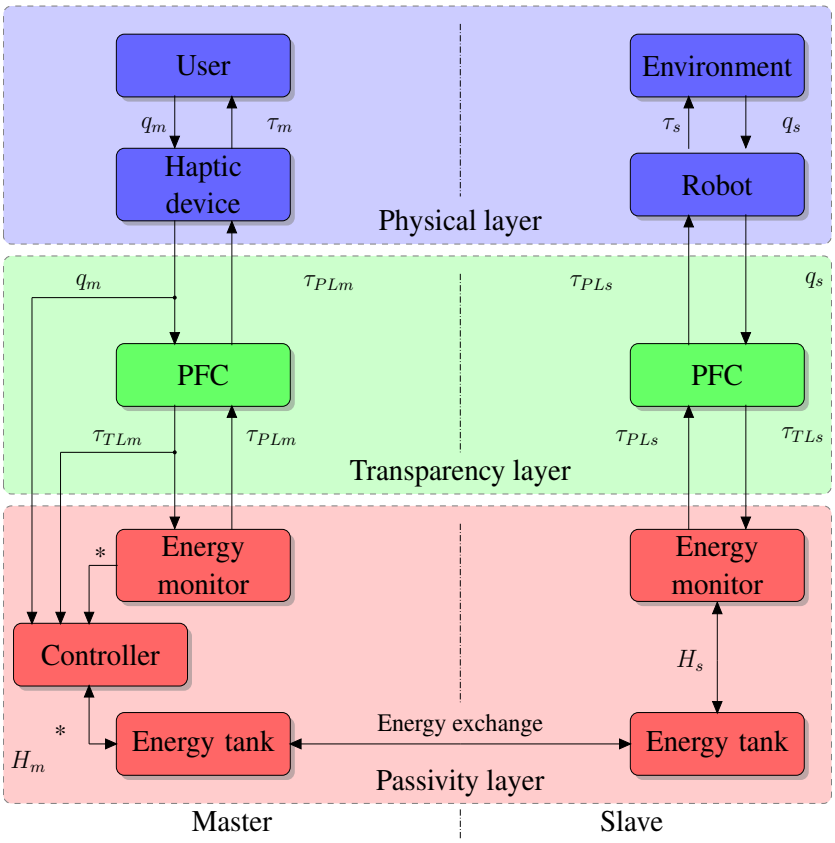

FIGURE 3.4. Controller architecture block diagram. The architecture of the controller is divided in three areas: a) the physical layer that defines forces as inputs and position as outputs for the devices. b) the transparency layer that computes position to force control. c) the passivity layer which computes the damping correction (only on the master side) and energy flow control.

where $\tau_e(k)$ is the measured interaction force at the master side, while K_p and K_d are suitable proportional and derivative controller gains, and T is the master-slave communication delay (possibly time-varying). The force vectors $\tau_{TLm}(k)$ and $\tau_{TLs}(k)$, once actuated at the respective sides, ensure full transparency for the teleoperation system. Such transparency might not be always achieved in a passive manner. The role of the *passivity layer* is to suitably modulate the forces $\tau_{TL}(k)$ generated by the PFCs at both sides in order to preserve passivity of the overall system, i.e., to ensure that (3.29) holds at all times. Due to the impossibility of monitoring the overall energy H_T in real time due to the presence of delays, in [35] the following paradigm is adopted.

A virtual energy tank H characterized by an energy level $H(k)$ is introduced at each side. Each tank can exchange virtual energy with its counterpart at the other side and functions as the energy budget available for performing the appropriate (master or slave) force control action.

When the tank level at one side is detected as being low, a correction to the actuated force $\tau_{TL}(k)$ is applied in order for the tank level not to drop below zero, therefore preserving passivity.

The passivity layer also integrates an energy exchange protocol whose role is to transfer virtual energy packets between the master and slave tanks according to a suitable algorithm. The purpose of this protocol is to balance energy levels at both sides, so as to relax the conservative condition that both tank levels be positive in order to guarantee overall passivity.

The details on the latter component are out of the scope of this work and the standard implementation of [35] is used here. In this section, the passivity layer without specific reference to the master or the slave side is described, it can be implemented and stick with the notation used in [35].

Let $q(k)$ be the sampled generalized device displacement, and denote with $\tau_r(\bar{k})$ the actuated force during $\bar{k}$, which is held constant since a zero-order-hold is used. The energy loss in tank H during $\bar{k}$ is therefore given by:

$$\Delta H(k) = \tau_r'(\bar{k})(q(k) - q(k-1)), \tag{3.32}$$

Hence, the tank level after the control action has performed the energy loss extraction as in the following equation:

$$H(k) = H(k-1) - \Delta H(k). \tag{3.33}$$

Taking into account a possible virtual energy exchange amounting to $H_{\pm}(k)$, performed according to the exchange protocol, the energy tank level at the end of the time interval $\bar{k}$ becomes:

$$H(\overline{k+1}) = H(k) + H_{\pm}(k). \tag{3.34}$$

The tank level $H(\overline{k+1})$ in (3.34) represents the available amount of energy to perform the force actuation task during the time interval $\overline{k+1}$. In [35], the passivity layer is implemented as a curtailed version $\tau_{PL}(k)$ of the force feedback $\tau_{TL}(k)$, computed according to the value of $H(\overline{k+1})$. In particular, the following two strategies are considered:

1. Simply cut-off all forces if there is no energy left, i.e.,

$$\tau_{PL}(k) = \begin{cases} 0 & \text{if } H(\overline{k+1}) \leq 0 \\ \tau_{TL}(k) & \text{otherwise.} \end{cases} \tag{3.35}$$

2. Provided the teleoperation system has only a single DoF, an estimate of the energy required for the control action in $\overline{k+1}$ is given by:

$$\Delta H(\overline{k+1}) = \tau_r(\overline{k+1})\dot{q}(k)T_s, \tag{3.36}$$

where $\tau(\overline{k+1})$ is the prospective actuated force. Based on this and on the available energy, a limitation on $\tau(\overline{k+1})$ is computed as:

$$\tau_{max}(k) = \frac{H(\overline{k+1})}{|\dot{q}(k)|T_s}. \tag{3.37}$$

The curtailed force $\tau_{PL}(k)$ is then computed as:

$$\tau_{PL}(k) = \begin{cases} 0 & \text{if } H(\overline{k+1}) \leq 0 \\ \mathbf{sgn}(\tau_{TL}(k))\mathbf{min}(|\tau_{TL}(k)|, \tau_{max}(k)) & \text{otherwise.} \end{cases}. \tag{3.38}$$

Finally, a certain amount τ_{TLC} of virtual damping force is added to τ_{PL} at the master side to prevent total tank depletion. Such damping is given by the dynamic damper $\tau_{TLC} = -d(k)\dot{(}q)_m(k)$ as in equation (3.5).

The aim of this methodology is to find a suitable τ_{TLC} such that the energy levels are kept above the desired level while prioritizing transparency along different directions. In [35], the problem of suitably shaping $\tau_{PL}(k)$ in the multi-DoF case, depending on the task and in order to preserve transparency under the passivity constraint is left open.

3.4.2 Optimal Passivity Layer Design

This thesis proposes an optimization-based design of the passivity layer which addresses the multi-DoF case and minimizes the loss of transparency on subsets of the task space which are relevant to the given task, while preserving passivity[2] Similarly to case (2) above, it is considered the estimated energy loss as a function of the prospective actuated force $\tau_r(\overline{k+1})$ as:

$$\Delta H(\overline{k+1}) = \tau_r'(\overline{k+1})\dot{q}(k)T_s. \tag{3.39}$$

Therefore, an estimate of the tank level after the control action has been performed is given by:

[2]Parts of this section have been published in: **Moreno, O.,** Bimbo, J., Pacchierotti, C., Prattichizzo, D., Barcelli D., & Bianchini, G.(2018, October). Transparency-optimal passivity layer design for time-domain control of multi-DoF haptic-enabled teleoperation. In *IEEE/RSJ International Conference on Intelligent Robots and Systems (IROS).*

$$H(k+1) = H(\overline{k+1}) - \tau_r'(\overline{k+1})\dot{q}(\bar{k})T_s. \tag{3.40}$$

Let $H_{min}(k) > 0$ be a possibly time-varying threshold level, chosen by the designer, corresponding to the amount of energy to be left in the tank after $\tau_r(\overline{k+1})$ has been applied during $\overline{k+1}$. In order for such a level to be guaranteed, according to the estimate in (3.40), the following constraint must hold:

$$H(k+1) = H(\overline{k+1}) - \tau_r'(\overline{k+1})\dot{q}(\bar{k})T_s \geq H_{min}(k). \tag{3.41}$$

It is easily seen from (3.41) that if $H(\overline{k+1}) - \tau_{TL}'(k)\dot{q}(k)T_s \geq H_{min}(k)$, then the unmodified $\tau_{TL}(k)$ can be safely actuated (i.e., $\tau_{PL}(k) = \tau_{TL}(k)$) and therefore perfect transparency can be achieved. To address the situation in which this is not possible, $\tau_{PL}(k)$ is computed as the solution of an optimization problem. For this purpose, it was convenient to implement the effect of the passivity layer as a force correction in the form of a suitable amount of virtual damping. In particular, it is defined $\tau_{PL}(k)$ as:

$$\tau_{PL}(k) = \tau_{TL}(k) + \tau_{TLC}(k) \tag{3.42}$$

where $\tau_{TLC}(k) = -B(k)\dot{q}(k)$ as presented above in equation (3.16), $B(k)$ is a symmetric matrix.

To formulate the optimization problem, let $\mathscr{S}_i(k)$, $i = 1,\dots m$ be a suitable set of subspaces of the task space, depending on the given task and possibly also on the time index k. Let us assign a priority index $p_i(k) \geq 0$ to each subspace $\mathscr{S}_i(k)$, also depending on the current task configuration. The idea of associating each subspace to a priority index is quite simple: the higher the priority $p_i(k)$, the stricter the requirement that the projection on $\mathscr{S}_i(k)$ of the optimal rendered force $\tau_{PL}(k)$ is as close as possible to the corresponding projection of $\tau_{TL}(k)$. Let $A_i(k)$ be a matrix whose columns form a basis of $\mathscr{S}_i(k)$. The projection of the force correction $\tau_{TLC}(k) = \tau_{PL}(k) - \tau_{TL}(k)$ on $\mathscr{S}_i(k)$ is given by:

$$\Pi_{\mathscr{S}_i}(\tau_{TLC}(k)) = T_i(k)\tau_{TLC}(k), \tag{3.43}$$

where the projection matrix $T_i(k)$ reads:

$$T_i(k) = A_i(k)[A_i'(k)A_i(k)]^{-1}A_i'(k). \tag{3.44}$$

Based on the arguments above, it is natural to define the following functional to be minimized:

$$J(B(k)) = \sum_{i=1}^{m} p_i(k)\,\|T_i(k)\tau_{TLC}(k)\|^2, \tag{3.45}$$

where $\tau_{TLC}(k)$ is as in (3.16) and the decision variables are represented by the entries of the damping matrix $B(k)$. Reshaping Eq. (3.22) in the standard form, the result is Eq. (3.45). The minimization of (3.45) must be carried out under the constraint (3.41). Furthermore, it must be ensured that the sign of all components of $\tau_{PL}(k)$ be the same as the corresponding components of $\tau_{TL}(k)$ as a result of the force correction in (3.42)-(3.16) corresponding to the minimum of $J(B(k))$. This constraint prevents the passivity layer from letting the tank gain energy from inverting the direction of rendered forces with respect to $\tau_{PL}(k)$, thus resulting in an excessive loss of transparency. Said in another way, the maximum allowed correction along each direction must act so as to zero out the rendered force. To ensure the latter condition, the following constraint is required:

$$\tau_{PL}(k) \odot \tau_{TL}(k) = (\tau_{TL}(k) - B(k)\dot{q}(k)) \odot \tau_{TL}(k) \geq 0 \tag{3.46}$$

Motivated by the above observations, the following algorithm for the implementation of the passivity layer is proposed (see Algorithm 2).

Algorithm 2 Optimal passivity layer implementation

1: Given: $H(\overline{k+1})$, $\tau_{TL}(k)$, $\dot{q}(k)$, $\{ p_i(k), T_i(k) \}$, $H_{min}(k)$
2: **if** $H(\overline{k+1}) - \tau'_{TL}(k)\dot{q}(k) \geq H_{min}(k)$ **then**
3: $\quad \tau_{PL}(k) = \tau_{TL}(k)$
4: **else**
5: $\quad$ Solve the optimization problem

$$\begin{aligned} & B^*(k) = \arg\min_B J(B) \\ & \text{subject to} \\ & H(\overline{k+1}) - \tau'_{TL}(k)\dot{q}(k) + \dot{q}'(k)B\dot{q}(k) \geq H_{min}(k) \\ & (\tau_{TL}(k) - B\dot{q}(k)) \odot \tau_{TL}(k) \geq 0 \end{aligned} \tag{3.47}$$

6: $\quad$ **if** Problem 5: is feasible **then**
7: $\quad\quad \tau_{PL}(k) = \tau_{TL}(k) - B^*(k)\dot{q}(k)$
8: $\quad$ **else**
9: $\quad\quad \tau_{PL}(k) = 0$
10: $\quad$ **end if**
11: **end if**
12: Actuate $\tau_r(\overline{k+1}) = \tau_{PL}(k)$

The optimization problem (3.45) is a convex quadratic program. Note that the condition in 6 (see Algorithm 2) presents numerical errors such as when one of the eigenvalues of the matrix $Q(k)$ (see Eq. (3.21)) are smaller than zero, as previously seen before. Just to remind the reader this is a quadratic programming problem. The global minimum can be efficiently computed using interior point methods. As it will be shown in the experimental section, the method can

be implemented without problems on a 3 DoF teleoperation system operating at a sampling frequency of 1 kHz.

So far the function that must be minimizes has been defined (see equation (3.45)). The constraints in equations (3.41) and (3.46) ensure passivity on the system. But for the optimal passivity layer design, a correction on the desired level H_d must be performed. This correction should guarantee that the energy budget (H_{min} is defined in Eq. (4.8)) is enough to perform movements in the slave side when the energy tank depletes in different scenarios. The correction also must satisfies the passivity condition without committing any violation, the discussion of the correction is described in Sec. 3.4.3.

3.4.3 Correction on the Desired Level: The Expected Performance

In order to spend energy efficiently, the desired level must be updated and adjusted in every iteration; thus, the amount of energy in the tank will ensure $H_d(K) \geq 0$, as first described in Sec. 3.2. To initialize the system, the desired level $H_d(0)$ is set as the fixed desired level with a value (as proposed in [35]): $H_d(0) = 0.1$.

Then, calculating $H(k)$ as the instantaneous and dynamical energy tank level value. Finally $\Delta H(k+1)$ represents the estimated energy budget for the next sample period as defined in equation (3.1) in Sec. 3.2. When the TOPL controller is operating four possible scenarios could appear:

1. Above the desired level and losing energy.

   In figure 3.5(a)-a, the first scenario is shown , when the tank level is above the desired level, and the energy tank level samples $H(k)$ decreases along time.

   $$\text{scenario } 1 \begin{cases} H(k) & > H_d(0), \\ \tau_r(k)\dot{q}(k) & > 0. \end{cases} \tag{3.48}$$

   In this case, the expected behaviour of the new desired level would be a function of the estimated energy budget $\Delta H(k+1)$. Preserving the new desired level above the estimated budget as long as the samples are above $H_d(0)$.

2. Above the desired level and gaining energy.

   In this scenario, the tank is gaining energy. There is no need to adjust the new value of the desired level. For this case, it is expected that the forces of the transparency layer equal the forces of the passivity layer $\tau_{TL} = \tau_{PL}$ and therefore, the damping forces equals to zero $\tau_{TLC} = 0$. (Possible case when the end effector is dragging over the surface and gaining energy due to friction).

$$\text{scenario } 2 \begin{cases} H(k) & > H_d(0), \\ \tau_r(k)\dot{q}(k) & < 0. \end{cases} \tag{3.49}$$

3. Below the desired level and losing energy.

   In this scenario probably the best way to spend the energy is adjusting the desired level gradually. The behaviour expected defines a new desired level rising up until the tank level reaches $H_d(0)$, and then the system performs as in (3.48).

$$\text{scenario } 3 \begin{cases} H(k) & < H_d(0), \\ \tau_r(k)\dot{q}(k) & > 0. \end{cases} \tag{3.50}$$

4. Below the desired level and gaining energy.

   For this scenario, if the energy tank level $H(1)$ is below the desired level H_d, there is not an adjustment of the desired level because the energy recovery is wanted as soon as possible. This behaviour should remain like this, until the energy tank level passes the desired level and acts as on scenario (3.49).

$$\text{scenario } 4 \begin{cases} H(k) & < H_d(0), \\ \tau_r(k)\dot{q}(k) & < 0. \end{cases} \tag{3.51}$$

The correction that better fits to H_d on the different scenarios showed is described in Sec. 4.2.2 as a dynamic desired level named H_{min}.

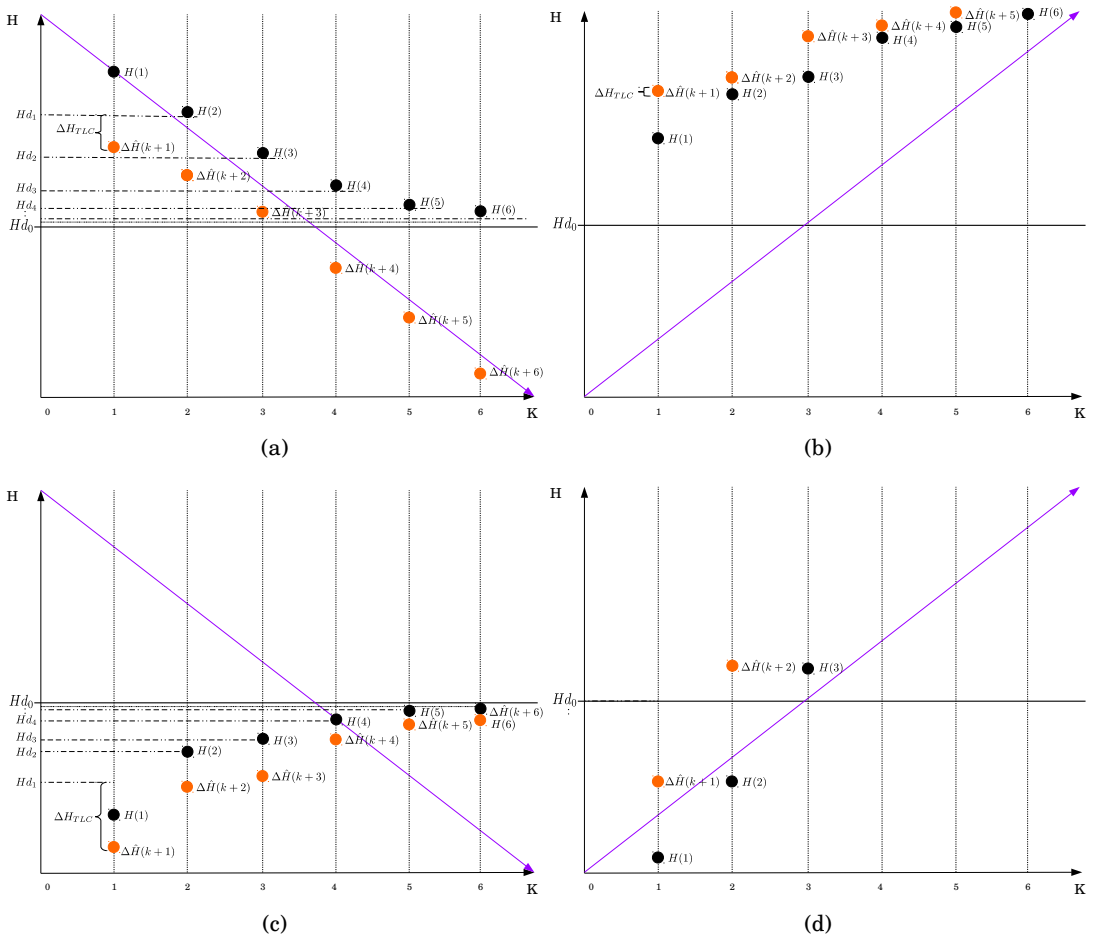

FIGURE 3.5. (a) Scenario 1: Above the desired level and losing energy. (b) Scenario 2: Above the desired level and gaining energy. (c) Scenario 3: Below the desired level and losing energy. (d) Scenario 4: Below the desired level and gaining energy.

CHAPTER 4

EXPERIMENTS AND RESULTS

In this chapter, the experiments and results of the TOPL method are presented and also the TOPL method is compared with other controllers in the set up and validation sections. The TOPL experiments and results are divided in two parts: *a) Poke/Drag Experiment* and *b) Palpation Experiment*. The first part of the experiment consist of poking a flat surface which presents friction on the virtual environment. The purpose of this experiment is to recognize the regions of operability using the NPC, STLC and TOPL controllers. The second part of the experiment is to compare the controllers performance presented in the two-layer approach (NPC, STLC, and TOPL) when executing a palpation task over a virtual surface.

Experiments *a)* and *b)* have a description on the experimental set up section that follows the order of the telemanipulation chain (see Fig. 2.1) which is the haptic device on the master side, and the virtual end-effector at the slave side. Since experiments *a)* and *b)* operate with the same haptic device for the experimental set up, the implementation of the device is described in Sec. 2.2.3 for both experiments.

4.1 TOPL: Poke/Drag Experiment (PODREX)

Previously a mathematical derivation of a prioritization of feedback forces was presented , the next step is to find an experimental procedure to choose suitable subspace bases and priorities (A_i, P_i) for different tasks. This set up must guarantee the passivity condition at all moments and display the desired behaviour. For this stage of the research it has been developed in a virtual environment using the Robot Operating System (ROS)[1] and the Omega 6 haptic device. As seen in Chapter 3, the goal is to implement the method in a virtual environment and test it on different

[1]Robot Operating System, Website: *http://www.ros.org/*

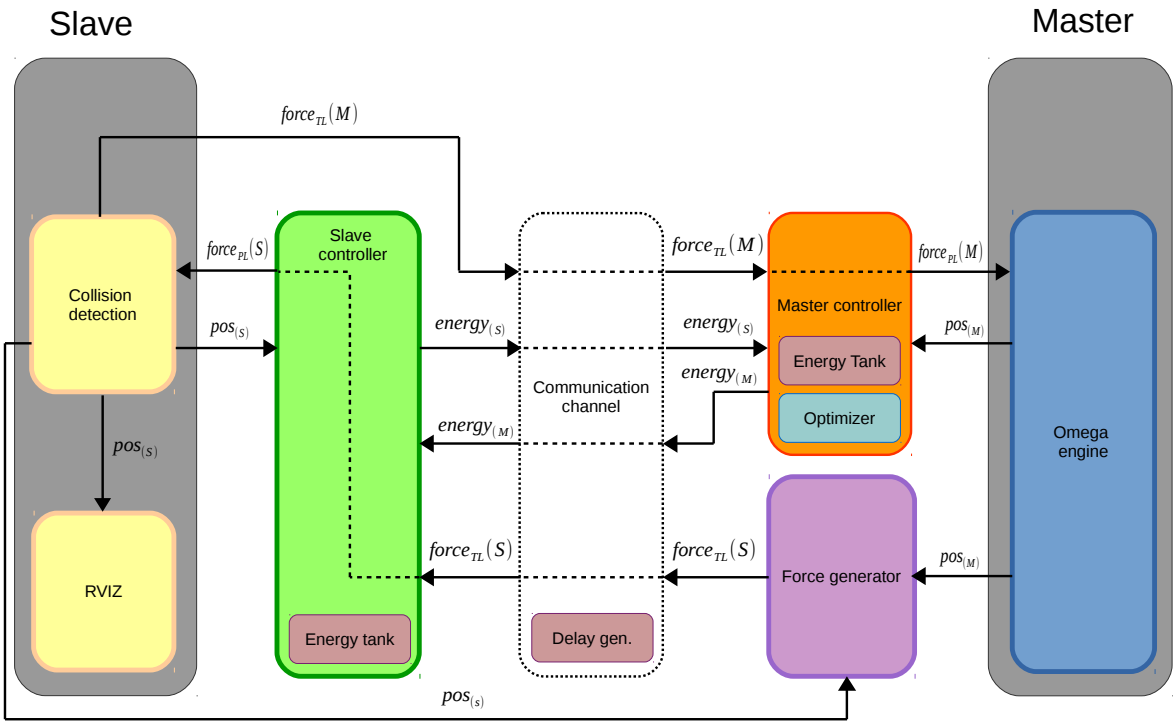

FIGURE 4.1. Block diagram of proposed bilateral telemanipulation system.

application scenarios. In this section, it is proposed an experiment called Poke/Drag Experiment (PODREX); the procedure is divided in Experimental Set up (see Sec. 4.1.1), Validation (see Sec. 4.1.2), and Results (see Sec. 4.1.3).

4.1.1 Experimental Set Up

In Fig. 4.1 it is shown the bilateral telemanipulation scheme proposed for this thesis. It is divided mainly in two sections: *a) master side* and *b) slave side*. Both sides uses the two-port architecture as described in Section 2.1.1 and the configuration resides on position-force control (see Section 2.1.2) where the forces f_i act as input and the positions q_i operate as output. In addition, both sides have an energy tank and only the master side has a TLC. The communication channel is placed in the center of the system, that element transmits the forces between sides and also exchanges energy package among controllers.

A) Virtual Environment

This element represents the slave side of the telemanipulation chain as depicted in Fig. 2.1 in Sec. 2.1. The remote location for the slave side is generated in a virtual environment using the

visualization tool RVIZ[2], which is package of the ROS[3] framework. The architecture of the virtual environment follows the description of the haptic rendering scheme presented in Fig. 2.11. In the scheme there is a ROS node that performs the collision detection and the physics engine, the RVIZ tool executes the simulation/graphics engine and the visualization.

4.1.2 Validation

The first part of the experiment consist of poking a plane surface on the virtual environment. Fig. 4.2 shows the sequence of the palpation with end-effector poking the surface on a virtual environment. The movements done by the user and then replicated by the end-effector mainly occur at the $z-$ axis. The avatar (virtual end-effector) is modelled as a single point element with position p_i and the contact position is p_i'. The remote object surface has a stiffness value regulated by a configurable parameter (penetration vector) K, the force F_{env} computed when the collision occurs is shown in the next equation as presented in [212]:

$$F_{env} = K(p_i - p_i'). \tag{4.1}$$

The surface has a friction implementation, the classical Coulomb Model as described in [271] and [272] is:

$$F_f = \begin{cases} F_c \cdot \mathbf{sgn}(\dot{x}) & \text{if} \quad \dot{x} \neq 0 \\ F_{app} & \text{if} \quad \dot{x} = 0 \quad F_{app} < F_c. \end{cases} \tag{4.2}$$

where F_{app} is the applied force, $\dot{x}$ is the sliding speed and F_c represents the Coulomb friction force defined by:

$$F_c = \mu F_N \tag{4.3}$$

in the previous equation μ is the Coulomb friction coefficient and F_N the normal load between two contact surfaces.

The second part of the experiment is to compare the controllers presented in the two-layer approach having as a reference the transparent system declared as NPC controller, the second controller is the 3 DoF extension of Franken *et al.* in [35] which has been defined as STLC controller, and the third is the TOPL controller. The experiment consist of testing the system response of each controller under diverse time and force parameters by poking or dragging the virtual surface described above. The validation was performed for time delay parameters

[2]RVIZ is a 3D visualization tool for ROS, Website: *http://wiki.ros.org/rviz*

[3]A brief description of ROS and RVIZ can be consulted in [269, 270].

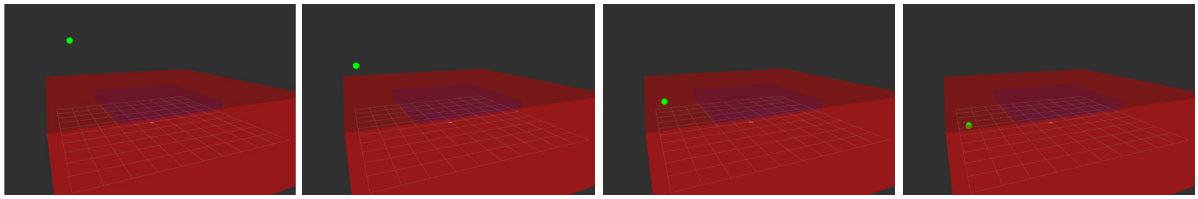

FIGURE 4.2. Sequence of palpation experiment by poking the surface with the end-effector on a virtual environment with the RVIZ tool.

among 0 – 100 ms, since the maximum force displayed by the haptic devices is 12 N, the stiffness parameters depicted on the graphics are scaled in sections of 0.29 N/mm.

The results are shown in Fig. 4.5, 4.6, 4.7, 4.8, 4.9, 4.10, and 4.12. These figures have been named tables of operability regions, each of the controllers were tested in two modalities by an expert user[4]: *a) soft grasp*, and *b) strong grasp*. The haptic device model used in this experiments is the Omega 6, which has a handle in the form of a pen. With this handler a soft grasp is defined as grabbing the haptic handler as a pen for writing; in contrast, with a strong grasp the haptic handler is grabbed by covering it with the whole fist (like grabbing a knife in an inverse way). Figure 4.3 depicts soft grasp and strong grasp modes.

a) b)

FIGURE 4.3. Haptic handle grasp: a) Soft grasp mode and b) strong grasp mode.

In the first case (soft grasp) the muscles of the arm are more tense, and in the second case (strong grasp) the muscles of the shoulder get tenser. It has been asked to the user to describe the response behaviour in three ways:

[4]The author of this thesis defined an expert user a person who has used haptic devices to perform tasks, and has an experience of more than 40 hrs with the haptic interface.

- **Stable behaviour** (Marked with a circle for soft grasp and a square for strong grasp on the graphics). It is considered stable behaviour when the task could be performed without losing the control of the virtual end-effector in the remote environment due to instabilities when poke and/or drag the surface, or receiving force feedback in a violent response.

- **Undetermined behaviour** (Marked with a triangle on the graphics). Undetermined behaviour means that the tasks can be performed partially, but one of the drag or poke performance is lost, it tends to stabilize, or the user forces the performance.

- **Unstable behaviour** (Marked with a cross on the graphics). Unstable behaviour occurs when the tasks can not be performed.

4.1.3 Results

To illustrate the functionality of 3 DoF extension, Fig. 4.4 shows the results of the poking interaction over the virtual surface.

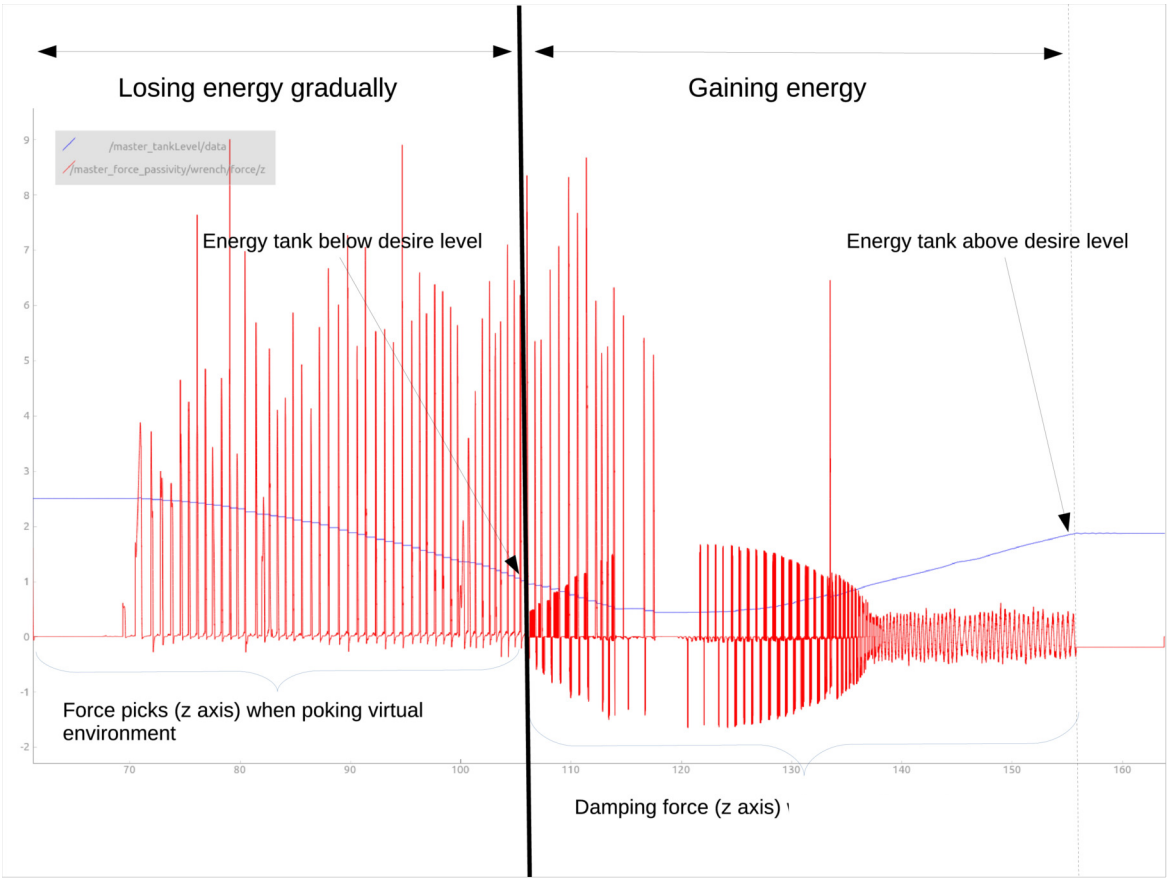

FIGURE 4.4. Experiment of the TOPL interaction when poking the surface with the end-effector with 1 kN of stiffness and 10 ms delay.

The blue line represents the energy tank level (master side), as seen, it starts with a high value in the tank above the upper limit. The red lines are the forces f_z which represent the poking when the virtual end-effector is penetrating the surface. At the beginning is clearly seen that the energy tank level is decreasing on every poke done to the surface, this interaction causes an energy lost gradually due to the energy cost of the movement. But when the energy tank level drops below the desired level H_d the virtual damper starts at the master side, making the user to introduce the energy by pumping-like movements. On the picture, after the black line that divides the poke sequence, it is observed the process of gaining energy (when the virtual damper kicks).

For the system response in soft grasp, Fig. 4.5 shows that with a greater time delay is not possible to perform the tasks when the level of stiffness increases. In Fig. 4.6 the performance of the task with the STLC controller seems to improve in small regions of high time delay and low stiffness, but more regions of instability appeared on low time delays and higher stiffness. Using the TOPL controller, in Fig. 4.7 is shown that the regions of operability with a stable behaviour have increased, on the same way the regions of undetermined behaviour.

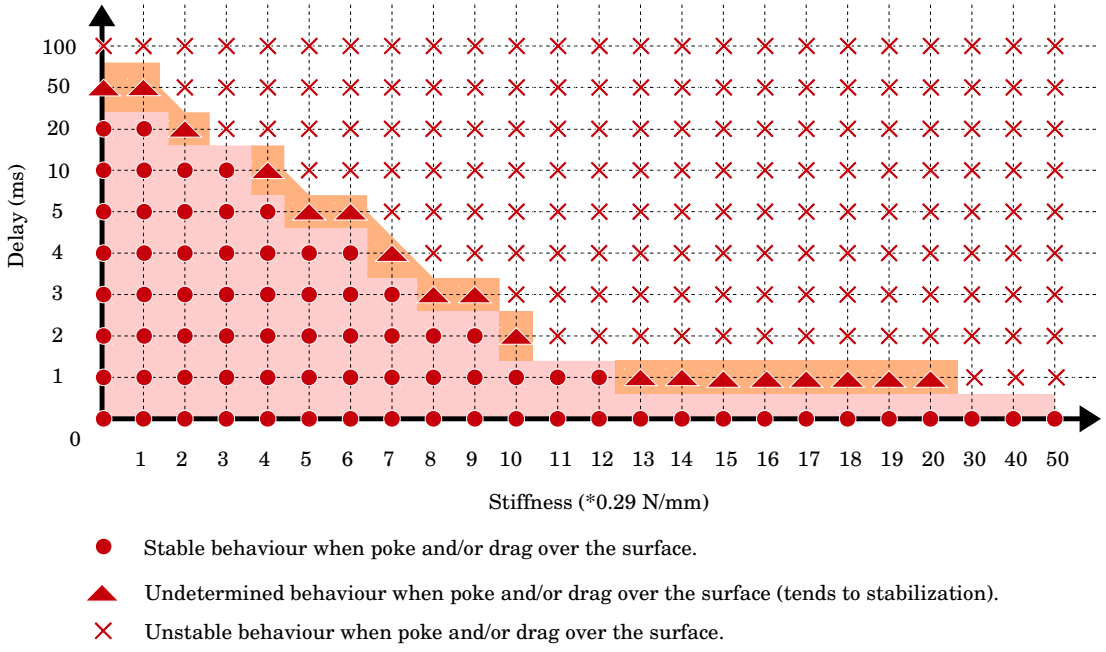

FIGURE 4.5. Table of operability regions: Soft grasp - NPC. Poke and drag on a surface with friction.

Lastly for soft grasp, Fig. 4.8 depicts the comparison on the different regions of stability, and how those regions were extended by using the TOPL controller.

In strong grasp analysis, Fig. 4.9 shows an extended region of stability when the user grasps the haptic handle stronger. In Fig. 4.10 the performance of the task with the STLC controller

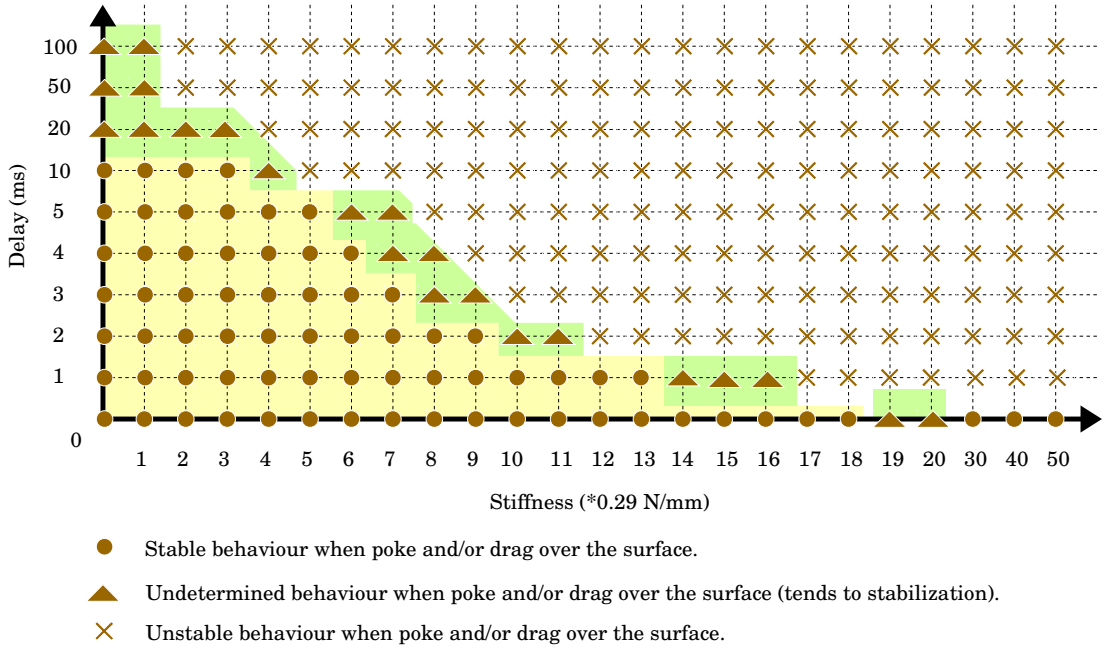

FIGURE 4.6. Table of operability regions: Soft grasp - STLC. Poke and drag on a surface with friction.

improves small regions of high time delay and low stiffness, and also a short region of stability occurred on low time delays and higher stiffness. When TOPL controller is on, in Fig. 4.11 is shown that the regions of stable performance are extended, on the same manner the regions of undetermined behaviour. Finally for strong grasp, Fig. 4.12 illustrates the comparison on the extended regions of stability.

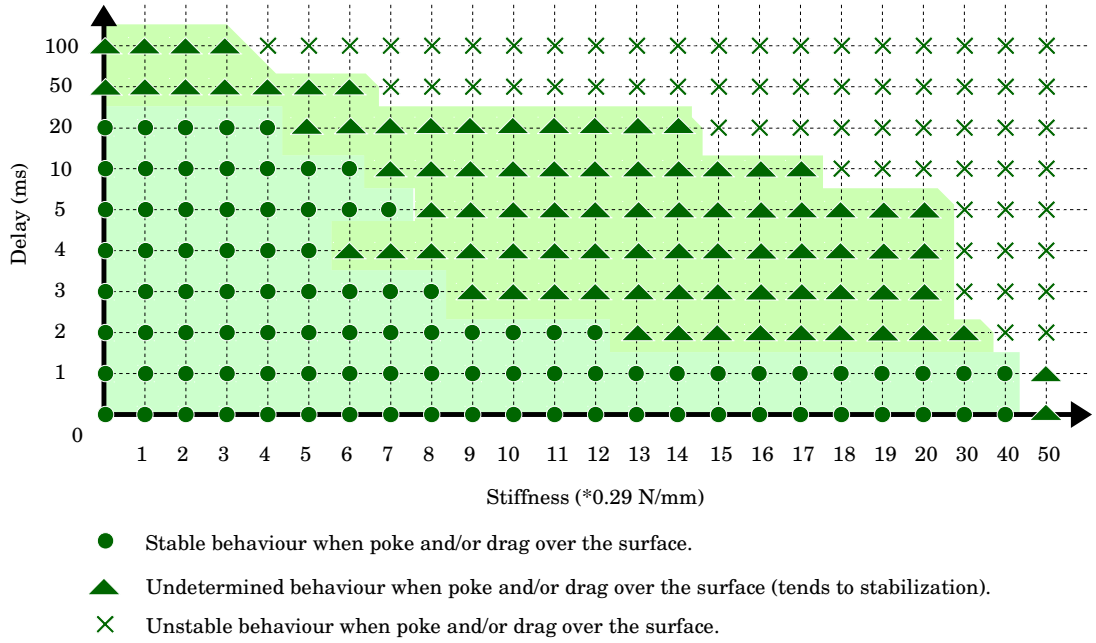

FIGURE 4.7. Table of operability regions: Soft grasp - TOPL. Poke and drag on a surface with friction.

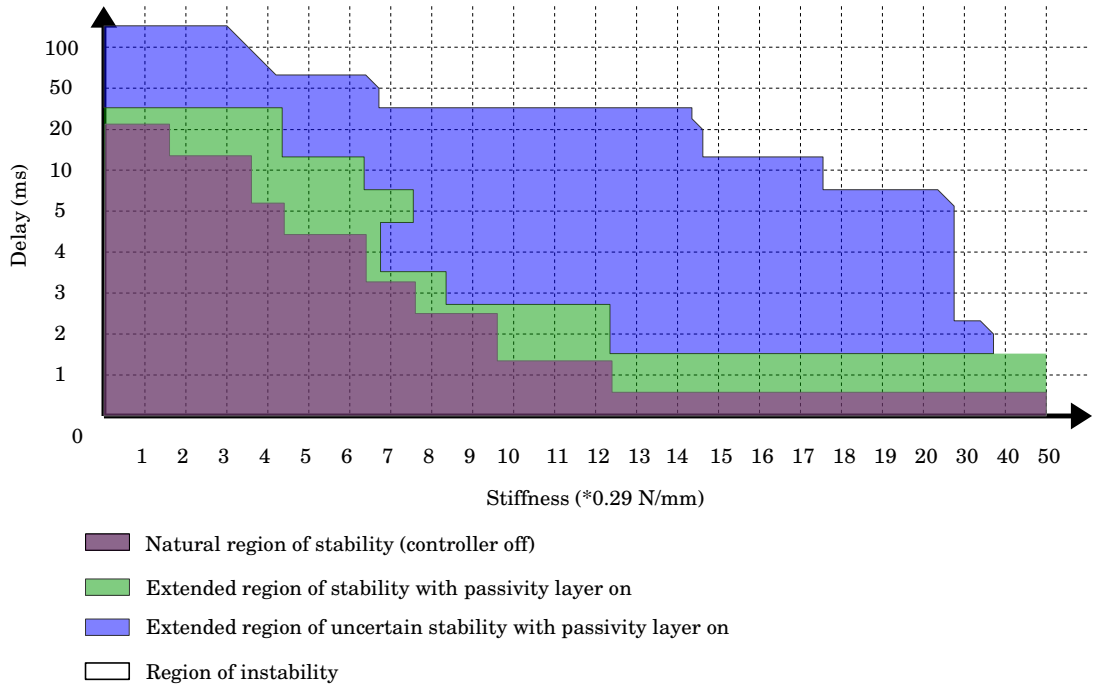

FIGURE 4.8. Table of operability regions: Soft grasp - Regions. Poke and drag on a surface with friction.

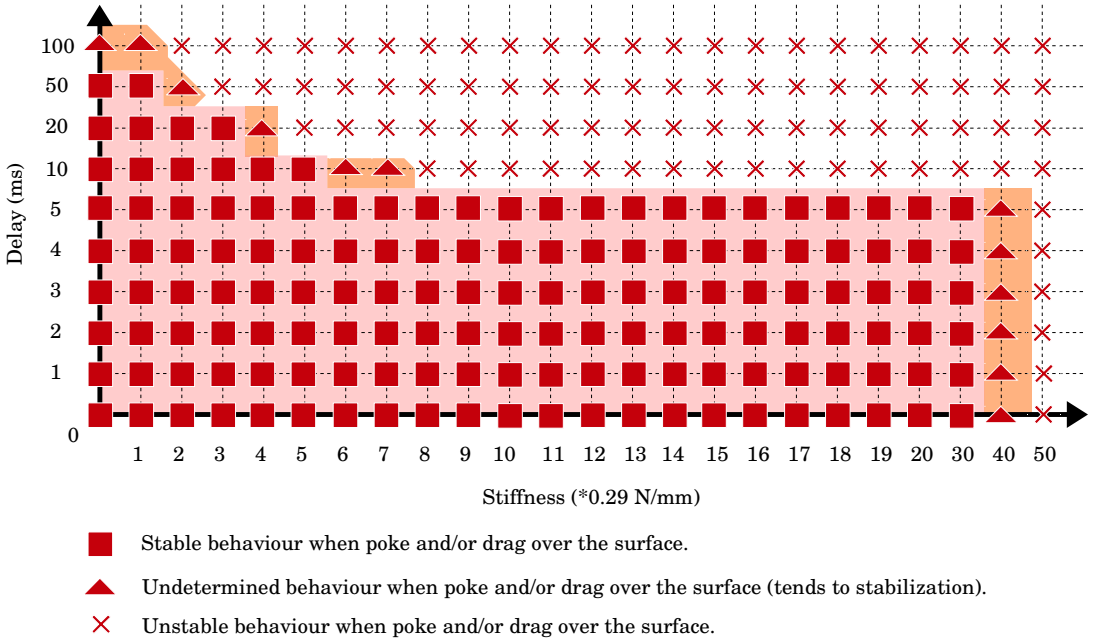

FIGURE 4.9. Table of operability regions: Strong grasp - NPC. Poke and drag on a surface with friction.

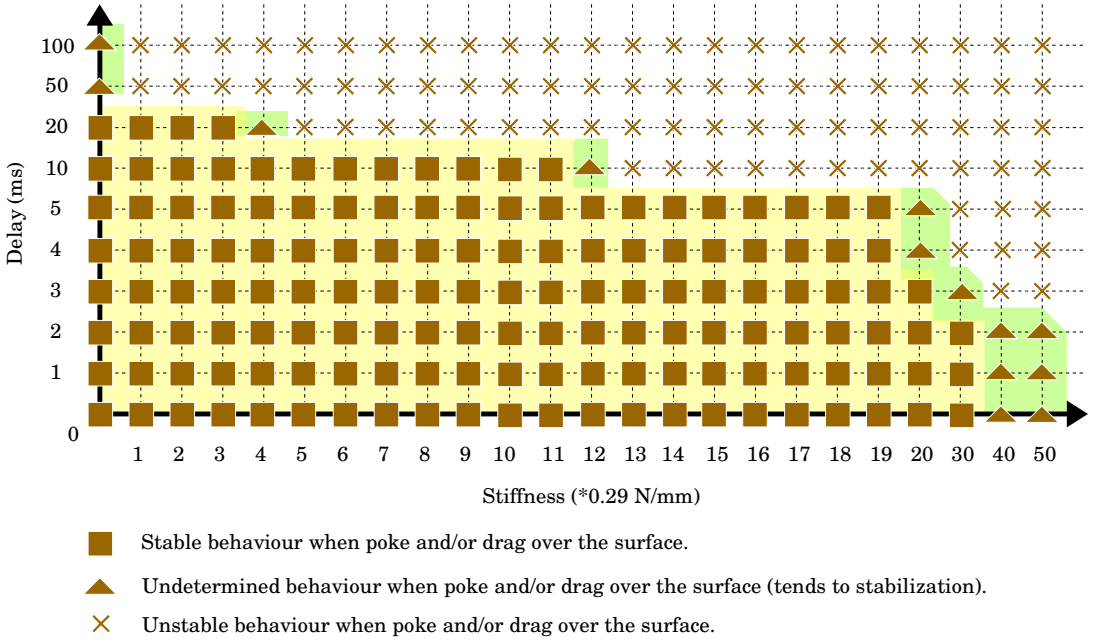

FIGURE 4.10. Table of operability regions: Strong grasp - STLC. Poke and drag on a surface with friction.

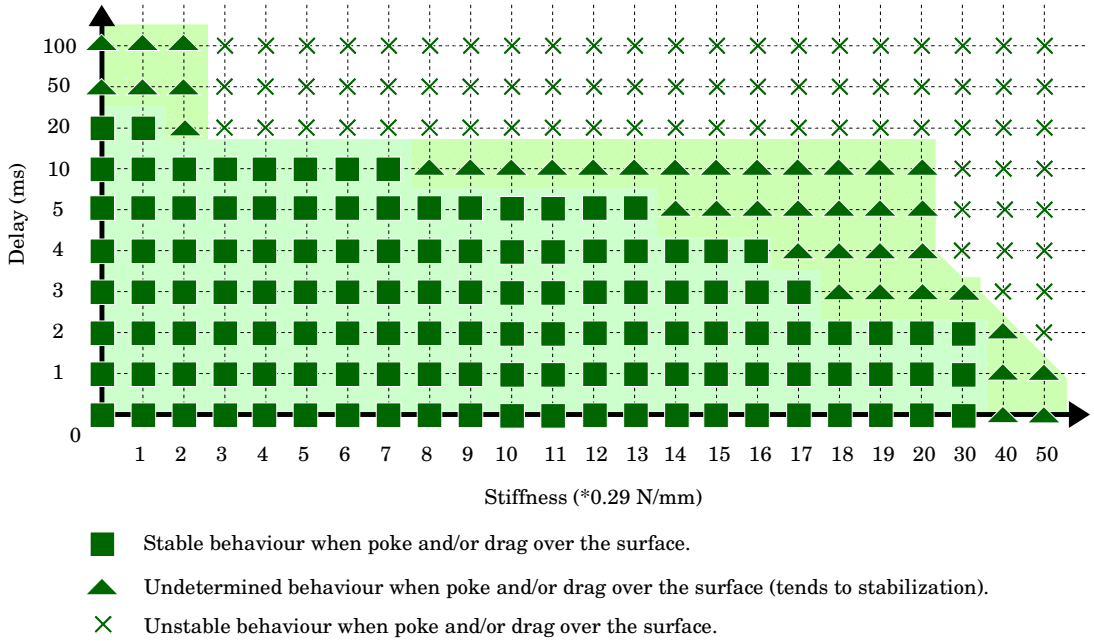

FIGURE 4.11. Table of operability regions: Strong grasp - TOPL. Poke and drag on a surface with friction.

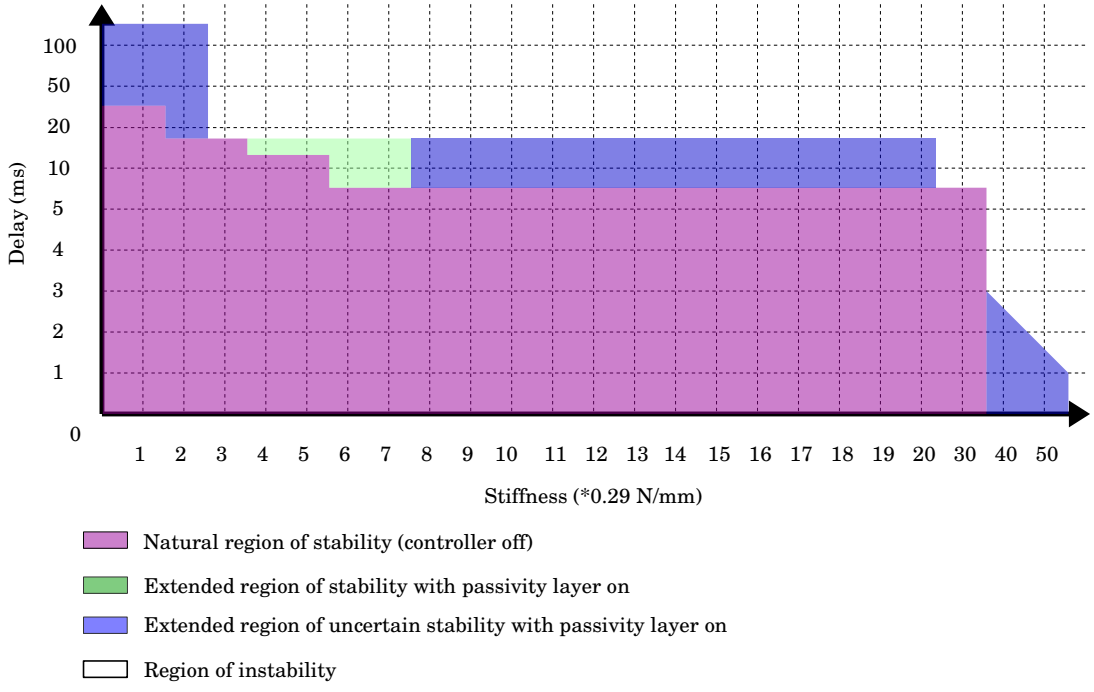

FIGURE 4.12. Table of operability regions: Strong grasp - Regions. Poke and drag on a surface with friction.

4.2 TOPL: Palpation Experiment (PE)

To evaluate the feasibility and effectiveness of the TOPL approach, a Palpation Experiment (PE) was carried out. A user with previous experience on haptic devices was asked to palpate a virtual surface and locate an area stiffer than the rest. The task performance was evaluated considering different controller types and experimental conditions, i.e., the delay T in the loop. Modifying some configuration parameters, such as time delay on the communication channel, or the stiffness of the remote environment, created conditions that may destabilize the system. The objective is to compare user performance in these different scenarios using the proposed controller with the controller proposed by Franken *et al.* [35] and with a controller that does not try to enforce the passivity of the system. Fig. 4.13 shows the experimental set up. A detailed explanation of each experimental component follows.

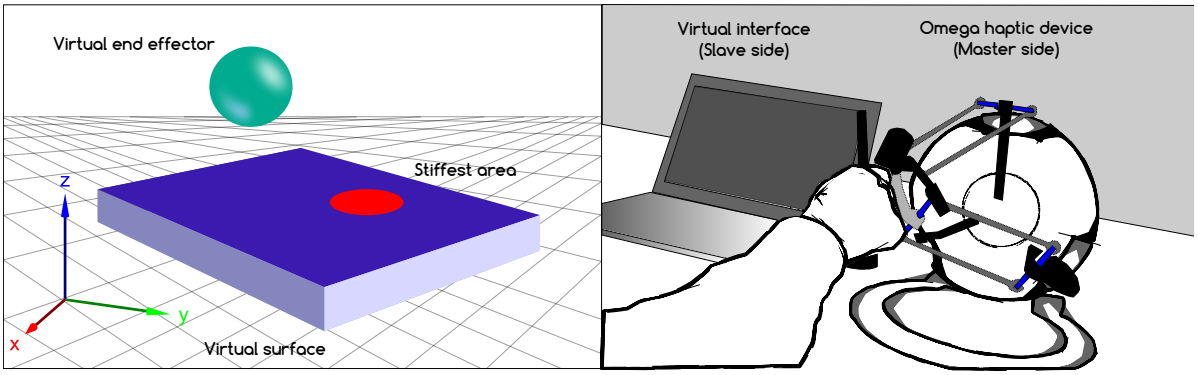

FIGURE 4.13. Experimental set up. On the left, the virtual environment (slave side) shows a contact area (the blue surface) with a stiffness value lower than the virtual "bump" (the red area). The end effector of the virtual environment is represented by the green sphere, and interacts with the surface, commanded by the master side. On the right side of the picture the Omega haptic device is shown. The virtual environment is an animated interface presented on the screen.

4.2.1 Experimental Set Up

The experimental set up consists of a system that follows the manipulation chain structure in Fig. 2.15 (see Sec. 2.3.3): master side, communication channel, and slave side. As shown in Fig. 4.13, the master side is composed of a human user holding the end-effector of a grounded haptic device, whose position is linked to the one of a virtual end effector in the virtual environment.

The user, by controlling the haptic interface, moves the virtual end effector and receives haptic feedback whenever it interacts with the virtual surface. The goal of the task is to identify, through palpation, the stiffest point on a virtual surface using the haptic device.

In order to perform the task and provide a reliable sensation of stiffness difference on the surface, a virtual "bump" is generated. A stiff circular region of 1 cm radius is positioned randomly on this virtual surface. In this region the stiffness is higher than in the surrounding surface, with the stiffest point lying on its centre (see Fig. 4.13). Differently from Fig. 4.13, during the experiment, the user was not provided with any visual information on the position of the stiffer region, and he had to rely only on force cues. Next, the user grasps the haptic device's end effector as a pen and is sitting on a chair in a comfortable position. After explaining the objective, a trial session is performed to get the user the experience of the environment interaction.

The task was performed nine times randomly by the user (see table 4.1), that means that the user does not experience different conditions with the same parameters. When each task is done, the user can see where the bump was, and a new task will run again. At the end, the user must fill up a survey.

Table 4.1: Experimental Task Sequence Example

Delay/Controller	NPC	STLC	TOPL
0.001 s	3	5	1
0.005 s	9	7	2
0.010 s	8	6	4

Table 4.1 describes an example of the experiment following three conditions. Each condition makes reference to the controller running on the system, for convenient proposes the name of the conditions are defined as follows:

- NPC: the system runs without controller,
- STLC: the system runs the Two-layer approach controller presented by Franken *et al.* [35],
- TOPL: the system performs the proposal described in Sec. 3.4.

Besides, each controller is configure to run with a time delay parameter. Every time delay parameter is considered as a region of performance, where the highest value is the most difficult region to develop the task. The user will experience each condition on the three regions with the next time delays: a) 0.001 sec, b) 0.005 sec, and c) 0.01 sec.

For a better understanding of the conditions, no controller means that the system is running on the most transparent way, the user performs the experience of manipulating the environment directly, and it is given from the forces at the slave side $\tau_s(t)$ to the master side $\tau_m(t)$ and the velocities as well $\dot{q}_s(t)$ and $\dot{q}_m(t)$ respectively. In this scenario, the forces rendered by the haptic device obey equation (3.31) [7, 236].

Finally, in the proposed controller condition, the forces rendered on the haptic device are dependant also on a transparency layer and passivity layer; but this last relays on the optimization process of (3.45) and (3.41) described in Section 3.4.

A) Communication Channel

This component represents the middle block of the telemanipulation chain as depicted in Fig. 2.1 in Section 2.1. The communication channel receives and distributes the signals between the master and slave sides. Those signals include the actions evaluated by transparency layer on the master side τ_{TLm} and the slave side τ_{TLs}. They also include the energy exchange information shared between master and slave. Finally, the communication channel introduces a time delay T (see (2.14)), which affects the forces and energy package distribution along sides.

$$\begin{aligned} \tau_m(t) &= \tau_s(t+T) \\ \dot{q}_m(t) &= \dot{q}_s(t+T) \end{aligned}. \tag{4.4}$$

It is carried out a palpation task simulating three communication delays T: 1 ms, 5 ms, and 10 ms. These delays were added up to the intrinsic delay of the system, which was measured to be on average 1.8 ms. At each time-step, a fraction β of the energy on one side is transmitted to the energy tank on the other.

B) Virtual environment

This element represents the slave side of the telemanipulation chain as depicted in Fig. 2.1 in Section 2.1. The virtual environment runs on a GNU/Linux machine using the Robot Operative System (ROS) framework. It was rendered using the RVIZ visualization tool, as shown in Fig. 4.13. It is composed of the virtual surface, which is modelled as a spring with elastic constant $K = 1$ N/cm (blue area in Fig. 4.13). Positions in the virtual environment are scaled by a factor of 100. As mentioned before, within this virtual surface, it was placed a stiffer 1-cm-radius circular region (red area in Fig. 4.13).

This stiffer area was modelled as a spring having elastic constant $K_H = 2$ N/cm. This area simulates a nodule or "bump", with maximum stiffness at its centre. When the end-effector penetrates the virtual surface the ideal force rendered on the z-axis, normal to the surface is:

$$\tau_e(k) = \begin{cases} -K_H(h_0(k) - q_z(k)) & \text{if on the stiffer area} \\ -K(h_0(k) - q_z(k)) & \text{otherwise} \end{cases} \tag{4.5}$$

Where K expresses the stiffness factor of the surface and K_H the stiffness factor of the stiffer region, given by (4.6), $h_0(k)$ is the z-position of the uncompressed surface and $q_z(k)$ the position of the virtual end effector along the z-axis. In equation (4.6), ρ is a fraction of the configurable stiffness K, $q(k)$ are the positions of the end effector, and r is the radius of the bump. The parameters of the virtual surface are defined in Table 4.2.

$$K_H = (2K + \rho)(q(k) - r). \tag{4.6}$$

When moving laterally across the surface, along axes x and y, the user is provided with force feedback about the friction of the surface, modelled using a standard Coulomb friction model with coefficient $\mu = 0.005$. Friction forces were implemented as described in Section 4.1.2. Also the haptic device (master side) is connected to the same computer system.

Table 4.2: Virtual Environment Properties

Subjects	2 (males)	
Task	dragging on the surface to find the bump	
Conditions	Stiffness (V. environment)	10 N/mm
	Friction coefficient (V. environment)	0.005
	Bump radius (V. environment)	1 cm
	Surface height (V. environment)	3 cm
	Surface width (V. environment)	11 cm

4.2.2 Controllers

To test the experimental set up, three controllers were used to have a comparison on the response and performance: a) No Passivity Controller (NPC), b) Simple Tank Level Controller (STLC) and c) Transparency-optimal Passivity Layer Controller (TOPL).

A) No Passivity Controller (NPC)

The first approach to be tested was a controller that directly transmits the forces and velocities between master and slave, without any concern for passivity, following equation (2.13) in Section 2.3.1.

B) Simple Tank Level Controller (STLC)

This controller follows the two-layer energy-based approach, presented by Franken *et al.* [35], where the force is limited by the energy available in the tank according to (4.7), and introduces a damping force on the master side. According to [35], the master side damping is implemented as:

$$
\begin{aligned}
F_{TLC} &= -d(k)\dot{q}_m(k) \\
d(k) &= \begin{cases} \alpha(H_d - H_m(k)) & \text{if } H_m < H_d \\ 0 & \text{otherwise.} \end{cases}
\end{aligned} \tag{4.7}
$$

where the damping gain α is set to 100, H_d is set to 0.2, and the energy exchange factor β described in Section 4.2.1 is set to 0.01.

C) Transparency-optimal Passivity Layer Controller (TOPL)

The approach described in Sec. 3.4.2 was implemented using the architecture in Fig. 3.4. First, the physical layer contains the haptic device (master) and the robotic manipulator (on this case a virtual end effector as a slave). On the physical layer the forces $\tau_m(t)$ and $\tau_s(t)$ act as inputs to the robots, and the positions $q_m(t)$ and $q_s(t)$ as outputs. These forces $\tau_{m,s}(t)$ are the result of the forces produced in the passivity layer and the transparency layer.

Second, the transparency layer manages the positions from the physical layer. The system uses Position to Force Control (PFC) in order to produce the forces $\tau_{TLm}(t)$ and $\tau_{TLs}(t)$. A switch block commutes the forces between the physical and transparency layer. When "no controller" mode is enable, the forces from the passivity layer $\tau_{PLm}(t)$ and $\tau_{PLs}(t)$ equal to zero.

Subsequently, the passivity layer contains the energy flow monitors, the energy tanks and the optimization process are marked as prioritizer (only on the master side), as seen in Fig. 3.4. The energy flow monitor performs the estimated loss of energy function described in (3.32); in the case of the master side, the energy flow monitor achieves the damping correction creating the force $\tau_{PLm}(t)$, when the transparent layer controller (TLC) sends to optimize forces ($\tau_{TLm}(t)$), velocities $\dot{q}_m(t)$ and desired level (H_{DK}) to the prioritizer block. In this controller, a dynamic threshold level $H_{min}(k)$ is implemented as follows:

$$H_{min}(k) = H(\overline{k+1}) + \eta(H_0 - H(\overline{k+1}))\|\dot{q}(k)\|^2, \tag{4.8}$$

the purpose of $H_{min}(k)$ is to shape the energy budget according to the available energy, the priorities defined in (3.45) and the current velocities, where H_0 represents a reference tank level to be maintained during transparent operation and $\eta > 0$ is a tunable parameter which acts as a proportional controller gain. The current energy level $H(k)$ modulates the damping correction forces $\tau_{TLC}(t)$, η is a configuration parameter that sets the instantaneous amount of energy that may be gained or lost. Equation (4.8) allows the system to recover energy when the level of energy is below the reference level H_0, as well as to limit the spending of energy when above. The norm of the current velocity is also weighted in the proportional controller gain in order to limit the damping forces generated by the passivity layer.

Given the aim of the experiment with respect to the virtual teleoperated environment, the subspaces $\mathscr{S}_i$, $i = 1,2,3$ have been defined as the three Cartesian axes x, y, z. The priorities $p_i(k)$ are taken to be constant. The highest priority was assigned to the projection on the z-axis, since the perception of the stiffness perpendicular to the surface is fundamental for the scope of the experiment, while friction forces on the horizontal (x, y) plane are assigned lower priorities. The priority values were set as $p_1(k) = p_2(k) = 0.1$, $p_3(k) = 0.5$. Lastly, the passivity layer contains the energy flow monitors, the energy tanks and the optimization process marked as prioritizer (only on the master side), as seen in Fig. 3.4.

The energy flow monitor performs the estimated loss of energy function described in (3.32); in the case of the master side, the energy flow monitor achieves the damping correction creating the force $\tau_{PLm}(t)$ when the transparent layer controller (TLC) sends forces, velocities and desired level to the prioritizer block. Finally, the energy tanks on the passivity layer perform the energy quantum exchange of $H_{-} = Hd(k)\beta$, that consist in exchanging constantly a small fraction of the energy contained in the tank from each side in order to maintain both tanks with the same level.

4.2.3 Validation

Beneficial to validate the proposed approach, a simple experiment was carried out, where a user teleoperated the slave robot to slide on the virtual surface over a stiffer region at a known location. The surface had a Coulomb friction coefficient $\mu = 0.005$, a maximum stiffness $K_H = 21.25$ N/mm at the centre of the stiffer region and $K = 10.00$ N/mm elsewhere. The communication between master and slave had a delay of $\Delta t = 1.7$ ms.

Fig. 4.14 shows a representative trial, capturing the moment when the user passes on the stiffer area of the environment. The forces computed by the transparency layer $\tau_{TL}(k)$ and the ones computed by the passivity layer $\tau_{PL}(k)$ along the z-axis are shown in the upper part of Figs. 4.14(a), 4.14(b), and 4.14(c). In the lower part of the same figures, it is possible to see the same forces $\tau_{TL}(k)$ and $\tau_{PL}(k)$ for x and y axes. In this case, a delay of 1 ms was present between master and slave.

When enforcing no passivity controller, the force measured in the virtual environment is directly provided to the user through the haptic interface, i.e., $\tau_{PL} = \tau_{TL}$ regardless of passivity constraints (see Section 4.2.2). Then, enforcing the STLC controller, a damping action is introduced along all directions when the energy tank level is below a predefined threshold (see Section 4.2.2). In the proposed TOPL approach, it is given a higher priority/importance to vertical forces, which are the most informative for the palpation task, at the expense of losing transparency when rendering the horizontal (friction) forces.

In this respect, it has seen that in Fig. 4.14(b) (STLC) corrective actions are taken along all directions. On the other hand, Fig. 4.14(c) shows that the proposed approach takes significant corrective actions along the non-preferred directions (x and y), while it preserves transparency along the preferred direction z, which is the most useful for the palpation task.

As the slave robot reaches the stiffer area, the user experiences a upwards force which leads to a velocity in the same direction. A damper acts against this movement and thus, the vertical force that is rendered to the user is not exactly the one measured at the slave side. Conversely, after the user passes the centre of the stiffer area, the downwards movement of the user causes an upwards damping force. In summary, these corrections cause the user to feel an erroneous impedance of the environment.

In the proposed controller (TOPL) shown in Fig. 4.14(c), the vertical forces that are rendered at the master side follow very closely the forces measured at the slave side. Passivity conditions

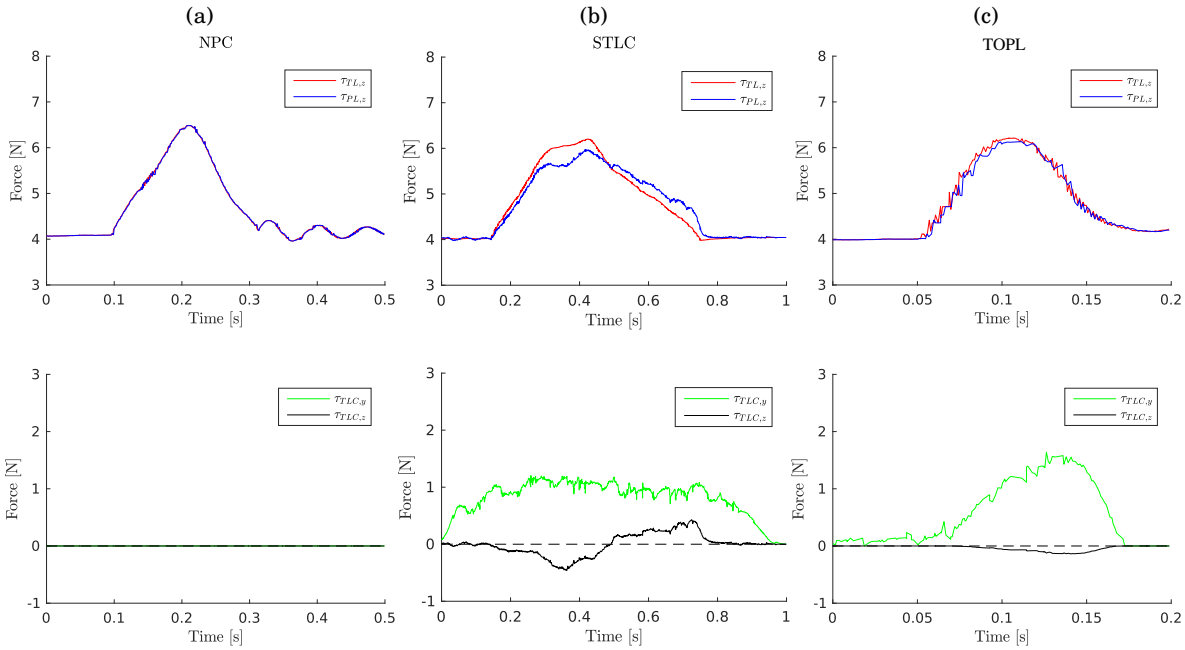

FIGURE 4.14. Forces of the three experimental conditions with a pass over the bump. (a) shows the $\tau_{TL,z}$ and $\tau_{PL,z}$ forces when the end effector passes over the bump; as seen, $\tau_{TL,z}$ follows $\tau_{PL,z}$ presenting the most transparent scenario (NPC). (b) presents $\tau_{TL,z}$ and $\tau_{PL,z}$ forces when STLC controller is running, as well the $\tau_{TLC,y}$ and $\tau_{TLC,z}$forces, that belong to the correction phase. (c) displays the $\tau_{TL,z}$ and $\tau_{PL,z}$ forces when TOPL controller is working and the damping correction on $\tau_{TLC,y}$ and $\tau_{TLC,z}$ forces.

are enforced by sacrificing transparency on the horizontal plane. This transparency along the direction normal to the surface allows the user to have a better feeling of the impedance of the environment.

The root mean square (RMS) of the y-axis force correction was 1.0 N for TLC and 0.99 N for the proposed controller, while for the vertical (z)-direction, the RMS of the correction forces was 0.24 N and 0.07 N respectively.

Also, when moving the end-effector across the virtual surface and passing over the stiffer circular area, the direction of motion therefore evolves along the axes parallel y and perpendicular z to the surface. The velocities and energy tank levels are included into the discussion for comparison and better understanding of the TOPL controller.

The results of the NPC case are depicted in Fig. 4.15. The forces τ_{TL} and velocities $\dot{q}$ are the same in the master side (left) and the slave side (right). The colour notation for the axis (forces and velocities) are: red for the x, blue for the y and green for the z[5]. In the absence of a controller,

[5]Parts of this section have been published in: Bianchini, G., Bimbo, J., Pacchierotti, C., Prattichizzo, D., & **Moreno, O.,** (2018, December). Transparency-oriented passivity control design for haptic-enabled teleoperation systems with multiple degrees of freedom. In *IEEE Conference on Decision and Control (CDC)*.

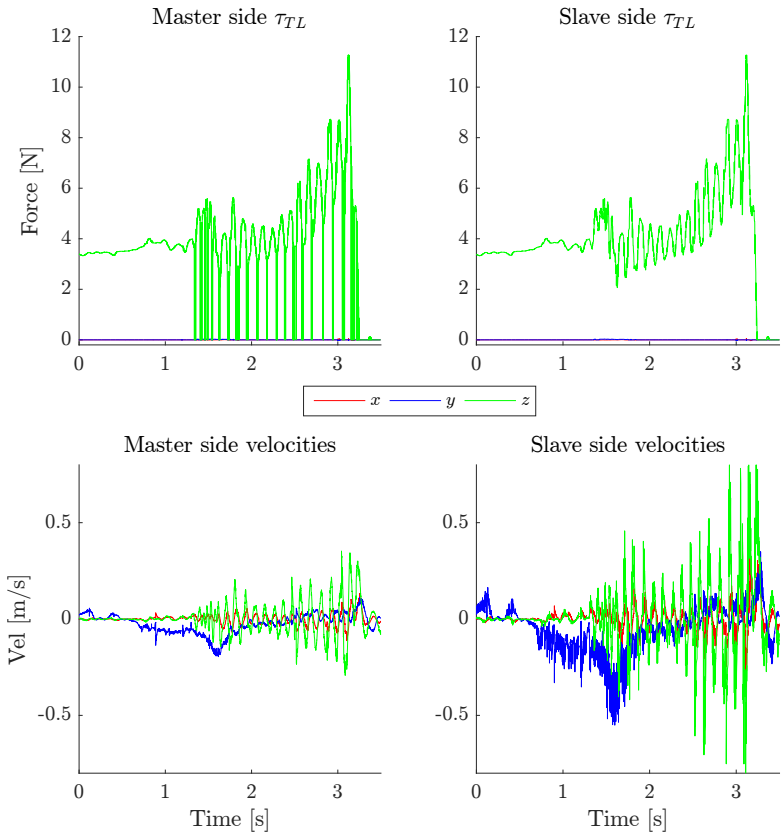

FIGURE 4.15. No Passivity Controller (NPC) case. [Top] Transparency layer forces τ_{TL} at master (left) and slave side (right). [Bottom] Velocities $\dot{q}$ of the master and slave sides.

it is apparent that persistent oscillatory behaviours show up for the considered values of the system parameters.

The STLC run is represented in Figs. 4.16. On the master side are depicted τ_{TL}, τ_{PL} and τ_{TLC} forces, also velocities $\dot{q}$ and energy tank level H. The slave side depicts the same information as in the master side except for τ_{TLC} forces, due to the TLC implementation belongs only to the master side. The colour notation for the z-axis in transparency and passivity layer are: green for τ_{TLz} and black for τ_{PLz}. The colour notation for the axis (forces and velocities) are: red for the x, blue for the y and green for the z. The colour notation for energy tank levels H are: red for the master and black for the slave. The force peak along z corresponds to the end effector passing over the stiffer spot. Note that relevant force corrections are applied by the passivity layer along all axes. On top, it is appreciated "the pass over the bump" and how the passivity layer τ_{PLz} follows the transparency layer τ_{TLz}. An oscillation as part of the surface mechanics and the user grasp is registered. In the middle, the τ_{TLC} forces are seen performing the correction, τ_{TLCz} presents the higher value of correction while τ_{TLCx} and τ_{TLCy} shows a lower level of damping.

Fig. 4.17 depicts master-side forces along the x and y axes on a different scale for clarity. The

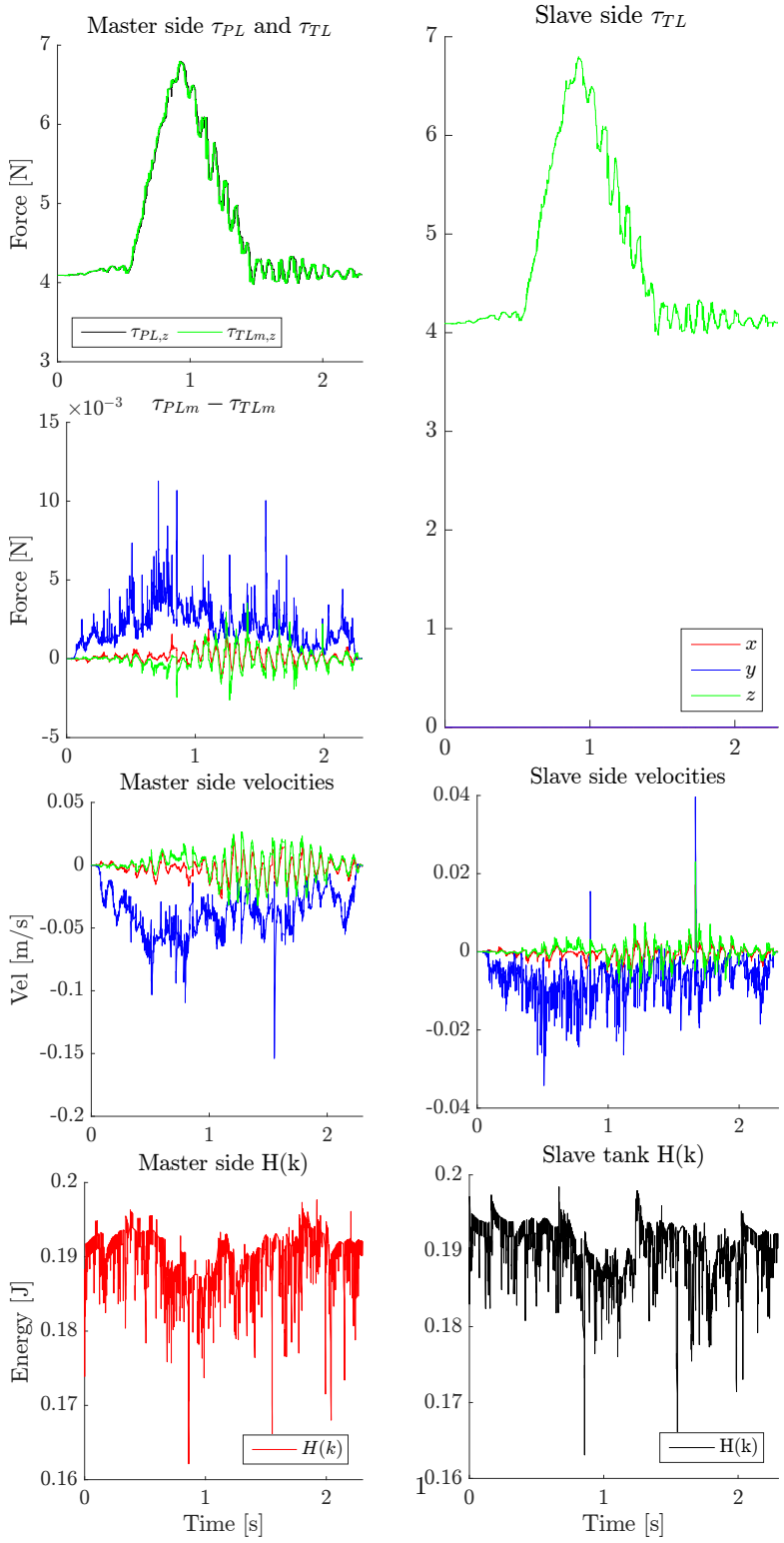

FIGURE 4.16. Standard Tank Level Controller (STLC). [Top] Forces τ_{TL} and τ_{PL} at the master (left) and slave (right) side. [Middle-top] Overall force correction $\tau_{PL} - \tau_{TL}$ enforced by the passivity layer at the master. [Middle-bottom] Velocities $\dot{q}$ in both sides. [Bottom] Energy tank levels H at both sides.

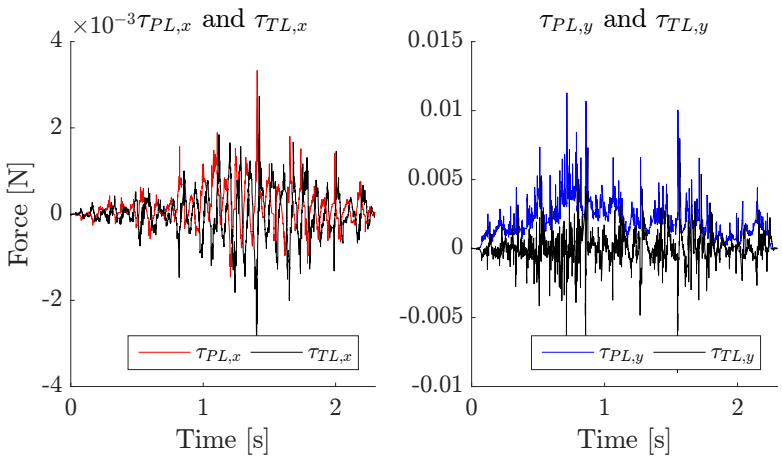

FIGURE 4.17. STLC. Transparency layer τ_{TL} and passivity layer τ_{PL} forces at the master side along the x (left) and y (right) axes.

colour notation for the x-axis are: red for τ_{PLx} and black for τ_{TLx}. The colour notation for the y-axis are: blue for τ_{PLy} and black for τ_{TLy}. Since the run over the "bump" is along the y-axis, the correction forces applied on that axis are higher than in the x-axis. The forces displayed on the x-axis show the non ideal trajectory followed by the user and the friction effect.

Finally, results from the TOPL run are depicted in Figs. 4.18. On the master side are shown τ_{TL}, τ_{PL} and τ_{TLC} forces, velocities $\dot{q}$ and energy tank level H. The slave side depicts same information as the master side except for τ_{TLC} forces. The colour notation for the z-axis in transparency and passivity layer are: green for τ_{TLz} and black for τ_{PLz}. The colour notation for the axis (forces and velocities) are: red for the x, blue for the y and green for the z. The colour notation for energy tank levels H are: red for the master tank level $H(k)$, blue for the master dynamic desired level H_{min} and black for the slave energy tank level $H(k)$. On top, it is appreciated "the pass over the bump" and how the passivity layer τ_{PLz} follows the transparency layer τ_{TLz}. An oscillation is registered as part of the surface mechanics and the user grasp. In the middle is seen the τ_{TLC} forces performing the correction with the TOPL controller. τ_{TLCy} presents the higher value of correction while τ_{TLCx} and τ_{TLCz} shows a lower level of damping. As opposite to the STLC case, the force correction τ_{TLC} introduced by the passivity layer is much more significant along the low-priority directions x and y than along z, thus indicating better transparency preservation on the latter subspace.

Fig. 4.19 shows master-side forces along the x and y axes on a different proportion for a better definition. The colour notation for the x-axis are: red for τ_{PLx} and black for τ_{TLx}. The colour notation for the y-axis are: blue for τ_{PLy} and black for τ_{TLy}. Similar to Fig. 4.17, the forces on the y-axis are higher in the x-axis, but, in comparison to Fig. 4.17, the forces are minor due to the optimization on the preferred direction.

In order to further test the proposed approach, a human subject carried out 48 repetitions of

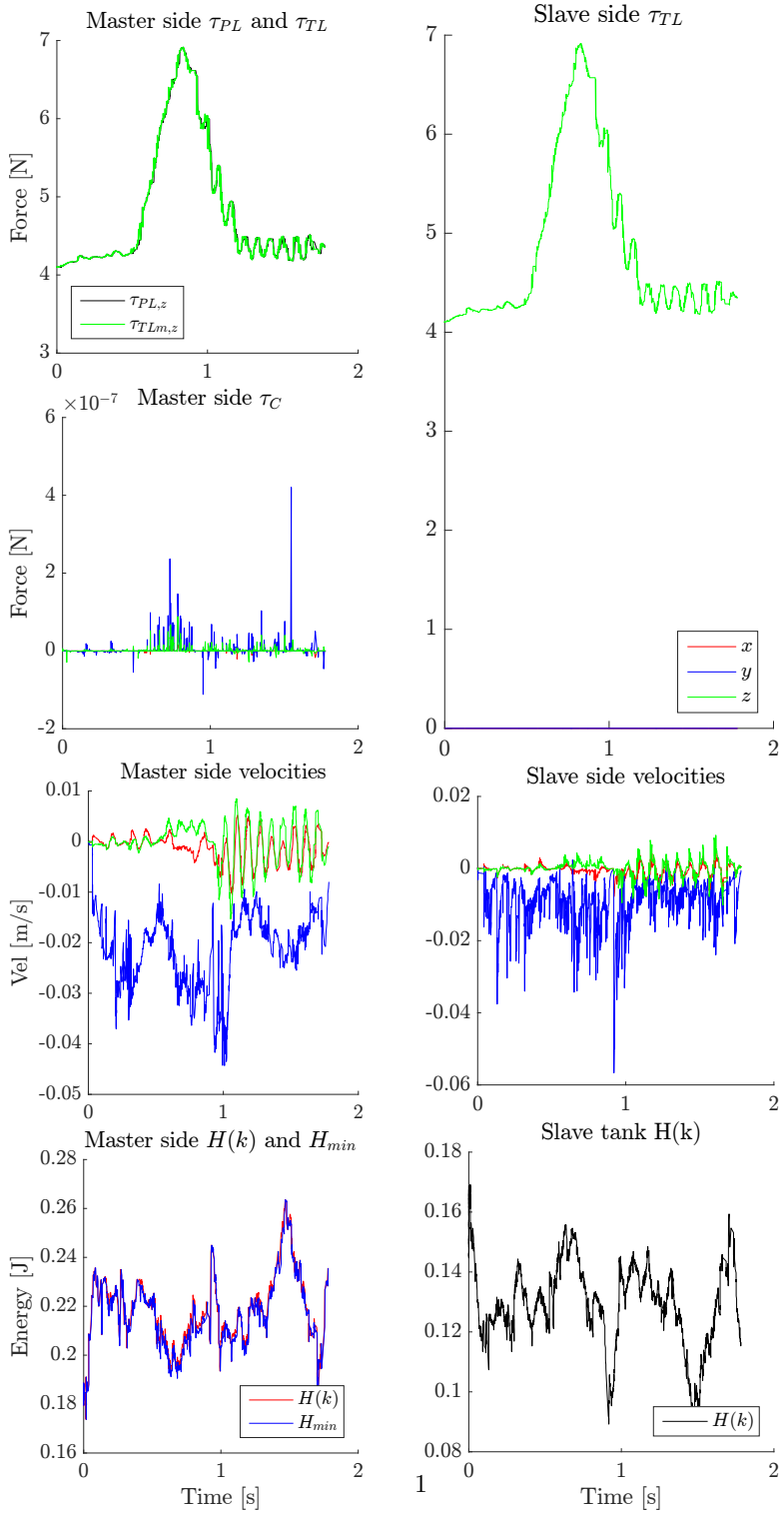

FIGURE 4.18. Transparency-Oriented Passivity Layer (TOPL). [Top] Forces τ_{TL} and τ_{PL} at the master (left) and slave (right) side. [Middle-top] Force correction τ_{TLC} enforced by the passivity layer at the master. [Middle-bottom] Velocities $\dot{q}$ at both sides. [Bottom-left] Energy tank level H and dynamic threshold value H_{min} at the master side. [Bottom-right] Energy tank level H at the slave side.

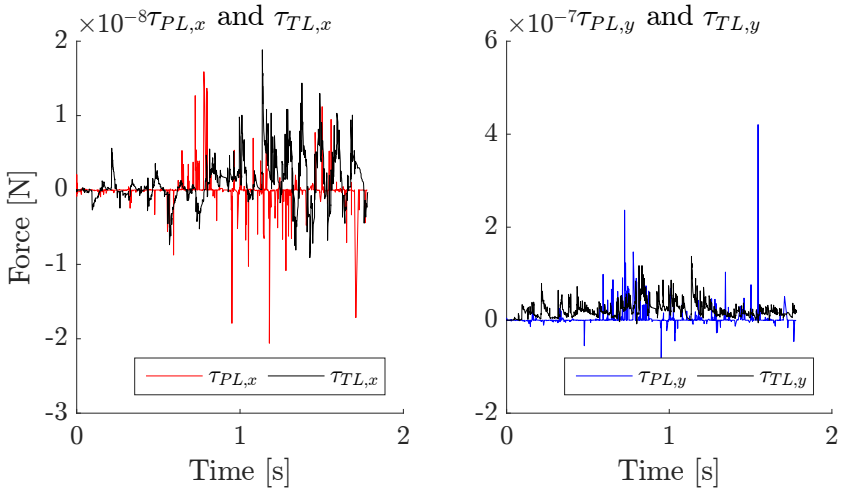

FIGURE 4.19. TOPL Transparency layer τ_{TL} and passivity layer τ_{PL} forces at the master side along the x (left) and y (right) axes.

the palpation task. The user was asked to find the location of a 3.14 cm^2 stiffer region placed on the virtual surface, as described in Section 4.2.1. The performance of the three controllers described in Section 4.2.2 have been compared, each tested when simulating three different communication delays between master and slave (1 ms, 5 ms, or 10 ms). To evaluate the effectiveness of the proposed system in correctly rendering the stiffness of the environment, the accuracy error in detecting the stiffer area within the virtual surface has been registered . Fig. 4.20 shows this result in the nine different experimental conditions.

To compare this metric among the conditions, a two-way repeated-measures ANOVA test on the data was ran. Time delay in the communication (1 ms vs. 5 ms vs. 10 ms) and stability controller (no controller, NPC vs. Franken *et al.* [35], STLC vs. the proposed approach, TOPL) were treated as within-subject factors. All data passed the Shapiro-Wilk normality test. Interaction effects between the factors were not statistically significant. Mauchly's Test of Sphericity indicated that the assumption of sphericity had been violated for both variables (delay, $\chi^2(2) = 23.148, p < 0.001$; controller, $\chi^2(2) = 15.987, p < 0.001$).

The two-way repeated-measure ANOVA with a Greenhouse-Geisser correction revealed statistically significant difference between the time delays ($F_{1.005,6.029} = 6.815, p = 0.011, a = 0.05$, partial $\eta^2 = 0.533$) and stability controllers ($F_{1.021,6.125} = 17.701, p < 0.001, a = 0.05$, partial $\eta^2 = 0.745$).

Post hoc analysis with Bonferroni adjustments revealed a statistically significant difference between having a 1 ms vs. a 5 ms delay ($p = 0.019$) and a 1 ms vs. a 10 ms delay ($p = 0.047$). Similarly, it revealed a statistically significant difference between enforcing NPC vs. STLC ($p = 0.007$), NPC vs. TOPL ($p = 0.017$), and STLC vs. TOPL ($p = 0.044$).

Fig. 4.21(a) shows the user accuracy in terms of detection error when using the three control

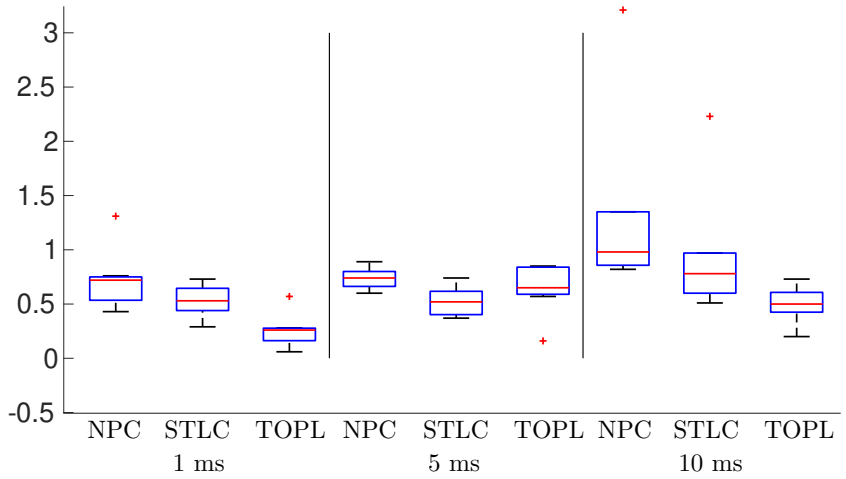

FIGURE 4.20. Mean accuracy error (cm) in detecting the stiffer area within the virtual surface. Controllers NPC, STLC and TOPL are plotted.

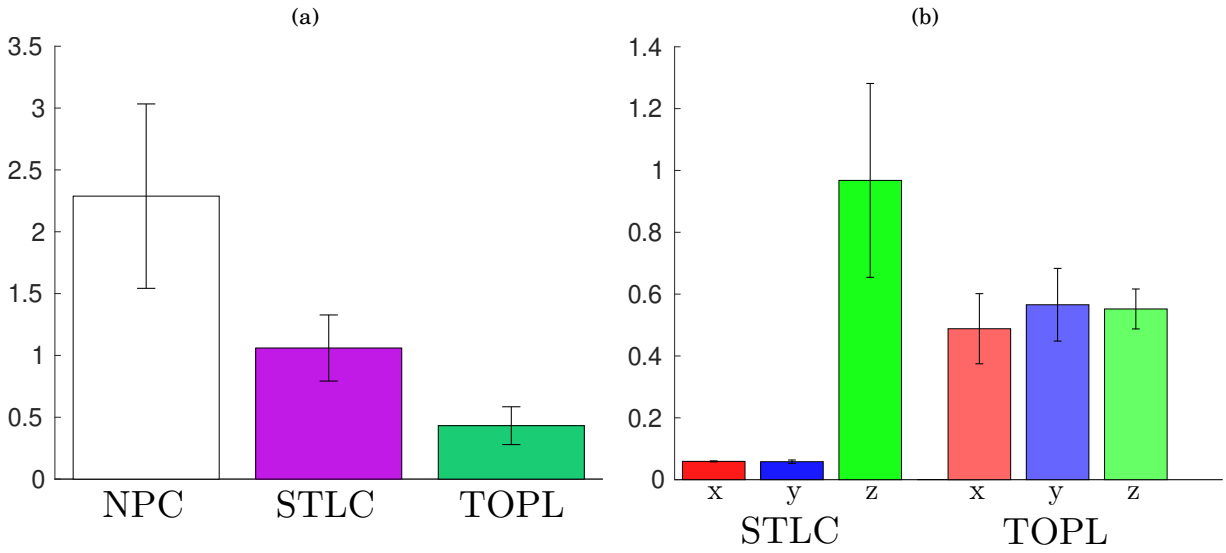

FIGURE 4.21. Results of the palpation experiment: (a) Accuracy (error) in detecting the stiffer area (cm). (b) Normalized RMS of the error between ideal and applied forces along the three axes.

modalities. As far as metric (ii) is concerned, Fig. 4.21(b) shows the RMS of the force correction enforced by the controller, i.e., the difference τ_{TLC} between the applied (τ_{PL}) and ideal (τ_{TL}) forces along the three axes, when using the STLC and TOPL control modalities.

4.3 Results

To evaluate the feasibility and performance of the proposed passivity approach (TOPL), an experiment was carried out in a simulated environment (see Sec. 4.1.1). The user was asked to palpate a virtual surface and search for a circular area of 2 cm diameter which is stiffer than the rest. The user's accuracy was tested in finding such area considering three different controllers (no controller (NPC), Franken *et al.* [35] (STLC), the proposed passivity approach (TOPL)), and three different communication delays between master and slave (1 ms, 5 ms, and 10 ms).

The hypotheses were that as the communication delay increases, if no controller is implemented, the teleoperation system becomes unstable; conversely, the system remains always stable if one of the two considered passivity controllers are enforced. Moreover, as the communication delay increases, it is also expected that the TOPL approach to better preserve the transparency along prioritized directions with respect to the approach of Franken *et al.* [35], which does not make any difference between directions. Both hypotheses were confirmed by the palpation experiment.

When a delay of 10 ms was introduced in the system, the experiment was very difficult to complete, as oscillations arose during the palpation. This unstable behaviour led to a significantly worse accuracy with respect to the other conditions (see Fig. 4.20) as well as to a very high task completion time (not reported in the figures). The subject repeatedly complained about this oscillation-prone behaviour, and he was often forced to increase the grasping force on the haptic interface handle to prevent it from vibrating uncontrollably.

On the other hand, the interaction was safe and stable when any of the two passivity controllers were in place. Between the two controllers, the proposed approach (TOPL) outperformed the one presented by Franken *et al.* [35]. This result is not surprising, as the TOPL controller makes use of additional information about the task, i.e., the importance of the different subspaces. This additional information is used by the TOPL controller to better distribute the energy available in the system, privileging forces rendered along the z-axis with respect to those rendered along the other axes.

Whenever it is needed to reduce transparency to preserve stability, Franken *et al.* [35] corrects the forces along all axis in a similar way. Conversely, the TOPL controller corrects very little along the privileged z-axis, while it significantly corrects the forces along the other axes. This behaviour resulted in higher transparency along z at the cost of sacrificing transparency along x and y.

Comparing the correction applied on $\tau_{TL}(k)$ on the z-axis between the (STLC) and the proposed (TOPL) controller, it is notable a higher correction in figure 4.14(b); which leads into a higher transparency displayed in figure 4.14(c). Finally, the correction of $\tau_{TL}(k)$ of the y-axis is higher on 4.14(c), rather than 4.14(b).

As presented in Fig. 4.20, the accuracy of the user is compared in three different regions of time (1 ms vs, 5 ms vs. 10 ms) where the highest time delay produces drastically more destabiliza-

tion on the system, which is translated of an non optimal force feedback sensation. In terms of performance, the user presents high accuracy on regions 1 ms vs. and 10 ms comparing the proposed TOPL controller and STLC controller. In the 5 ms region the proposed controller performs accurately as the STLC controller. The proposed TOPL controller generates damping correction forces displayed at the haptic device, and with this correction provides enough information on a preferred direction, thus, the user finds the bump.

Forces shown in figure 4.14 represent a pass of the end effector over the stiffest area according to the running controller (NPC, STLC, and TOPL). The transparency $\tau_{TL}(k)$ and passivity $\tau_{PL}(k)$ forces of the z-axis are shown on the top of figure 4.14(a), 4.14(b), 4.14(c). The bottom of the image presents the correction $\tau_{TLC}(k)$ forces of the axis x and y. When NPC mode is running, the $\tau_{TL}(k)$ force equals $\tau_{PL}(k)$ force, in contrast with STLC controller and the TOPL controller, the $\tau_{TL}(k)$ force tends to follow $\tau_{PL}(k)$ force in order to be as much transparent as possible. Comparing the correction applied on $\tau_{TL}(k)$ of the z-axis between the STLC controller and the proposed controller, it is notable a higher correction in figure 4.14(b); which leads into a higher transparency displayed in figure 4.14(c). Finally, the correction of $\tau_{TL}(k)$ of the y-axis is higher on 4.14(c), rather than 4.14(b).

CHAPTER 5

SOFTWARE IMPLEMENTATION

The first part of this chapter introduces an interactive simulator to provide customized functions suited to the user when working with energy-based tank controller. The second part describes the software (developed in ROS) used in the experiments shown in this thesis.

5.1 Interactive Simulator of Energy Tanks Behaviour for Passivity Control

On research, simulation has been adopted as a validation tool to support experimental implementations. The simulation permits diverse interfaces and applications to be analysed and evaluated without having the equipment/machine/device physically present [273]. A wide variety of simulators are developed to target specific applications, and the lack of functionalities or missing capabilities could invalidate a proper experimental set up, risking the potential of a real implementation. For this reason, it is proposed a standardized tool as a visual element that depicts the energy tank behaviour on telemanipulated systems.

The aim is to replicate the energy tanks behaviour of a telemanipulation system based on the two-layer approach (see Section 2.3.3) when the user interacts with a virtual environment. In a more specific way, this simulator was designed to reproduce the energy package exchange protocol and visualize this process on an interactive platform.

The typical telemanipulation system (see Fig. 5.1) is divided in two elements: *a) Master* and *b) Slave* sides; in the middle a communication channel provides the medium to exchange information between both sides. In this medium, information such forces $\tau(k)$, positions $q(k)$ or energy $H(k)$ is transmitted from the master to the slave and vice-versa; in this topic, energy

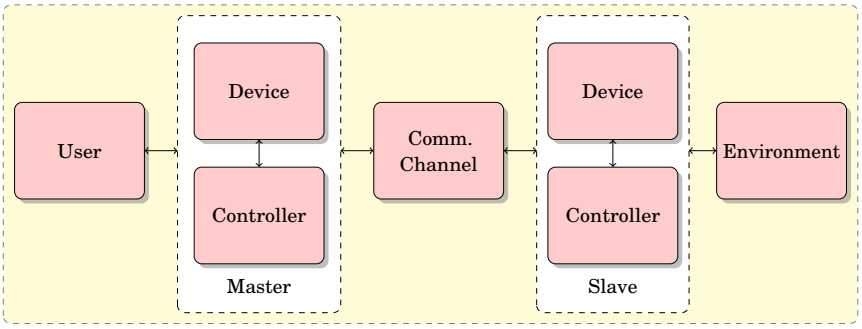

FIGURE 5.1. Schematic diagram of the telemanipulation chain.

plays an important role regarding the passivity of the system. As mentioned before, in order to preserve passivity the two-layer approach based on energy tanks is implemented; the energy provided to the slave side is limited by the energy obtained from the user at the master side. This energy is generated by a damping-like element that is activated when the current energy level is under the desired level. This process is visualized with an interactive tool to simulate the load and download of energy at the tanks.

5.1.1 Proposed Simulator Design

As Fry mention in [274], when abstract data is used, a visualization tool gains relevance in order to understand its functionality. The issue of perception wires the human brain to understand visual stimuli and aids the limited mental capacity with external cognition. As mention by Reas in [275], one the main ideas of a behavioural model of interaction is to develop a method that could engage the user with the next qualities:

- perception of control,
- responsiveness,
- unpredictability,
- engagement with the body,
- nuance of communication.

To reach these qualities, the simulator proposed here was designed in the Processing[1] framework as an interactive platform. This tool shows a graphical interface of the telemanipulation chain, where all the components are virtual except the user. Therefore, it is possible to interact with an environment and adjust parameters, such as the tank desired level, distance of the environment, and master's end effector. Visual animation and signal plotting are also available

[1]Processing Framework. Website: *https://processing.org/*

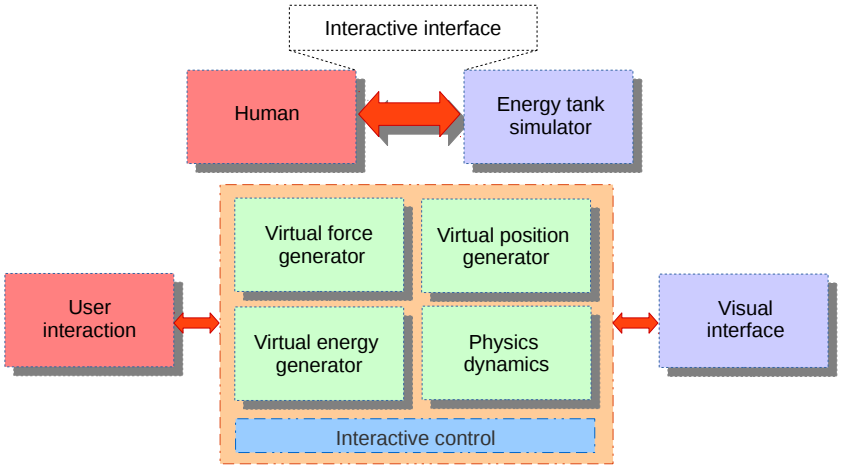

FIGURE 5.2. Energy tank simulator interactive interface design.

whilst the user interacts with the platform. Fig. 5.2 depicts the interactive interface which contains the following elements:

- Virtual force generator. Since there is no force sensor to measure the user's interaction, the forces are computed as a relation of the velocities. Using values on a range of "real force values" that are operable by the mechanic haptic device and the remote robot.
- Virtual positions generator. The virtual positions are computed according to the end-effectors' distance difference when the user interacts with the interface.
- Virtual energy generator. The energy is processed using the virtual force and velocity with the energy exchange model presented in Section 3.2.
- Physics dynamics. The interactive interface provides a physic dynamics engine to compute collisions and displacements of the simulation.

The simulator runs in two modes: *a) Direct transparency* and *b) Tank level controller*. For the first mode, there is no energy transfer protocol regulated in neither of the tanks, the slave side is commanded directly by the master, and the impedance reflection in the master is not affected by the force feedback signal from the slave. In the second mode, the tank level controller regulates the energy transfer protocol following the rules as described above. Also, a force sensor as a feedback signal is provided at the slave's side for interaction with the environment.

A) Processing Framework

As defined by Fry and Reas [276], *Processing* is an environment and programming language designed for the media arts community. One of the most important aspects of the framework lies in the component visual form, motion, and interaction of the data. On a general feature,

Processing provides a simple interface for users starting from scratch, where rapid prototyping can be developed with a small fraction of code[2]. The environment is set up as a collection of sketches, it is possible to combine those from several developers among the Processing community, also from the Library import section[3]. The literature referenced for the interface design can be consulted in [277–281].

Processing was chosen in this work for the multi-cross platform flexibility, the visual factor of the interface, and the support of standardized code such as C and C++ language. By the author's criteria is important to considerer the animations are designed in a 2D environment, while the real approach is developed in a 3D one. Undoubtedly, it is also important having the interactive interface for a better understanding of the Energy Tank concept; the algorithms used in the animations are portable to real environments, for instance the Robotics Operative System (ROS) [269] that interacts with the physical world. Finally the released version of the Energy Tank Simulator is located in the Processing Forum community for use and consulting[4].

B) Simulator Description

The architecture of the energy tank simulator is defined according to the telemanipulation chain block diagram: master's objects on the right and slave's objects on the left. Each side is composed of three windows areas as shown in Fig. 5.3: *a) Signal plotting*, *b) Tank level*, and *c) Device's end-effectors*. The resolution of the main window is 800 x 600 pixels to fit in standard monitors.

At the top of the window is visible the signal plotting area. In this zone are plotted the displacements, tanks levels, and forces signals for both sides. There is an interactive menu selector to print on screen the name of the signal for a better reference.

In the middle of the window there is the tank level animation area, it presents two tanks for the master and the slave's sides respectively. Under the master's tank there is a slider to set up the desired level. It is not possible to run the tank level controller mode of the simulator if the user has not set up yet the desired energy level. The mode selector switch is located under the slave's tank area.

At last, there are the end effectors areas, the master's side one is interactive, whilst the slave's side one is animated. To interact with the master side, the user just makes a simple click on the effector realising the mouse button; to stop the interaction the mouse button should be pressed again over the master's end effector. Every moment there is a impedance reflection on the master side, a damper icon will appear on the master's end effector. Above the slave's end effector, there is a slider to adjust the distance of the environment ("wall") to the end effector. Finally, the slave's end effector has a force sensor on the right side presented as a blue line in the animation.

[2]Processing Integrated Development Environment. Website: *https://processing.org/reference/environment/*
[3]Processing Libraries. Website: *https://processing.org/reference/libraries/*
[4]Processing Forum Community. Website: *https://discourse.processing.org/*

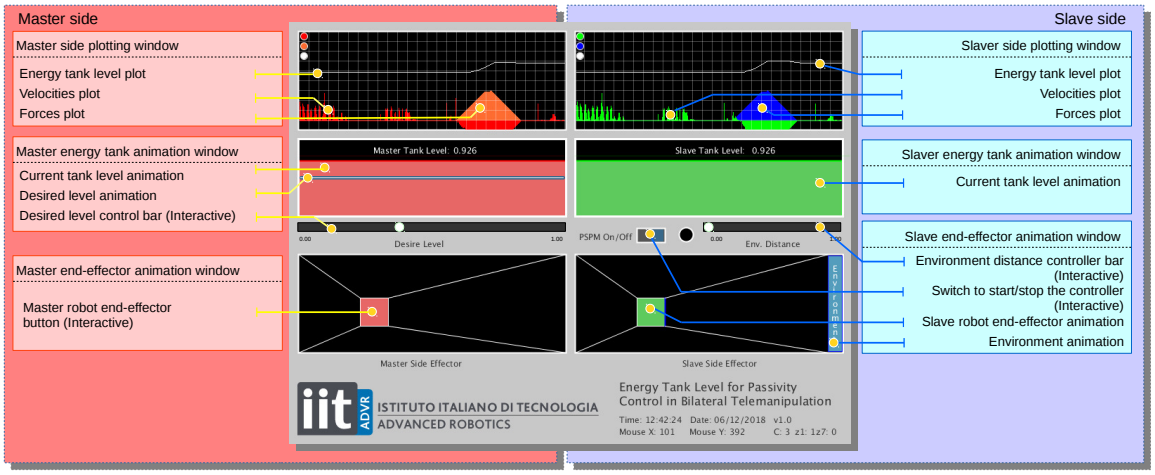

FIGURE 5.3. Energy tank simulator interface description.

C) Simulator Method

Animations in the Processing Framework are described by mathematical expressions. In order to generate signals in the plotting area, the model for the displacement signal is given by the average of $\Delta|x|$ and $\Delta|y|$ (5.1), which is the difference in position between the current and the previous displacement.

$$p = \frac{\Delta|x| + \Delta|y|}{2}, \; |x| \geq 0, \; |y| \geq 0 \tag{5.1}$$

where $\Delta|x|$ and $\Delta|y|$ are described by the parameters of current and previous sampled positions $x(t)$ and $x(t-1)$, and $y(t)$ and $y(t-1)$, respectively.

$$p = \frac{(|x(t-1) - x(t)|) + (|y(t-1) - y(t)|)}{2}, \; |x| \geq 0, \; |y| \geq 0\,. \tag{5.2}$$

Since the only information input source for the user is the mouse, the simulation of the force is given by the following equation where K represents a constant value (for simulation purposes) and $\Delta(p)$ is the difference between the last sampled position and the current one.

$$F = -K\Delta(p)\,. \tag{5.3}$$

The energy tank behaviour is governed by the transfer protocol controller algorithm. As described in (5.1), there is a fraction of the energy (β) exchanged among the tanks. For simulation purposes the value of β is set to 0.1, the code shown next contains the sequence of the TLC behaviour; the variables "vt1" and "vt2" stand for virtual tanks (master and slave respectively),

"tx12" is the transfer variable from master to slave's side, and "tx21" represents the opposite transfer variable. Finally, "lim" is the limit variable and depends on the plotting area, when the energy tank level reaches the maxim, the energy is virtually dissipated. It is important to to place the fraction energy (β) in the transfer variables before making the energy exchanges between the tanks.

Transfer Protocol Controller Algorithm

```
if (vt1>=0) {
    if (vt1>lim) {
      vt1=lim;
    }
    if (vt2>lim) {
      vt2=lim;
    }
    tx12 = vt1*0.1;
    tx21 = vt2*0.1;
    vt1=vt1-tx12;
    vt2=vt2+tx12;
    vt2=vt2-tx21;
    vt1=vt1+tx21;
  } else {
    vt1=0;
    vt2=0;
  }
}.
```

(Code from Energy Tank section, main Processing Framework sketch)

Lastly, the virtual force feedback sensor "fss" is modelled as a contact sensor that increases its value as it stays in touch with the environment until a limit. When the contact stops, the sensor value will decrease to zero. The behaviour is described by:

$$fss = \sum_{i=0}^{lim} fss(i) + 1\,. \tag{5.4}$$

The next section presents the operability of the simulator on a normal run.

5.1.2 Simulation Run

A simulation run is perform to describe the functionality of the simulator. Fig. 5.4 describes the sequence of the *fill-up run* in order to start the energy exchange protocol and interact with the environment.

First, in Fig. 5.4-a, the system is completely inactive. On the top, the plotting areas do not show any information. In the middle, the energy tank animation windows display zero energy levels. The master and slave end-effector are placed in an initial position (at the center of the interactive windows respectively). The switch is set "OFF", and the user must turn it on to start the sequence.

Second, once the switch is "ON" (see Fig. 5.4-b), the master virtual end-effector shows a damper icon ($\tau_{TLC} = ON$), this will be turn until the energy tank level reaches the desired level. The user must set a desired level H_d with a configurable value from 0.0 to 1.0.

Third, the user must "pick up" the master virtual end-effector and start moving it on axes x and y, similar to be manipulating a pump. While the damper icon is on, those pump like movements generate the position difference as in (5.1) and the energy tanks start to fill up (see sequence in Fig. 5.4-c-d-e). The plotting windows are displaying the energy tank levels and the positions (in this scenario on the master side). The energy tank animation windows show the current level as being filled up. The end-effector window presents the damper activated on the master side.

Finally, in Fig. 5.4-f, the energy tank level has reached the desired level, the master visual end-effector displays the damper icon as "OFF". In the general configuration of the simulator, the slave virtual end-effector performs movements only when the energy level is above the desired level. When this condition is not satisfied, the virtual end-effector returns to the initial position and the master virtual end-effector displays the damper icon on. This animation was developed to simulate the damper like behaviour in the real system.

The next part of the sequence is *emptying* the tanks. Fig. 5.5 shows the stages of the process. The last part of the *fill up run* is depicted in Fig. 5.5-a, there is energy budget on the tanks to perform movements and both master and slave end-effectors are displacing.

Starting with Fig. 5.5-b-c, during the interactions of the slave's virtual end-effector and the environment, the energy cost of the movements when it collides with the virtual wall causes the tank level to drop. These movements in the simulator are realized with soft touches to the virtual wall, decreasing the tanks in the animation slowly.

Next, to exemplify a greater energy level drop, the simulator allows the user to operate the environment dynamically. That means to manipulate the environment and displace a virtual wall along the environment until it reaches the slave's virtual end-effector. When the virtual wall creates a collision with the virtual end-effector the tank level drops down "faster" in the animation. These movements are replicated in Fig. 5.5-d-e.

Lastly, once the tank level is smaller than the desired level ($H(k) \leq H_d$), the damper icon on the master's virtual end-effector turns on again; and the animation of the tanks replenishment is ready to perform (see Fig. 5.5-f).

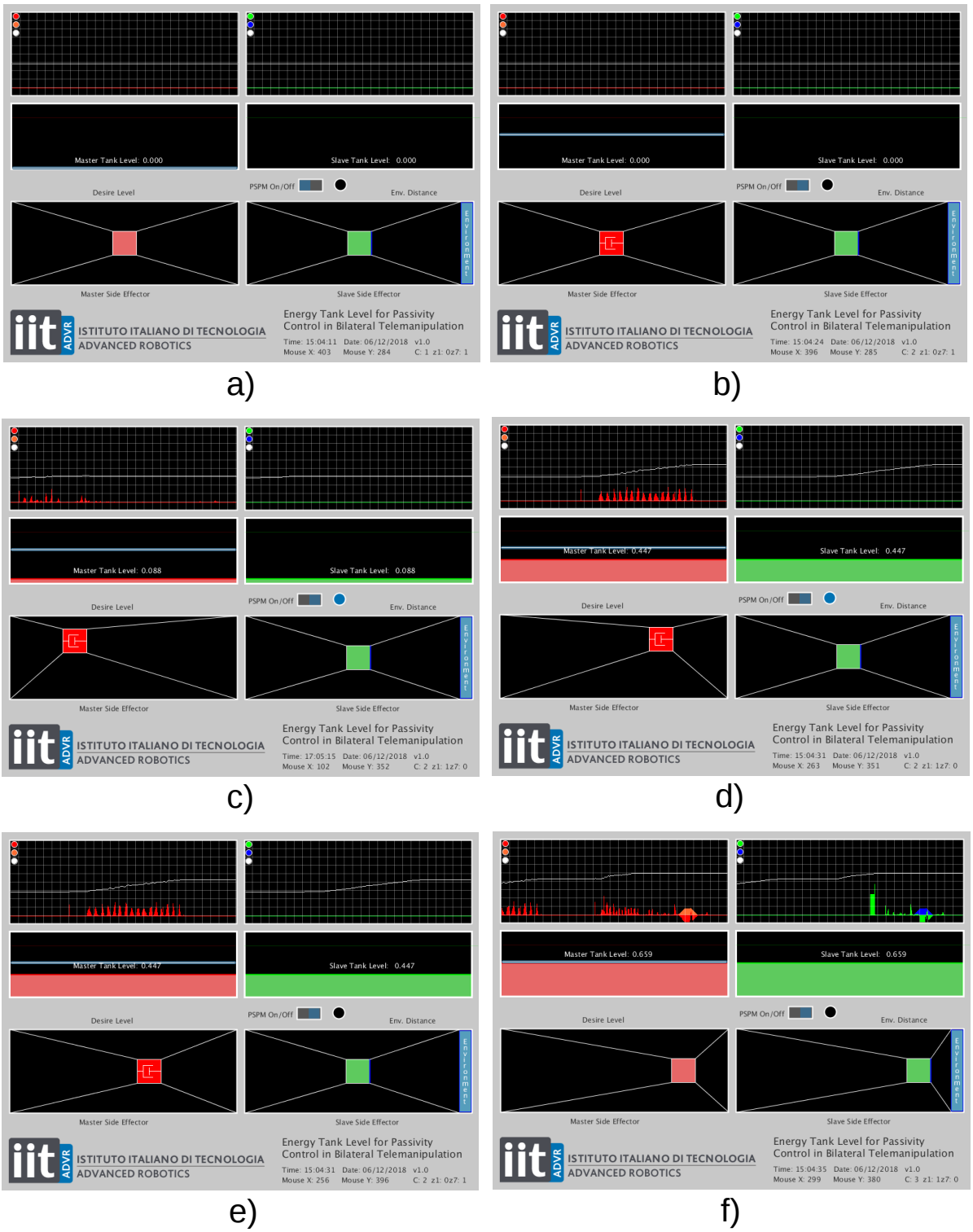

FIGURE 5.4. Energy tank simulator sequence: fill up.

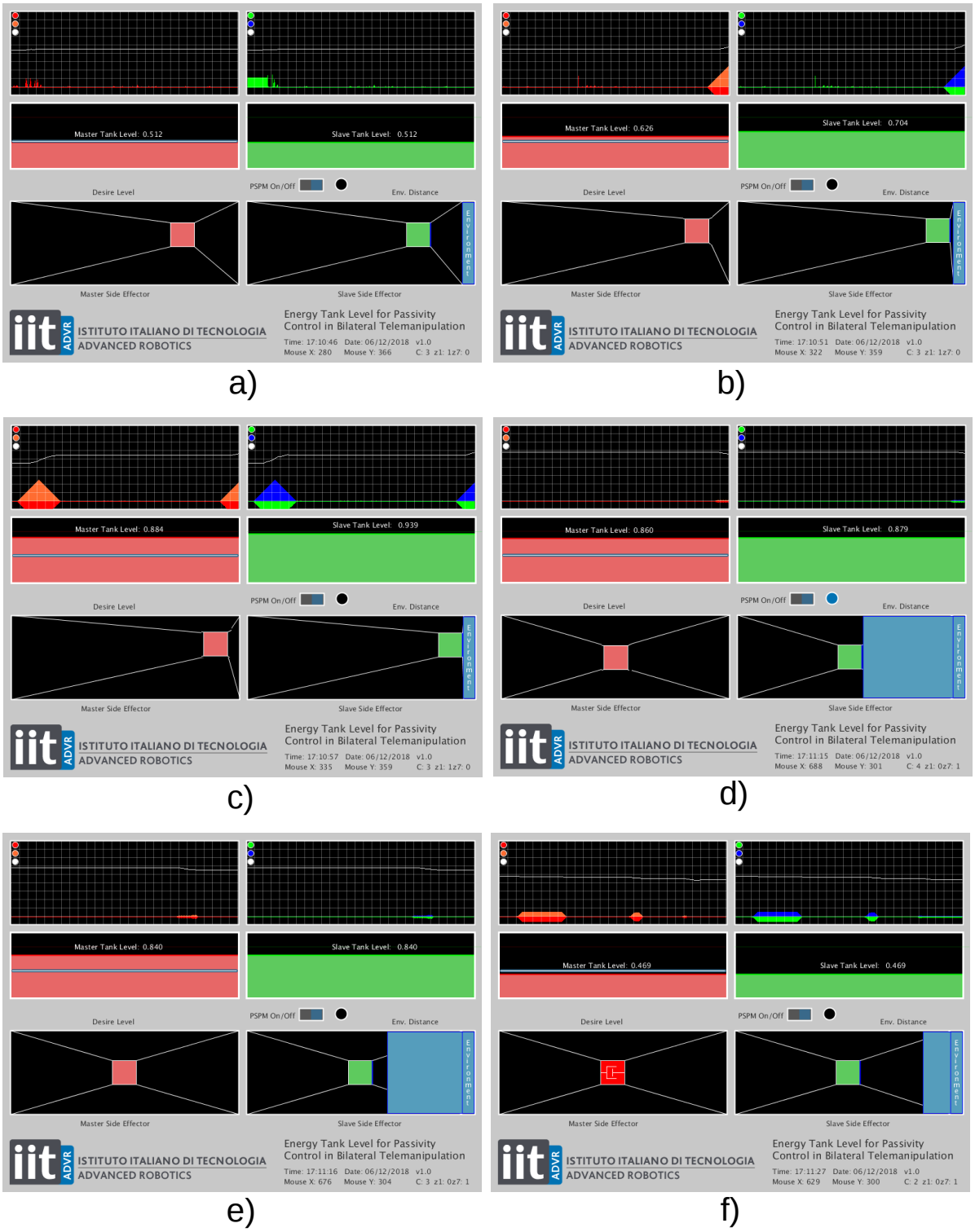

FIGURE 5.5. Energy tank simulator sequence: empty.

5.1.3 Discussion

To illustrate the functionality of the Energy Tank Simulator, two runs were performed. The first one displayed in Fig. 5.4, shows the sequence of the tanks filling up in the presence of sufficient energy budget in the tank ($H(k) \geq H_d$). The second sequence presented in Fig. 5.5, depicts the process to empty the tanks until the previous sequence ($H(k) \leq H_d$).

The replenishment or emptiness of the tanks is controlled totally by the energy exchange protocol (see equation (3.1) in Section 3.2). This energy monitor computes the energy exchange from the physical world (mechanical system) to the impedance controller (in this case the virtual impedance controller). The dynamics of the energy exchange protocol are defined by:

$$\Delta H(k) = -\tau_r(\overline{k})\Delta q_a(k) \begin{cases} -\Delta H(k) & \text{if} \quad \tau_r(\overline{k})\Delta q_a(k) > 0 \\ +\Delta H(k) & \text{if} \quad \tau_r(\overline{k})\Delta q_a(k) < 0. \end{cases} \tag{5.5}$$

When forces and displacements are positive ($\tau_r(\overline{k})\Delta q_a(k) > 0$), the energy exchange has a negative value; on the other hand, when forces and displacements are negative ($\tau_r(\overline{k})\Delta q_a(k) < 0$), the energy exchange turns a positive value. One can understand how it affects the energy tank dynamics from the following equation which describes the computation of the energy tank level:

$$H(k) = H(\overline{k}) + H_+(k) - \Delta H_I(k). \tag{5.6}$$

According to the TLC passivity layer work-flow algorithm in Section 3.2, first all the energy packages received in the queue $H_+(k)$ are summed into a single variable (see equation (3.7)). Then, the energy exchange $\Delta H_I(k)$ is computed to have the transition of energy from the mechanical model to the impedance controller (see equation (3.1)). Finally, as described in equation (5.6), the computation of the tank level depends on the current tank level value $H(\overline{k})$ at the moment of the sample plus the energy packages received $H_+(k)$ and what is the case of the energy exchange result $\Delta H_I(k)$.

Using equation (5.5) in (5.6), a positive value in $\Delta H_I(k)$ will reduce energy to the tank, while on the contrary a negative value in $\Delta H_I(k)$ will add the tank level. On the simulator, the animations are designed to magnify the tank level behaviour to obtain a clear representation of the dynamics as show on previous sequences.

To finish, the energy transferred among the tanks follows the description on equation (3.6) in Section 3.2. There, from the energy is assumed that a constant time delay ($\Delta T_m, \Delta T_s$) occurs in both sides, in the simulator these time delays are not considered when the energy is transferred from side to side. Besides, the β coefficient which regulates the amount of energy (as a tank level fraction) to be transferred from side to side is set to 0.1. That means that 10% of the tank level is shared with the other side, hence by modifying this variable, it is possible to replenish or empty the tank with a higher or lower frequency.

5.2 ROS System Architecture

Robot Operating System (ROS) is a trending robot application development platform that provides various features such as message passing, distributed computing, code reusing, and so on. In particular, ROS has revolutionized the developer community, providing it with a set of tools, infrastructure and best practices to build new applications and robots (like the Baxter research robot). A key pillar of the ROS effort is the notion of not re-inventing the wheel by providing easy to use libraries for different capabilities like navigation, manipulation, control (and more). The ROS community is growing very fast and there are many users and developers worldwide. Most of the high-end robotics companies are now porting their software to ROS. This trend is also visible in industrial robotics, in which companies are switching from proprietary robotic application to ROS [269].

ROS works with nodes and topics. A node is a process that performs computation. Nodes are combined together into a graph and communicate with one another using streaming topics, RPC services, and the Parameter Server. These nodes are meant to operate at a fine-grained scale; a robot control system usually comprise many nodes. For example, one node controls a laser range-finder, one node controls the robot's wheel motors, one node performs localization, one node performs path planning, one node provides a graphical view of the system, and so on.

On the other hand, topics are named buses over which nodes exchange messages. Topics have anonymous publish/subscribe semantics, which decouples the production of information from its consumption. In general, nodes are not aware of who they are communicating with. Instead, nodes that are interested in data subscribe to the relevant topic; nodes that generate data publish to the relevant topic. There can be multiple publishers and subscribers to a topic.

5.2.1 Proposed Implementation Design

The proposed implementation using ROS as a software tool to generate the teleoperated architecture presented in this thesis is depicted in Fig. 5.6. There are seven nodes running in parallel, the system is divided according to the features of a telemanipulation chain: *a) master side*, *b) communication channel*, and *c) slave side*.

- Master side:
  - Node: Omega engine. This node processes the information of the haptic device positions and sends it to the master controller node. Additionally, the node displays the forces coming from the master controller node at the haptic device. It contains one input topic and two outputs topics which interact with the master controller node.
  - Node: Master controller. This node runs the optimization process for the TOPL approach under the work flow of the Two-layer Approach. The node realizes the energy exchange from the physical world to the impedance controller. The node contains three

topics as inputs and six topics as outputs, it interacts with omega engine node and communication channel node. The quadratic programming tool used to optimize the function defined in Section 3.3 is Mosek. Mosek is a software package for solving large optimization problems with a great number of constraints and variables. The Application Programming Interface (API) is designed to perform low-level optimization for programming languages as C, C++, MATLAB, Java, .NET and Python.

- Communication channel:
  - Node: Communication channel. Inside the node there is a time delay generator, from 0 to 1 second the user can set the time delay and induce it into the system. The node contains four input topics and 5 output topics that interact with the master controller node and slave controller node.
- Slave side:
  - Node: Slave controller. This node follows the Two-layer Approach work flow but without the optimization part. The node realizes the energy exchange from the virtual environment to the impedance controller. The node contains three topics as inputs and six topics as outputs, it interacts with the collision detector node and communication channel node.
  - Node: Collision detector. Here, it is developed a physics engine processor to detect when objects overlap or collide when interacting. The outcome are the reaction forces displayed in the haptic device. The node contains three input topics and three output topics, and interacts with the slave controller node and the marker array generator node.
  - Node: Marker array generator. This node is part of the ROS framework, it provides a series of geometrical shapes to be displayed in the virtual environment. The user configures the number, size, color and shape of the geometrical objects, the behaviour of the shapes is commanded by the positions set to it. The node contains two input topics and three output topics that interact with the collision detector node and the RVIZ node.
  - Node: RVIZ. It is a visualization tool that provides a visual environment to display the geometric shapes, signals, and adjustable parameters. The node contains one topic as input that interacts with the marker array generator node.

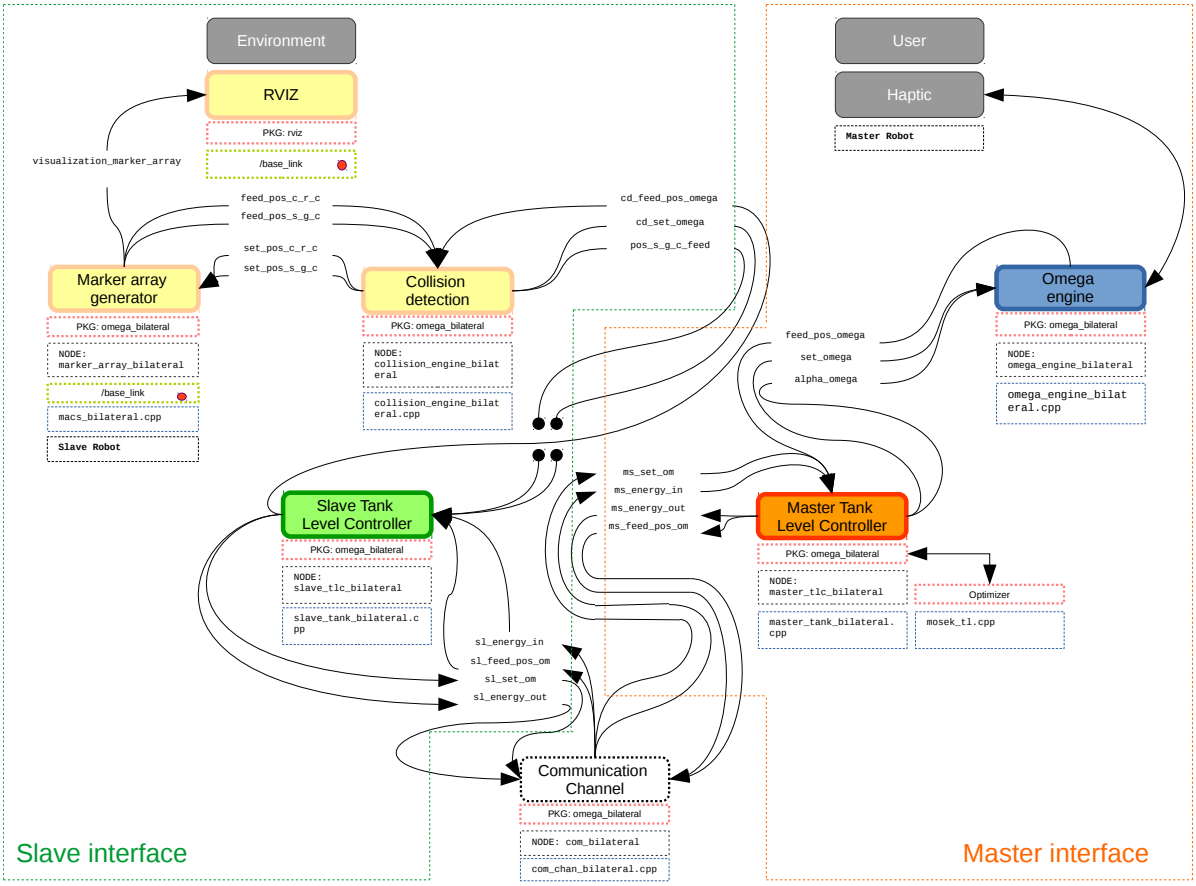

FIGURE 5.6. Connection diagram of the ROS Two-Layer Approach Passivity Control Transparency Optimize Package.

CHAPTER 6

CONCLUSIONS

In this thesis an innovative optimization-based passivity control algorithm for haptic-enabled bilateral teleoperation systems with multiple DoF was presented. This contribution focused on implementing a novel passivity layer for the existing time-domain scheme of Franken *et al.*[35]. While guaranteeing passivity, it was ensured optimal transparency of the interaction along subsets of the environment space, in which were chosen as the most important ones for the given task. The involved optimization problem is convex and amenable to real-time implementation. The feasibility and effectiveness of the proposed approach was validated with a palpation experiment performed on a virtual environment. Results showed that the proposed controller outperformed the time-domain scheme of Franken *et al.*[35] while guaranteeing the stability and safety of the system. In order to maintain the stability on the system, a passivity approach must be integrated. An optimal passivity layer design was presented in Section 3.4.2. The goal was to reach higher transparency forces on a preferred direction by optimizing the damping correction forces. Based on the Franken *et al.*[35] approach, an energy tank structure was implemented to preserve passivity on the system. A set of experiment trials were carried out as described in Section 4.2.3. As seen in figure 4.14 the proposed controller was able to provide more transparency while correcting less on the preferred direction.

Different methods of passivity control were studied, for instance the scattering/wave-variable-based approach using wave variables; the TDPC approach in which the elements passivity observer and controller are introduced; the EBA, where the virtual energy generated at the system is limited by dissipation; and last, the passive set-position modulation, which presents a spring-damper controller to acquire energy from the user. Among these methods, the two-layer approach gives a solution to provide stability on the system without jeopardizing passivity. This approach uses the energy tank concepts with the damper-like force corrector.

In this thesis, a mathematical derivation of a prioritization of feedback forces has been achieved for the 3 DoF extension of the two-layer approach. The next step is to find an experimental procedure to choose suitable subspace bases and priorities (A_i, P_i) for different tasks. This set up must guarantee the passivity condition at all moments and display the desired behaviour. Currently, research is being developed on a virtual environment using ROS and the Omega.6 haptic device.

Since humans wanted to explore, reach, manipulate, and control remote scenarios (from hazardous material manipulation to outer space exploration) without compromising people's safety, a tool was needed to solve this dilemma. Bilateral telemanipulation offers a solution to overcome the problem but with some limitations. Some of the disadvantages are the technological aspects on telemanipulated systems, such as mechanical device constraints, sampling frequency, communication infrastructure, etc. The technological relevance of the telemanipulated system is proven by the operability, remote features, communication support and synchronization.

In this thesis, the objective was to obtain of maximum degree of transparency based on a preferred direction and guaranteeing passivity. The optimization of the damping coefficients parameters by the TOPL passivity layer design was presented. In addition, the dynamic desired level function H_{min} was modelled to prevent energy loss in the TOPL controller. Besides, a simulator on energy tanks was developed, to provide a visual and interactive tool that depicts the tanks behaviours. Finally, the whole control system was implemented on the ROS structure, generating a package for bilateral control.

The two-layer approach uses the passivity control theory and introduces the damper-like correction on the master side. With this technique, the user exerts a force on the haptic when needed, thus, the energy is inserted into the system. This approach presented by Franken *et al.* [35], considers the negative influences that affects the bilateral telemanipulation chain. The approach divides the controller in two layers: *i) transparency layer* to compute forces and positions, and *ii) passivity layer* to manage the energy balance of the system. The two-layer approach implements the energy tanks, where an energy exchange is done between the physical world and the impedance controller.

Since the damping-like force is displayed in all directions in the two-layer approach, a method to improve transparency on a given preferred direction was proposed. Given a set of priorities P_i and the directions A_i, a minimization function is proposed in equation (3.15) in Section 3.3, using theτ_{TLC} forces, composed by a symmetric matrix B that contains the damping coefficients. The minimization is performed by a quadratic programming algorithm that solves the vector of the minimal damping coefficients. The minimization is limited in such a way that it never misses energy in the tank. A poke/drag experiment to validate the proposed method was implemented. Using a haptic device and a virtual environment, the user interacts with a surface with friction moving a virtual end-effector.

To simplify the demonstration of optimization the tables of operability regions were introduced.

The poke/drag experiment was tested using three different controllers: *i) NPC* (full transparent system), *ii) STLC* (3 DoF two-layer approach of [35]), and *iii) TOPL* (the approach proposed in this thesis). The user was asked to poke/drag the surface in two modalities: *i) soft grasp*, and *ii) strong grasp*, with regards of the haptic grasper. The objective of the tables of operability was to illustrate how the operability of the experiment were extended in terms of transparency when different stiffness values and time delays were set. The comparison of the tables of operability showed the extension of operability in certain regions, the proof of a better performance with the TOPL approach.

Regarding to the importance of the user's experience. The haptic device is a mechanical tool, the user must be trained to understand the device's functionality and operation. The experiments performed with inexperience users were not even complete on the trial tests. Some of them declared its first time using a haptic device and their performances were open to a subjective interpretation. Such interpretations did not provide enough information about the tactile "feeling" (sensation) on the interaction they were performed. Despite the designed task was simple to perform in terms of tactile sensations (identify a "bump" element over a surface wit friction), inexperience users were not able to identify the elements required to validate the task (such as the difference of stiffness over the surface and friction); furthermore, when time delay was induced on the task, inexperience users were not able to grasp and control the haptic device handler with their own hands, making the task inoperable. The expert user (with 40 hrs using a haptic device) was able to manipulate an interpret the information provided by the mechanical device, because of previous training with the tool, also was able to anticipate actions when time delay was induce. The designed task was a procedure to identify difference of stiffness among two objects over the same surface, this procedure takes time and effort to achieve.

In a different setting, a simulator was developed to exemplify the functionality of the energy tanks. This interactive visual tool exhibits the energy tanks behaviour of a bilateral telemanipulation chain when the user interacts with the remote environment. The simulator depicts the action of replenishing the tank and emptying Two sequences to show these actions were performed, and the computation which lied on the energy tank exchange protocol shown in Eq. (3.1) of Sec. 3.2 and the energy transfer protocol defined in Eq. (3.7).

Finally, on the optimal transparency-passivity layer design, a new constraint was given. The new constraint prevents the passivity layer from letting the tank gain energy when inverting the directions of the rendering forces with respect to the passivity layer forces $\tau_{PL}(k)$. That means the maximum allowed correction along each direction must act so as to zero out the rendered force (see equation (3.46) in Section 3.4.2). To maintain the energy above the desired level continuously, a correction to the desired level H_d was studied in Section 3.4.3. The outcome was a dynamic desired level with the name $H_{min}(k)$ described in equation (4.8).

6.1 Impact

A novel passivity control algorithm for haptic-enabled bilateral teleoperation systems with multiple degrees of freedom has been introduced within the framework of [35]. The proposed approach is aimed at enhancing the transparency of the interaction along subsets of the environment space designated as the most important ones for the given task, and involves the solution of an optimization problem which is convex and amenable to real-time implementation. The feasibility and effectiveness of the method has been validated on a human subject palpation experiment performed on a virtual environment. Regards haptic rendering, a virtual environment model that provides a geometrical scenario where objects can collide was presented. The processing of this model consists of the reaction when geometrical shapes overlap. These reactions send information to a physical engine to produce forces which are displayed at the haptic device.

6.2 Future Work

In the future, the goal is to implement the method in a real environment and test it on different application scenarios (see Fig. 6.1). With respect to this, it is planned to study how to automatically assign priority indexes to the subspaces given one (or more) representative runs of the considered task. Moreover, to run real-world experiments using a robotic manipulator such as the 7 DoF KUKA LBR robot and a grounded haptic interface such as the 7 DoF Sigma 7 device is planned. Besides, this work will focus on improving the performance of this proposed optimal correction approach as well as running a more extensive human subject evaluation.

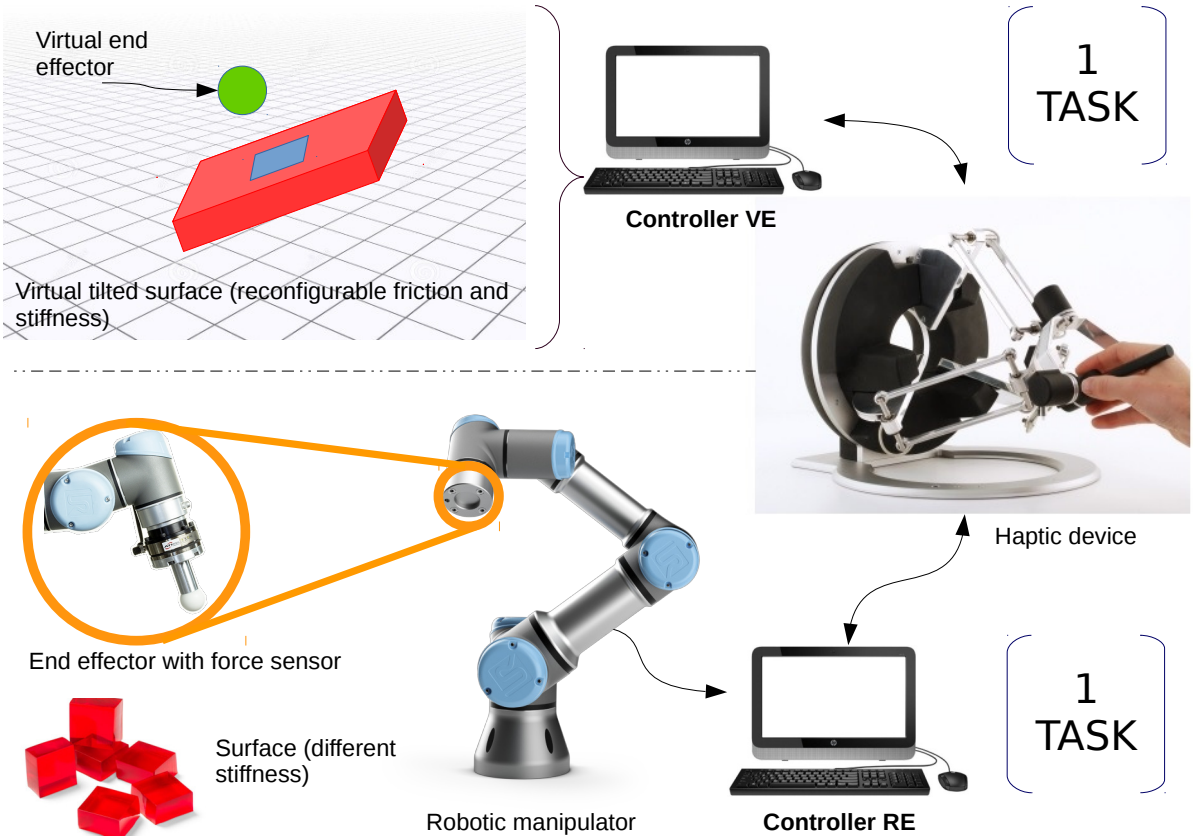

FIGURE 6.1. Scheme of the TOPL tasks. Top task depicts the experimental set up in a virtual environment. Bottom task illustrates the experimental set up in a real scenario.

BIBLIOGRAPHY

[1] R. C. Goertz, "Mechanical Master-Slave Manipulator," *Nucleonics (U.S.) Ceased publication*, vol. 12, Nov. 1954.

[2] R. C. Goertz and J. R. G. Schmitt, "Remote-control manipulator," Nov. 1954.
US Patent 2695715A.

[3] R. C. Goertz, "Manipulator System Development at ANL," *Argonne National Laboratory Reviews (U.S.) Supersedes Argonne Natl. Lab., News Bull. Changed to Argonne Rev.*, vol. 2, July 1965.

[4] W. R. Ferrell, "Remote manipulation with transmission delay," *IEEE Transactions on Human Factors in Electronics*, vol. HFE-6, pp. 24–32, Sept. 1965.

[5] B. Siciliano, "Control in robotics: open problems and future directions," in *Proceedings of the 1998 IEEE International Conference on Control Applications (Cat. No.98CH36104)*, vol. 1, pp. 81–85 vol.1, Sept. 1998.

[6] R. Anderson and M. Spong, "Bilateral control of teleoperators with time delay," *IEEE Transactions on Automatic Control*, vol. 34, pp. 494–501, May 1989.

[7] M. C. J. Franken, S. Stramigioli, R. Reilink, C. Secchi, and A. Macchelli, "Bridging the gap between passivity and transparency," in *Proc. Robotics: Science and Systems*, July 2009.

[8] J.-H. Ryu, D.-S. Kwon, and B. Hannaford, "Stable teleoperation with time-domain passivity control," *IEEE Transactions on Robotics and Automation*, vol. 20, pp. 365–373, Apr. 2004.

[9] J.-P. Kim, C. Seo, and J. Ryu, "A Multirate Energy Bounding Algorithm for High Fidelity Stable Haptic Interaction Control," in *SICE-ICASE, 2006. International Joint Conference*, pp. 215–220, Oct. 2006.

[10] D. Lee and M. W. Spong, "Passive Bilateral Teleoperation With Constant Time Delay," *IEEE Transactions on Robotics*, vol. 22, pp. 269–281, Apr. 2006.

[11] S. Avgousti, A. S. Panayides, E. G. Christoforou, A. Argyrou, A. Jossif, P. Masouras, C. Novales, and P. Vieyres, "Medical Telerobotics and the Remote Ultrasonography Paradigm

Over 4g Wireless Networks," in *2018 IEEE 20th International Conference on e-Health Networking, Applications and Services (Healthcom)*, pp. 1–6, Sept. 2018.

[12] M. Di Castro, M. Ferre, and A. Masi, "CERNTAURO: A Modular Architecture for Robotic Inspection and Telemanipulation in Harsh and Semi-Structured Environments," *IEEE Access*, vol. 6, pp. 37506–37522, 2018.

[13] M. Di Castro, M. L. B. Tambutti, M. Ferre, R. Losito, G. Lunghi, and A. Masi, "i-TIM: A Robotic System for Safety, Measurements, Inspection and Maintenance in Harsh Environments," in *2018 IEEE International Symposium on Safety, Security, and Rescue Robotics (SSRR)*, pp. 1–6, Aug. 2018.

[14] X. Mai, J. Chen, Y. Wang, S. Bi, Y. Cheng, and N. Xi, "A Teleoperation Framework of Hot Line Work Robot," in *2018 IEEE International Conference on Mechatronics and Automation (ICMA)*, pp. 1872–1876, Aug. 2018.

[15] T. Abut and S. Soyguder, "Haptic industrial robot control and bilateral teleoperation by using a virtual visual interface," in *2018 26th Signal Processing and Communications Applications Conference (SIU)*, (Izmir), pp. 1–4, IEEE, May 2018.

[16] P. D. Lillo, D. D. Vito, E. Simetti, G. Casalino, and G. Antonelli, "Satellite-Based Tele-Operation of an Underwater Vehicle-Manipulator System. Preliminary Experimental Results," in *2018 IEEE International Conference on Robotics and Automation (ICRA)*, pp. 7504–7509, May 2018.

[17] C. A. Garcia, J. E. Naranjo, L. A. Campana, M. Castro, C. Beltran, and M. V. Garcia, "Flexible Robotic Teleoperation Architecture Under IEC 61499 Standard for Oil and Gas Process," in *2018 IEEE 23rd International Conference on Emerging Technologies and Factory Automation (ETFA)*, vol. 1, pp. 1269–1272, Sept. 2018.

[18] M. H. Rahman, T. K-Ouimet, M. Saad, J. P. Kenne, and P. S. Archambault, "Tele-operation of a robotic exoskeleton for rehabilitation and passive arm movement assistance," in *2011 IEEE International Conference on Robotics and Biomimetics*, pp. 443–448, Dec. 2011.

[19] M. Panzirsch, R. Balachandran, B. Weber, M. Ferre, and J. Artigas, "Haptic Augmentation for Teleoperation through Virtual Grasping Points," *IEEE Transactions on Haptics*, vol. 11, pp. 400–416, July 2018.

[20] J. Artigas, *"Time domain passivity control for delayed teleoperation"*. Ph.D. dissertation, Dept. Ind. Eng., Madrid Poly. Univ., 2014.

[21] C. Tzafestas, S. Velanas, and G. Fakiridis, "Adaptive impedance control in haptic teleoperation to improve transparency under time-delay," in *Robotics and Automation, 2008. ICRA 2008. IEEE International Conference on*, pp. 212–219, IEEE, 2008.

[22] D. Lawrence, "Stability and transparency in bilateral teleoperation," *IEEE Transactions on Robotics and Automation*, vol. 9, pp. 624–637, Oct. 1993.

[23] K. M. Tsui, M. Desai, H. A. Yanco, and C. Uhlik, "Exploring use cases for telepresence robots," in *2011 6th ACM/IEEE International Conference on Human-Robot Interaction (HRI)*, pp. 11–18, Mar. 2011.

[24] B. Willaert, D. Reynaerts, H. Van Brussel, and E. B. Vander Poorten, "Bilateral teleoperation: quantifying the requirements for and restrictions of ideal transparency," *IEEE transactions on control systems technology*, vol. 22, no. 1, pp. 387–395, 2014.

[25] M. H. Khong and Y. C. Liu, "Design and implementation of a three-axis force sensor for applications to bilateral teleoperation systems," in *2015 IEEE International Conference on Advanced Intelligent Mechatronics (AIM)*, pp. 1760–1765, July 2015.

[26] B. T. Bethea, A. M. Okamura, M. Kitagawa, T. P. Fitton, S. M. Cattaneo, V. L. Gott, W. A. Baumgartner, and D. D. Yuh, "Application of Haptic Feedback to Robotic Surgery," *Journal of Laparoendoscopic & Advanced Surgical Techniques*, vol. 14, pp. 191–195, June 2004.

[27] R. Muradore and P. Fiorini, "A Review of Bilateral Teleoperation Algorithms," *Acta Polytechnica Hungarica*, vol. 13, Jan. 2016.

[28] T. B. Sheridan, "Space teleoperation through time delay: review and prognosis," *IEEE Transactions on Robotics and Automation*, vol. 9, pp. 592–606, Oct. 1993.

[29] D. W. Hainsworth, "Teleoperation User Interfaces for Mining Robotics," *Autonomous Robots*, vol. 11, no. 1, pp. 19–28, 2001.

[30] A. Hodzic and E. Mujcic, "Teleoperation system control based on the method for supervisory control with variable time delay," in *2015 23rd Telecommunications Forum Telfor*, pp. 345–348, Nov. 2015.

[31] W.-H. Zhu and S. E. Salcudean, "Stability guaranteed teleoperation: an adaptive motion/force control approach," *IEEE Transactions on Automatic Control*, vol. 45, pp. 1951–1969, Nov. 2000.

[32] L. A. Sanchez, M. Q. Le, C. Liu, N. Zemiti, and P. Poignet, "The impact of interaction model on stability and transparency in bilateral teleoperation for medical applications," in

2012 IEEE International Conference on Robotics and Automation, pp. 1607–1613, May 2012.

[33] J.-P. Kim and J. Ryu, "Robustly Stable Haptic Interaction Control using an Energy-bounding Algorithm," *The International Journal of Robotics Research*, vol. 29, pp. 666–679, May 2010.

[34] D. Lee and K. Huang, "Passive-Set-Position-Modulation Framework for Interactive Robotic Systems," *IEEE Transactions on Robotics*, vol. 26, pp. 354–369, Apr. 2010.

[35] M. Franken, S. Stramigioli, S. Misra, C. Secchi, and A. Macchelli, "Bilateral Telemanipulation With Time Delays: A Two-Layer Approach Combining Passivity and Transparency," *IEEE Transactions on Robotics*, vol. 27, pp. 741–756, Aug. 2011.

[36] V. Duindam and S. Stramigioli, "Port-Based Asymptotic Curve Tracking for Mechanical Systems," *European Journal of Control*, vol. 10, no. 5, pp. 411–420, 2004.

[37] A. Franchi, C. Secchi, H. I. Son, H. Bulthoff, and P. Giordano, "Bilateral Teleoperation of Groups of Mobile Robots With Time-Varying Topology," *IEEE Transactions on Robotics*, vol. 28, pp. 1019–1033, Oct. 2012.

[38] C. Secchi, A. Franchi, H. Bulthoff, and P. Giordano, "Bilateral teleoperation of a group of UAVs with communication delays and switching topology," in *2012 IEEE International Conference on Robotics and Automation (ICRA)*, pp. 4307–4314, May 2012.

[39] F. Ferraguti, N. Preda, A. Manurung, M. Bonfe, O. Lambercy, R. Gassert, R. Muradore, P. Fiorini, and C. Secchi, "An Energy Tank-Based Interactive Control Architecture for Autonomous and Teleoperated Robotic Surgery," *IEEE Transactions on Robotics*, vol. 31, pp. 1073–1088, Oct. 2015.

[40] R. Muradore, P. Fiorini, G. Akgun, D. E. Barkana, M. Bonfe, F. Boriero, A. Caprara, G. D. Rossi, R. Dodi, O. J. Elle, F. Ferraguti, L. Gasperotti, R. Gassert, K. Mathiassen, D. Handini, O. Lambercy, L. Li, M. Kruusmaa, A. O. Manurung, G. Meruzzi, H. Q. P. Nguyen, N. Preda, G. Riolfo, A. Ristolainen, A. Sanna, C. Secchi, M. Torsello, and A. E. Yantac, "Development of a cognitive robotic system for simple surgical tasks," *International Journal of Advanced Robotic Systems*, Apr. 2015.

[41] C. Pacchierotti, L. Meli, F. Chinello, M. Malvezzi, and D. Prattichizzo, "Cutaneous haptic feedback to ensure the stability of robotic teleoperation systems," *The International Journal of Robotics Research*, pp. 1773–1787, Oct. 2015.

[42] C. Pacchierotti, A. Tirmizi, G. Bianchini, and D. Prattichizzo, "Enhancing the Performance of Passive Teleoperation Systems via Cutaneous Feedback," *IEEE Transactions on Haptics*, vol. 8, pp. 397–409, Oct. 2015.

[43] C. Schindlbeck and S. Haddadin, "Unified passivity-based Cartesian force/impedance control for rigid and flexible joint robots via task-energy tanks," in *2015 IEEE International Conference on Robotics and Automation (ICRA)*, pp. 440–447, May 2015.

[44] P. Pitakwatchara, "Wave Correction Scheme for Task Space Control of Time-Varying Delayed Teleoperation Systems," *IEEE Transactions on Control Systems Technology*, vol. 26, pp. 2223–2231, Nov. 2018.

[45] Y. Chang, C. Yang, and H. Lin, "Adaptive control for bilateral teleoperation systems with time-varying delays," in *2018 IEEE International Conference on Applied System Invention (ICASI)*, pp. 1111–1114, Apr. 2018.

[46] Z. Chen, F. Huang, W. Song, and S. Zhu, "A Novel Wave-Variable Based Time-Delay Compensated Four-Channel Control Design for Multilateral Teleoperation System," *IEEE Access*, vol. 6, pp. 25506–25516, 2018.

[47] J. A. Vences-Jimenez, A. Rodriguez-Angeles, and J. Alvarez-Gallegos, "Bilateral time delay compensation in bilateral master slave teleoperation of differential mobile robots using IMC," in *2018 13th IEEE Conference on Industrial Electronics and Applications (ICIEA)*, pp. 1302–1307, May 2018.

[48] D. Heck, A. Saccon, R. Beerens, and H. Nijmeijer, "Direct Force-Reflecting Two-Layer Approach for Passive Bilateral Teleoperation With Time Delays," *IEEE Transactions on Robotics*, vol. 34, pp. 194–206, Feb. 2018.

[49] D. J. F. Heck, A. Saccon, N. van de Wouw, and H. Nijmeijer, "Switched position-force tracking control of a manipulator interacting with a stiff environment," in *2015 American Control Conference (ACC)*, pp. 4832–4837, July 2015.

[50] U. Ahmad and Y. Pan, "A Time Domain Passivity Approach for Asymmetric Multilateral Teleoperation System," *IEEE Access*, vol. 6, pp. 519–531, 2018.

[51] G. Feng, W. Li, and H. Zhang, "Space Robot Teleoperation Experiment and System Evaluation Method," in *2018 2nd IEEE Advanced Information Management,Communicates,Electronic and Automation Control Conference (IMCEC)*, pp. 346–351, May 2018.

[52] A. Schiele, M. D. Bartolomei, and F. V. D. Helm, "Towards Intuitive Control of Space Robots: A Ground Development Facility with Exoskeleton," in *2006 IEEE/RSJ International Conference on Intelligent Robots and Systems*, pp. 1396–1401, Oct. 2006.

[53] M. Folgheraiter, B. Bongardt, J. Albiez, and F. Kirchner, "A bio-inspired haptic interface for tele-robotics applications," in *2008 IEEE International Conference on Robotics and Biomimetics*, pp. 560–565, Feb. 2009.

[54] S. Kumra, S. Mehta, and R. Singh, "Development of anthropomorphic multi-D.O.F master-slave manipulator," in *2013 3rd IEEE International Advance Computing Conference (IACC)*, pp. 1631–1635, Feb. 2013.

[55] S. Yim and S. Kim, "Origami-inspired printable tele-micromanipulation system," in *2015 IEEE International Conference on Robotics and Automation (ICRA)*, pp. 2704–2709, May 2015.

[56] C. Meeker, T. Rasmussen, and M. Ciocarlie, "Intuitive Hand Teleoperation by Novice Operators Using a Continuous Teleoperation Subspace," in *2018 IEEE International Conference on Robotics and Automation (ICRA)*, pp. 1–7, May 2018.

[57] J. v. Oosterhout, C. J. M. Heemskerk, M. R. d. Baar, F. C. T. v. d. Helm, and D. A. Abbink, "Tele-Manipulation with Two Asymmetric Slaves: Two Operators Perform Better Than One," *IEEE Transactions on Haptics*, vol. 11, pp. 128–139, Jan. 2018.

[58] M. Shahbazi, S. F. Atashzar, and R. V. Patel, "A Systematic Review of Multilateral Teleoperation Systems," *IEEE Transactions on Haptics*, vol. 11, pp. 338–356, July 2018.

[59] K. A. Tahboub, "Natural and manmade shared-control systems: an overview," in *Proceedings 2001 ICRA. IEEE International Conference on Robotics and Automation (Cat. No.01CH37164)*, vol. 3, pp. 2655–2660 vol.3, May 2001.

[60] S. Jiang, C. Lin, K. Huang, and K. Song, "Shared Control Design of a Walking-Assistant Robot," *IEEE Transactions on Control Systems Technology*, vol. 25, pp. 2143–2150, Nov. 2017.

[61] S. Islam, P. X. Liu, and A. E. Saddik, "Haptics based bilateral shared telemanipulation of aerial vehicle over open communication network," in *2017 IEEE International Conference on Systems, Man, and Cybernetics (SMC)*, pp. 2340–2342, Oct. 2017.

[62] S. Islam, P. X. Liu, A. E. Saddik, R. Ashour, J. Dias, and L. D. Seneviratne, "Artificial and Virtual Impedance Interaction Force Reflection-Based Bilateral Shared Control for Miniature Unmanned Aerial Vehicle," *IEEE Transactions on Industrial Electronics*, vol. 66, pp. 329–337, Jan. 2019.

[63] F. Barbagli, D. Prattichizzo, and K. Salisbury, "Multirate analysis of haptic interaction stability with deformable objects," in *Proceedings of the 41st IEEE Conference on Decision and Control, 2002.*, vol. 1, pp. 917–922 vol.1, Dec. 2002.

[64] K. E. MacLean, "Haptic Interaction Design for Everyday Interfaces," *Reviews of Human Factors and Ergonomics*, vol. 4, pp. 149–194, Oct. 2008.

[65] J. K. Salisbury and M. A. Srinivasan, "Phantom-based haptic interaction with virtual objects," *IEEE Computer Graphics and Applications*, vol. 17, pp. 6–10, Sept. 1997.

[66] B. l. Torre, D. Prattichizzo, F. Barbagli, and A. Vicino, "The FeTouch project," in *2003 IEEE International Conference on Robotics and Automation (Cat. No.03CH37422)*, vol. 1, pp. 1259–1263 vol.1, Sept. 2003.

[67] D. Prattichizzo, B. la Torre, F. Barbagli, A. Vicino, F. M. Severi, and F. Petraglia, "The FeTouch project: an application of haptic technologies to obstetrics and gynaecology," *The international journal of medical robotics + computer assisted surgery: MRCAS*, vol. 1, pp. 83–87, June 2004.

[68] J. Semmoloni, R. Manganelli, A. Formaglio, and D. Prattichizzo, "Control design issues for a microinvasive neurosurgery teleoperator system," in *2009 International Conference on Advanced Robotics*, pp. 1–5, June 2009.

[69] C. Pacchierotti, A. Tirmizi, G. Bianchini, and D. Prattichizzo, "Improving transparency in passive teleoperation by combining cutaneous and kinesthetic force feedback," in *2013 IEEE/RSJ International Conference on Intelligent Robots and Systems*, pp. 4958–4963, Nov. 2013.

[70] O. A. Moreno, J. Bimbo, C. Pacchierotti, G. Bianchini, and D. Prattichizzo, "Optimizing Damping Factors in a 3dof Passive Two-layer Approach for Bilateral Telemanipulation," in *World Haptics 2017*, (Furstenfeldbruck (Munich), Germany), June 2017.

[71] O. A. Moreno, J. Bimbo, C. Pacchierotti, D. Prattichizzo, D. Barcelli, and G. Bianchini, "Transparency-optimal passivity layer design for time-domain control of multi-DoF haptic-enabled teleoperation," in *IROS 2018 - IEEE/RSJ International Conference on Intelligent Robots and Systems*, pp. 4988 – 4994, IEEE, Oct. 2018.

[72] G. Bianchini, J. Bimbo, C. Pacchierotti, D. Prattichizzo, and O. A. Moreno, "Transparency-oriented passivity control design for haptic-enabled teleoperation systems with multiple degrees of freedom," in *CDC 2018 - 57th IEEE Conference on Decision and Control*, pp. 2011–2016, IEEE, Dec. 2018.

[73] S. Eppinger and W. Seering, "Understanding bandwidth limitations in robot force control," in *1987 IEEE International Conference on Robotics and Automation Proceedings*, vol. 4, pp. 904–909, Mar. 1987.

[74] T. B. Sheridan, *Telerobotics, Automation, and Human Supervisory Control*. Cambridge, MA, USA: MIT Press, 1992.

[75] V. Hayward and O. R. Astley, "Performance Measures for Haptic Interfaces," in *Robotics Research* (G. Giralt and G. Hirzinger, eds.), pp. 195–206, Springer London, 1996.

[76] M. A. Goodrich and A. C. Schultz, “Human-robot Interaction: A Survey,” *Found. Trends Hum.-Comput. Interact.*, vol. 1, pp. 203–275, Jan. 2007.

[77] J. Hua, Y. Wang, and N. Xi, “A Hybrid Control Method for Telerobotic Systems,” in *2006 IEEE International Conference on Information Acquisition*, pp. 510–515, Aug. 2006.

[78] J. G. Park, *Improving teleoperation with models and tasks*.
Ph.D. dissertation, Stanford University, 2010.

[79] R. T. Azuma, “A Survey of Augmented Reality,” *Presence: Teleoper. Virtual Environ.*, vol. 6, pp. 355–385, Aug. 1997.

[80] J. Hills, P. Green, J. Jensen, Y. Gorfu, and A. Shah, “Telepresence surgery demonstration system,” in *, 1994 IEEE International Conference on Robotics and Automation, 1994. Proceedings*, pp. 2302–2307 vol.3, May 1994.

[81] G. S. Guthart and J. K. Salisbury, “The Intuitive/sup TM/ telesurgery system: overview and application,” in *Proceedings 2000 ICRA. Millennium Conference. IEEE International Conference on Robotics and Automation. Symposia Proceedings (Cat. No.00CH37065)*, vol. 1, pp. 618–621 vol.1, Apr. 2000.

[82] J. Suthakorn, “A concept on Cooperative Tele-Surgical System based on Image-Guiding and robotic technology,” in *2012 Pan American Health Care Exchanges*, pp. 41–45, Mar. 2012.

[83] G. Fau, T. Matsunaga, and K. Ohnishi, “Development of a five degrees of freedom Master/Slave robot for tele-operated laparoscopic surgical operations,” in *2014 7th International Conference on Human System Interactions (HSI)*, pp. 172–177, June 2014.

[84] C. Papachristos, V. N. Tsoulkas, and A. A. Pantelous, “Advances in Medical Education on Surgical Techniques Using Satellite Communications,” in *2009 Third UKSim European Symposium on Computer Modeling and Simulation*, pp. 361–366, Nov. 2009.

[85] S. Park, S. Baek, and J. Ryu, “Optimization for discriminability of soft tissues in haptic tele-surgery system with flexible surgical tool,” in *2016 IEEE International Conference on Advanced Intelligent Mechatronics (AIM)*, pp. 1382–1385, July 2016.

[86] J. Shang, K. Leibrandt, P. Giataganas, V. Vitiello, C. A. Seneci, P. Wisanuvej, J. Liu, G. Gras, J. Clark, A. Darzi, and G. Yang, “A Single-Port Robotic System for Transanal Microsurgery,ÄîDesign and Validation,” *IEEE Robotics and Automation Letters*, vol. 2, pp. 1510–1517, July 2017.

[87] Z. Su, K. Hausman, Y. Chebotar, A. Molchanov, G. E. Loeb, G. S. Sukhatme, and S. Schaal, “Force estimation and slip detection/classification for grip control using a biomimetic

tactile sensor," in *2015 IEEE-RAS 15th International Conference on Humanoid Robots (Humanoids)*, pp. 297–303, Nov. 2015.

[88] S. Shirwalkar, A. Singh, K. Sharma, and N. Singh, "Telemanipulation of an industrial robotic arm using gesture recognition with Kinect," in *2013 International Conference on Control, Automation, Robotics and Embedded Systems (CARE)*, pp. 1–6, Dec. 2013.

[89] D. Cannon and M. Siegel, "Perceived mental workload and operator performance of dexterous manipulators under time delay with master-slave interfaces," in *2015 IEEE International Conference on Computational Intelligence and Virtual Environments for Measurement Systems and Applications (CIVEMSA)*, pp. 1–6, June 2015.

[90] D. Yoerger and J. Slotine, "Supervisory control architecture for underwater teleoperation," in *1987 IEEE International Conference on Robotics and Automation Proceedings*, vol. 4, pp. 2068–2073, Mar. 1987.

[91] S. Mohan, J. Kim, and Y. Kim, "A null space control of an underactuated underwater vehicle-manipulator system under ocean currents," in *2012 Oceans - Yeosu*, pp. 1–5, May 2012.

[92] C. Pham and P. From, "Control allocation for mobile manipulators with on-board cameras," in *2013 IEEE/RSJ International Conference on Intelligent Robots and Systems (IROS)*, pp. 5002–5008, Nov. 2013.

[93] N. Babu, "Design and analysis of multipurpose mobile manipulator for defence application and study the dynamic effects on stability of an unmanned tracked vehicle," in *2015 International Conference on Robotics, Automation, Control and Embedded Systems (RACE)*, pp. 1–6, Feb. 2015.

[94] J. Kang, H. Choi, N. Nguyen, J. Kim, and D. Kim, "Simulation and experimental validation for dynamic stability of underwater vehicle-manipulator system," in *OCEANS 2017 - Anchorage*, pp. 1–5, Sept. 2017.

[95] H. Stuart, S. Wang, O. Khatib, and M. R. Cutkosky, "The Ocean One hands: An adaptive design for robust marine manipulation," *The International Journal of Robotics Research*, vol. 36, pp. 150–166, Feb. 2017.

[96] T. Piumsomboon, G. A. Lee, B. Ens, B. H. Thomas, and M. Billinghurst, "Superman vs Giant: A Study on Spatial Perception for a Multi-Scale Mixed Reality Flying Telepresence Interface," *IEEE Transactions on Visualization and Computer Graphics*, pp. 1–1, 2018.

[97] L. Fritsche, F. Unverzag, J. Peters, and R. Calandra, "First-person tele-operation of a humanoid robot," in *2015 IEEE-RAS 15th International Conference on Humanoid Robots (Humanoids)*, pp. 997–1002, Nov. 2015.

[98] N. Katayama, T. Inoue, and H. Shigeno, "Sharing the Positional Relationship with the Bidirectional Telepresence Robots," in *2018 IEEE 22nd International Conference on Computer Supported Cooperative Work in Design ((CSCWD))*, pp. 325–329, May 2018.

[99] S. R. Soomro, O. Eldes, and H. Urey, "Towards Mobile 3d Telepresence Using Head-Worn Devices and Dual-Purpose Screens," in *2018 IEEE Conference on Virtual Reality and 3D User Interfaces (VR)*, pp. 1–2, Mar. 2018.

[100] T. L. Brooks and I. Ince, "Operator vision aids for telerobotic assembly and servicing in space," in *Proceedings 1992 IEEE International Conference on Robotics and Automation*, pp. 886–891 vol.1, May 1992.

[101] K. Landzettel, C. Preusche, A. Albu-Schaffer, D. Reintsema, B. Rebele, and G. Hirzinger, "Robotic On-Orbit Servicing - DLR's Experience and Perspective," in *2006 IEEE/RSJ International Conference on Intelligent Robots and Systems*, pp. 4587–4594, Oct. 2006.

[102] C. Preusche, D. Reintsema, K. Landzettel, and G. Hirzinger, "Robotics Component Verification on ISS ROKVISS - Preliminary Results for Telepresence," in *2006 IEEE/RSJ International Conference on Intelligent Robots and Systems*, pp. 4595–4601, Oct. 2006.

[103] M. A. Seif, A. Hassan, A. H. El-Shaer, A. Alfar, S. Misra, and I. S. M. Khalil, "A magnetic bilateral tele-manipulation system using paramagnetic microparticles for micromanipulation of nonmagnetic objects," in *2017 IEEE International Conference on Advanced Intelligent Mechatronics (AIM)*, pp. 1095–1102, July 2017.

[104] P. Schmaus, D. Leidner, T. Kruger, A. Schiele, B. Pleintinger, R. Bayer, and N. Y. Lii, "Preliminary Insights From the METERON SUPVIS Justin Space-Robotics Experiment," *IEEE Robotics and Automation Letters*, vol. 3, pp. 3836–3843, Oct. 2018.

[105] S. Curtis, M. Brandt, G. Bowers, G. Brown, C. Cheung, C. Cooperider, M. Desch, N. Desch, J. Dorband, K. Gregory, K. Lee, A. Lunsford, F. Minetto, W. Truszkowski, R. Wesenberg, J. Vranish, M. Abrahantes, P. Clark, T. Capon, M. Weaker, R. Watson, P. Olivier, and M. L. Rilee, "Tetrahedral Robotics for Space Exploration," in *2007 IEEE Aerospace Conference*, pp. 1–9, Mar. 2007.

[106] J. Z. Sasiadek, "Space robotics: Present and past challenges," in *2014 19th International Conference on Methods and Models in Automation and Robotics (MMAR)*, pp. 926–929, Sept. 2014.

[107] E. Ackerman, "Are Telepresence Robots the Best Way to Explore Other Worlds?," *IEEE Spectrum: Technology, Engineering, and Science News*, June 2017.
Automaton blog.

[108] Y. Tanaka, H. Lee, D. Wallace, Y. Jun, P. Oh, and M. Inaba, "Toward deep space humanoid robotics inspired by the NASA Space Robotics Challenge," in *2017 14th International Conference on Ubiquitous Robots and Ambient Intelligence (URAI)*, pp. 14–19, June 2017.

[109] E. Ackerman, "JAXA Wants Telepresence Robots for In-Space Construction and Exploration," *IEEE Spectrum: Technology, Engineering, and Science News*, Sept. 2018. Automaton blog.

[110] G. Hirzinger, B. Brunner, J. Dietrich, and J. Heindl, "ROTEX-the first remotely controlled robot in space," in *, 1994 IEEE International Conference on Robotics and Automation, 1994. Proceedings*, pp. 2604–2611 vol.3, May 1994.

[111] A. Owen-Hill, J. Breosa, M. Ferre, J. Artigas, and R. Aracil, "A Taxonomy for Heavy-Duty Telemanipulation Tasks Using Elemental Actions," *International Journal of Advanced Robotic Systems*, p. 1, 2013.

[112] A. Bejczy, W. Kim, and S. Venema, "The phantom robot: predictive displays for teleoperation with time delay," in *, 1990 IEEE International Conference on Robotics and Automation, 1990. Proceedings*, pp. 546–551 vol.1, May 1990.

[113] J. Colgate, M. Stanley, and J. Brown, "Issues in the haptic display of tool use," in *1995 IEEE/RSJ International Conference on Intelligent Robots and Systems 95. 'Human Robot Interaction and Cooperative Robots', Proceedings*, vol. 3, pp. 140–145 vol.3, Aug. 1995.

[114] J. Colgate, "Robust impedance shaping telemanipulation," *IEEE Transactions on Robotics and Automation*, vol. 9, pp. 374–384, Aug. 1993.

[115] W. Kim, B. Hannaford, and A. Fejczy, "Force-reflection and shared compliant control in operating telemanipulators with time delay," *IEEE Transactions on Robotics and Automation*, vol. 8, pp. 176–185, Apr. 1992.

[116] B. Hannaford, "Stability and performance tradeoffs in bi-lateral telemanipulation," in *, 1989 IEEE International Conference on Robotics and Automation, 1989. Proceedings*, pp. 1764–1767 vol.3, May 1989.

[117] D. C. Ruspini, K. Kolarov, and O. Khatib, "The Haptic Display of Complex Graphical Environments," in *Proceedings of the 24th Annual Conference on Computer Graphics and Interactive Techniques*, SIGGRAPH '97, (New York, NY, USA), pp. 345–352, ACM Press/Addison-Wesley Publishing Co., 1997.

[118] D. C. Ruspini, K. Kolarov, and O. Khatib, "Haptic interaction in virtual environments," in *Proceedings of the 1997 IEEE/RSJ International Conference on Intelligent Robot and Systems. Innovative Robotics for Real-World Applications. IROS '97*, vol. 1, pp. 128–133 vol.1, Sept. 1997.

[119] D. Ruspini and O. Khatib, "Haptic display for human interaction with virtual dynamic environments," *Journal of Robotic Systems*, vol. 18, pp. 769–783, Dec. 2001.

[120] P. Mitra and G. Niemeyer, "Dynamic proxy objects in haptic simulations," in *IEEE Conference on Robotics, Automation and Mechatronics, 2004.*, vol. 2, pp. 1054–1059 vol.2, Dec. 2004.

[121] R. J. Adams and B. Hannaford, "Stable haptic interaction with virtual environments," *IEEE Transactions on Robotics and Automation*, vol. 15, pp. 465–474, June 1999.

[122] B. Hannaford and J.-H. Ryu, "Time-domain passivity control of haptic interfaces," *IEEE Transactions on Robotics and Automation*, vol. 18, pp. 1–10, Feb. 2002.

[123] J.-H. Ryu, D.-S. Kwon, and B. Hannaford, "Stability guaranteed control: time domain passivity approach," *IEEE Transactions on Control Systems Technology*, vol. 12, pp. 860–868, Nov. 2004.

[124] B. Hannaford, "A design framework for teleoperators with kinesthetic feedback," *IEEE Transactions on Robotics and Automation*, vol. 5, pp. 426–434, Aug. 1989.

[125] G. J. Raju, G. C. Verghese, and T. B. Sheridan, "Design issues in 2-port network models of bilateral remote manipulation," in *1989 International Conference on Robotics and Automation Proceedings*, pp. 1316–1321 vol.3, May 1989.

[126] K. J. Kuchenbecker, J. Fiene, and G. Niemeyer, "Improving contact realism through event-based haptic feedback," *IEEE Transactions on Visualization and Computer Graphics*, vol. 12, pp. 219–230, Mar. 2006.

[127] R. J. Anderson and M. W. Spong, "Asymptotic stability for force reflecting teleoperators with time delays," in *1989 International Conference on Robotics and Automation Proceedings*, pp. 1618–1625 vol.3, May 1989.

[128] N. Chopra, M. W. Spong, and R. Lozano, "Synchronization of bilateral teleoperators with time delay," *Automatica*, vol. 44, pp. 2142–2148, Aug. 2008.

[129] P. Arcara and C. Melchiorri, "A Comparison of Control Schemes for Teleoperation with Time Delay," *IFAC Proceedings Volumes*, vol. 34, pp. 1–6, July 2001.

[130] Y. Yokokohji and T. Yoshikawa, "Bilateral control of master-slave manipulators for ideal kinesthetic coupling-formulation and experiment," *IEEE Transactions on Robotics and Automation*, vol. 10, pp. 605–620, Oct. 1994.

[131] C. A. Lawn and B. Hannaford, "Performance testing of passive communication and control in teleoperation with time delay," in *[1993] Proceedings IEEE International Conference on Robotics and Automation*, pp. 776–783 vol.3, May 1993.

[132] I. G. Polushin, A. Takhmar, and R. V. Patel, "Projection-Based Force-Reflection Algorithms With Frequency Separation for Bilateral Teleoperation," *IEEE/ASME Transactions on Mechatronics*, vol. 20, pp. 143–154, Feb. 2015.

[133] A. Okamura, "Methods for haptic feedback in teleoperated robot-assisted surgery," *The Industrial robot*, vol. 31, pp. 499–508, Dec. 2004.

[134] F. Barbagli and K. Salisbury, "The effect of sensor/actuator asymmetries in haptic interfaces," in *11th Symposium on Haptic Interfaces for Virtual Environment and Teleoperator Systems, 2003. HAPTICS 2003. Proceedings.*, pp. 140–147, Mar. 2003.

[135] K. Hashtrudi-Zaad and S. E. Salcudean, "Adaptive transparent impedance reflecting teleoperation," in *Proceedings of IEEE International Conference on Robotics and Automation*, vol. 2, pp. 1369–1374 vol.2, Apr. 1996.

[136] A. Abdossalami and S. Sirouspour, "Adaptive Control of Haptic Interaction with Impedance and Admittance Type Virtual Environments," in *2008 Symposium on Haptic Interfaces for Virtual Environment and Teleoperator Systems*, pp. 145–152, Mar. 2008.

[137] Y. C. Fung, *Biomechanics: Mechanical Properties of Living Tissues*.
Springer-Verlag New York, 2 ed., 1993.

[138] K. J. Kuchenbecker, *Characterizing and controlling the high-frequency dynamics of haptic interfaces*.
Ph.D. dissertation, Stanford University, Department of Mechanical Engineering, 2006.

[139] A. De Greef, T. Delwiche, L. Catoire, and M. Kinnaert, "Experimental Study of Position-Position and Force-Position Control Methods in Teleoperation," *IFAC Proceedings Volumes*, vol. 39, pp. 301–306, Jan. 2006.

[140] I. Aliaga, A. Rubio, and E. Sanchez, "Experimental quantitative comparison of different control architectures for master-slave teleoperation," *IEEE Transactions on Control Systems Technology*, vol. 12, pp. 2–11, Jan. 2004.

[141] E. K. Samygina, L. N. Rassudov, and A. P. Balkovoi, "Comparison of linear position and velocity control strategies for a direct servodrive," in *2018 25th International Workshop*

on Electric Drives: Optimization in Control of Electric Drives (IWED), pp. 1–5, Jan. 2018.

[142] K. Kawashima, K. Tadano, G. Sankaranarayanan, and B. Hannaford, "Model-based passivity control for bilateral teleoperation of a surgical robot with time delay," in *2008 IEEE/RSJ International Conference on Intelligent Robots and Systems*, pp. 1427–1432, Sept. 2008.

[143] R. Daniel and P. McAree, "Fundamental Limits of Performance for Force Reflecting Teleoperation," *The International Journal of Robotics Research*, vol. 17, pp. 811–830, Aug. 1998.

[144] R. Cortesao, J. Park, and O. Khatib, "Real-time adaptive control for haptic telemanipulation with Kalman active observers," *IEEE Transactions on Robotics*, vol. 22, pp. 987–999, Oct. 2006.

[145] T. Osa, S. Uchida, N. Sugita, and M. Mitsuishi, "Hybrid Rate: Admittance Control With Force Reflection for Safe Teleoperated Surgery," *IEEE/ASME Transactions on Mechatronics*, vol. 20, pp. 2379–2390, Oct. 2015.

[146] R. Q. Van Der Linde, "The HapticMaster, a new high-performance haptic interface," *Proc. EuroHaptics, Edinburgh, 2002*, pp. 1–5, 2002.

[147] C. Ott, R. Mukherjee, and Y. Nakamura, "Unified Impedance and Admittance Control," in *2010 IEEE International Conference on Robotics and Automation*, pp. 554–561, May 2010.

[148] A. K. H. Bejczy, "Experimental results with a six-degree-of-freedom force-reflecting hand controller," in *Proceedings 17th Annual Conference on Manual Control*, (Los Angeles, CA), Oct. 1981.

[149] B. Hannaford and R. Anderson, "Experimental and simulation studies of hard contact in force reflecting teleoperation," in *1988 IEEE International Conference on Robotics and Automation Proceedings*, pp. 584–589 vol.1, Apr. 1988.

[150] C. R. Carignan and K. R. Cleary, "Closed-Loop Force Control for Haptic Simulation of Virtual Environments," *Haptics-e [Online]*, vol. 2, Feb. 2000.
Available: http://www.haptics-e.org.

[151] J. J. Gil, I. Diaz, X. Justo, and P. Ciaurriz, "Educational haptic controller based on Arduino platform," in *2014 XI Tecnologias Aplicadas a la Ensenanza de la Electronica (Technologies Applied to Electronics Teaching) (TAEE)*, pp. 1–7, June 2014.

[152] V. Hayward, O. R. Astley, M. Cruz-Hernandez, D. Grant, and G. Robles De la Torre, "Haptic interfaces and devices," *Sensor Review*, vol. 24, pp. 16–29, Mar. 2004.

[153] M. Benali-Khoudjaa, M. Hafez, J. M. Alexandre, and A. Kheddar, "Tactile interfaces : a state-ofthe-art survey," in *Proceedings 35th International Symposium on Robotics*, (Paris, France), 2004.

[154] K. B. Shimoga, "Finger Force and Touch Feedback Issues in Dexterous Telemanipulation," in *Fourth Annual Conference on Intelligent Robotic Systems for Space Exploration Proceedings*, pp. 159–178, Sept. 1992.

[155] D. G. Caldwell, S. Lawther, and A. Wardle, "Tactile perception and its application to the design of multi-modal cutaneous feedback systems," in *Proceedings of IEEE International Conference on Robotics and Automation*, vol. 4, pp. 3215–3221 vol.4, Apr. 1996.

[156] A.-S. Augurelle, A. M. Smith, T. Lejeune, and J.-L. Thonnard, "Importance of cutaneous feedback in maintaining a secure grip during manipulation of hand-held objects," *Journal of Neurophysiology*, vol. 89, pp. 665–671, Feb. 2003.

[157] M. O. Ernst and H. H. Bulthoff, "Merging the senses into a robust percept," *Trends in Cognitive Sciences*, vol. 8, pp. 162–169, Apr. 2004.

[158] J. Hu, D. Xin, and R. Wang, "Dependence of tactile sensation on deformations within soft tissues of fingertip," *World Journal of Modelling and Simulation*, vol. 3, no. 1, pp. 73–78, 2007.

[159] J. Colgate and J. Brown, "Factors affecting the Z-Width of a haptic display," in *, 1994 IEEE International Conference on Robotics and Automation, 1994. Proceedings*, pp. 3205–3210 vol.4, May 1994.

[160] K. Totorkulov and J.-H. Ryu, "Stable haptic interaction with admittance type virtual environments based on time-domain passivity approach," in *2012 9th International Conference on Ubiquitous Robots and Ambient Intelligence (URAI)*, pp. 111–113, Nov. 2012.

[161] N. Hogan, "Impedance Control: An Approach to Manipulation," in *1984 American Control Conference*, pp. 304–313, June 1984.

[162] N. Hogan, "Controlling impedance at the man/machine interface," in *1989 International Conference on Robotics and Automation Proceedings*, pp. 1626–1631 vol.3, May 1989.

[163] N. Hogan and S. P. Buerger, "Impedance and Interaction Control," in *Robotics and Automation Handbook*, p. 24, CRC Press, Oct. 2004.

[164] L. Burstrom, "The influence of biodynamic factors on the mechanical impedance of the hand and arm," *International Archives of Occupational and Environmental Health*, vol. 69, no. 6, pp. 437–446, 1997.

[165] C. J. Hasser and M. R. Cutkosky, "System identification of the human hand grasping a haptic knob," in *Proceedings 10th Symposium on Haptic Interfaces for Virtual Environment and Teleoperator Systems. HAPTICS 2002*, pp. 171–180, Mar. 2002.

[166] T. L. Gibo, A. J. Bastian, and A. M. Okamura, "Grip Force Control during Virtual Object Interaction: Effect of Force Feedback, Accuracy Demands, and Training," *IEEE Transactions on Haptics*, vol. 7, pp. 37–47, Jan. 2014.

[167] K. J. Kuchenbecker, J. G. Park, and G. Niemeyer, "Characterizing the Human Wrist for Improved Haptic Interaction," in *Proceedings of International Mechanical Engineering Congress and Exposition*, pp. 591–598, Jan. 2003.

[168] M. J. Fu and M. C. Eavusoglu, "Three-dimensional human arm and hand dynamics and variability model for a stylus-based haptic interface," in *2010 IEEE International Conference on Robotics and Automation*, pp. 1339–1346, May 2010.

[169] J. D. Hwang, M. D. Williams, and G. Niemeyer, "Toward event-based haptics: rendering contact using open-loop force pulses," in *12th International Symposium on Haptic Interfaces for Virtual Environment and Teleoperator Systems, 2004. HAPTICS '04. Proceedings.*, pp. 24–31, Mar. 2004.

[170] T. Sansanayuth, I. Nilkhamhang, and K. Tungpimolrat, "Teleoperation with inverse dynamics control for PHANToM Omni haptic device," in *2012 Proceedings of SICE Annual Conference (SICE)*, pp. 2121–2126, Aug. 2012.

[171] B. Varalakshmi, J. Thriveni, and V. K R, "Haptics: State of the Art Survey," *International Journal of Computer Science Issues (IJCSI)*, vol. 9, Jan. 2012.

[172] K. S. Hale and K. M. Stanney, *Handbook of Virtual Environments: Design, Implementation, and Applications*.
Boca Raton, FL, USA: CRC Press, Inc., 2nd ed., 2014.

[173] D. Feth, A. Peer, and M. Buss, "Incorporating human haptic interaction models into teleoperation systems," in *2010 IEEE/RSJ International Conference on Intelligent Robots and Systems*, pp. 4257–4262, Oct. 2010.

[174] N. Colonnese and A. Okamura, "M-Width: Stability and Accuracy of Haptic Rendering of Virtual Mass," in *Robotics: Science and System*, vol. 08, July 2012.

[175] M. Tavakoli, R. V. Patel, and M. Moallem, "Bilateral control of a teleoperator for soft tissue palpation: design and experiments," in *Proceedings 2006 IEEE International Conference on Robotics and Automation, 2006. ICRA 2006.*, pp. 3280–3285, May 2006.

[176] C. King, M. O. Culjat, M. L. Franco, C. E. Lewis, E. P. Dutson, W. S. Grundfest, and J. W. Bisley, "Tactile Feedback Induces Reduced Grasping Force in Robot-Assisted Surgery," *IEEE Transactions on Haptics*, vol. 2, pp. 103–110, Apr. 2009.

[177] R. H. Taylor, J. Funda, B. Eldridge, S. Gomory, K. Gruben, D. LaRose, M. Talamini, L. Kavoussi, and J. Anderson, "A telerobotic assistant for laparoscopic surgery," *IEEE Engineering in Medicine and Biology Magazine*, vol. 14, pp. 279–288, May 1995.

[178] Y. Kurita, H. Ohtsuka, K. Nagata, and T. Tsuji, "Haptic rendering of a needle insertion by enhancing the real force response of a base object," in *2014 IEEE Haptics Symposium (HAPTICS)*, pp. 357–360, Feb. 2014.

[179] L. Meli, C. Pacchierotti, and D. Prattichizzo, "Experimental evaluation of magnified haptic feedback for robot-assisted needle insertion and palpation," *The International Journal of Medical Robotics and Computer Assisted Surgery*, vol. 13, Dec. 2017.

[180] M. C. Cavusoglu, A. Sherman, and F. Tendick, "Design of bilateral teleoperation controllers for haptic exploration and telemanipulation of soft environments," *IEEE Transactions on Robotics and Automation*, vol. 18, pp. 641–647, Aug. 2002.

[181] O. Korner and R. Manner, "Implementation of a haptic interface for a virtual reality simulator for flexible endoscopy," in *11th Symposium on Haptic Interfaces for Virtual Environment and Teleoperator Systems, 2003. HAPTICS 2003. Proceedings.*, pp. 278–284, Mar. 2003.

[182] S. Chakravarthy, M. Krishna, and G. K. Ananthasuresh, "[D76] Haptic playback for endoscopy," in *2014 IEEE Haptics Symposium (HAPTICS)*, pp. 1–1, Feb. 2014.

[183] N. G. Tsagarakis and D. G. Caldwell, "A 5 dof haptic interface for pre-operative planning of surgical access in hip arthroplasty," in *First Joint Eurohaptics Conference and Symposium on Haptic Interfaces for Virtual Environment and Teleoperator Systems. World Haptics Conference*, pp. 519–520, Mar. 2005.

[184] N. Forrest, S. Baillie, and H. Z. Tan, "Haptic stiffness identification by veterinarians and novices: A comparison," in *World Haptics 2009 - Third Joint EuroHaptics conference and Symposium on Haptic Interfaces for Virtual Environment and Teleoperator Systems*, pp. 646–651, Mar. 2009.

[185] P. Abolmaesumi, K. Hashtrudi-Zaad, D. Thompson, and A. Tahmasebi, "A haptic-based system for medical image examination," in *The 26th Annual International Conference of the IEEE Engineering in Medicine and Biology Society*, vol. 1, pp. 1853–1856, Sept. 2004.

[186] S. Avgousti, E. G. Christoforou, A. S. Panayides, S. Voskarides, C. Novales, L. Nouaille, C. S. Pattichis, and P. Vieyres, "Medical telerobotic systems: current status and future trends," *BioMedical Engineering OnLine*, vol. 15, p. 96, Aug. 2016.

[187] C. Moussette, *Simple haptics : Sketching perspectives for the design of haptic interactions*. PhD Thesis, Umea University, Umea, Sweden, 2012.

[188] J. Forsslund, M. Yip, and E.-L. Sallnas, "WoodenHaptics : A Starting Kit for Crafting Force-Reflecting Spatial Haptic Devices," in *Proceedings of the Ninth International Conference on Tangible, Embedded, and Embodied*, pp. 133–140, ACM Digital Library, 2015.

[189] T. H. Massie, *Design of a three degree of freedom force-reflecting haptic interface*. Thesis, Massachusetts Institute of Technology, 1993.

[190] T. H. Massie and J. K. Salisbury, "The PHANToM haptic interface: A device for probing virtual objects," in *Proceedings of the ASME Dynamic Systems and Control Division*, pp. 295–301, 1994.

[191] L. A. Bonanni, "TapTap: A Haptic Wearable for Asynchronous Distributed Touch Therapy." MIT Media Lab Website.

[192] C. Neupert, S. Matich, N. Scherping, M. Kupnik, R. Werthschutzky, and C. Hatzfeld, "Pseudo-Haptic Feedback in Teleoperation," *IEEE Transactions on Haptics*, vol. 9, pp. 397–408, July 2016.

[193] P. Letier, E. Motard, and J. Verschueren, "EXOSTATION : Haptic exoskeleton based control station," in *2010 IEEE International Conference on Robotics and Automation*, pp. 1106–1107, May 2010.

[194] C. Pacchierotti, F. Ongaro, F. v. d. Brink, C. Yoon, D. Prattichizzo, D. H. Gracias, and S. Misra, "Steering and Control of Miniaturized Untethered Soft Magnetic Grippers With Haptic Assistance," *IEEE Transactions on Automation Science and Engineering*, vol. 15, pp. 290–306, Jan. 2018.

[195] W. Chou, T. Wang, and J. Xiao, "Haptic interaction with virtual environment using an arm type exoskeleton device," in *IEEE International Conference on Robotics and Automation, 2004. Proceedings. ICRA '04. 2004*, vol. 2, pp. 1992–1997 Vol.2, Apr. 2004.

[196] W. Yang and W. Chen, "Haptic Rendering of Virtual Hand Moving Objects," in *2011 International Conference on Cyberworlds*, pp. 113–119, Oct. 2011.

[197] C. B. Zilles and J. K. Salisbury, "A constraint-based god-object method for haptic display," in *Proceedings 1995 IEEE/RSJ International Conference on Intelligent Robots and Systems. Human Robot Interaction and Cooperative Robots*, vol. 3, pp. 146–151 vol.3, Aug. 1995.

[198] R. Kikuuwe, N. Takesue, A. Sano, H. Mochiyama, and H. Fujimoto, "Admittance and Impedance Representations of Friction Based on Implicit Euler Integration," *IEEE Transactions on Robotics*, vol. 22, pp. 1176–1188, Dec. 2006.

[199] N. Diolaiti, G. Niemeyer, F. Barbagli, and J. K. Salisbury, "Stability of Haptic Rendering: Discretization, Quantization, Time Delay, and Coulomb Effects," *IEEE Transactions on Robotics*, vol. 22, pp. 256–268, Apr. 2006.

[200] K. Salisbury, D. Brock, T. Massie, N. Swarup, and C. Zilles, "Haptic rendering: Programming touch interaction with virtual objects," in *Proc. Symposium on Interactive 3D graphics*, pp. 123–130, ACM, 1995.

[201] K. Salisbury, F. Conti, and F. Barbagli, "Haptic rendering: introductory concepts," *IEEE Computer Graphics and Applications*, vol. 24, pp. 24–32, Mar. 2004.

[202] N. Colonnese, S. M. Sketch, and A. M. Okamura, "Closed-loop stiffness and damping accuracy of impedance-type haptic displays," in *2014 IEEE Haptics Symposium (HAPTICS)*, pp. 97–102, Feb. 2014.

[203] H. Culbertson, J. J. L. Delgado, and K. J. Kuchenbecker, "[D11] The Penn Haptic Texture Toolkit," in *2014 IEEE Haptics Symposium (HAPTICS)*, pp. 1–1, Feb. 2014.

[204] G. Campion, A. H. C. Gosline, and V. Hayward, "Passive Viscous Haptic Textures," in *2008 Symposium on Haptic Interfaces for Virtual Environment and Teleoperator Systems*, pp. 379–380, Mar. 2008.

[205] S. Yim, S. Jeon, and S. Choi, "Data-driven haptic modeling and rendering of frictional sliding contact with soft objects for medical training," in *2014 11th International Conference on Ubiquitous Robots and Ambient Intelligence (URAI)*, pp. 66–67, Nov. 2014.

[206] L. Wei, L. Huynh, H. Zhou, and S. Nahavandi, "Immersive Visuo-Haptic Rendering in Optometry Training Simulation," in *2015 IEEE International Conference on Systems, Man, and Cybernetics*, pp. 436–439, Oct. 2015.

[207] R. Hover, M. Harders, and G. Szekely, "Data-Driven Haptic Rendering of Visco-Elastic Effects," in *2008 Symposium on Haptic Interfaces for Virtual Environment and Teleoperator Systems*, pp. 201–208, Mar. 2008.

[208] S. Shin and S. Choi, "Geometry-based haptic texture modeling and rendering using photometric stereo," in *2018 IEEE Haptics Symposium (HAPTICS)*, pp. 262–269, Mar. 2018.

[209] D. Fortmeier, M. Wilms, A. Mastmeyer, and H. Handels, "Direct Visuo-Haptic 4d Volume Rendering Using Respiratory Motion Models," *IEEE Transactions on Haptics*, vol. 8, pp. 371–383, Oct. 2015.

[210] D. J. Meyer, M. Wiertlewski, M. A. Peshkin, and J. E. Colgate, "Dynamics of ultrasonic and electrostatic friction modulation for rendering texture on haptic surfaces," in *2014 IEEE Haptics Symposium (HAPTICS)*, pp. 63–67, Feb. 2014.

[211] E. Klingbeil, S. Menon, K. Go, and O. Khatib, "Using haptics to probe human contact control strategies for six degree-of-freedom tasks," in *2014 IEEE Haptics Symposium (HAPTICS)*, pp. 93–95, Feb. 2014.

[212] R. B. Singapogu, S. T. Sander, T. C. Burg, and D. Lee, "A Five DOF haptic rendering algorithm using multiple contact points," in *IEEE SoutheastCon 2008*, pp. 262–267, Apr. 2008.

[213] G. Yu, D. Wang, Y. Zhang, and J. Xiao, "Simulating Sharp Geometric Features in Six Degrees-of-Freedom Haptic Rendering," *IEEE Transactions on Haptics*, vol. 8, pp. 67–78, Jan. 2015.

[214] L. Corenthy, M. A. Otaduy, L. Pastor, and M. Garcia, "Volume Haptics with Topology-Consistent Isosurfaces," *IEEE Transactions on Haptics*, vol. 8, pp. 480–491, Oct. 2015.

[215] I. Susa, Y. Takehana, A. Balandra, H. Mitake, and S. Hasegawa, "Haptic rendering based on finite element simulation of vibration," in *2014 IEEE Haptics Symposium (HAPTICS)*, pp. 123–128, Feb. 2014.

[216] Y. Li, Y. Zhang, X. Ye, and S. Zhang, "Haptic rendering method based on generalized penetration depth computation," *Signal Processing*, vol. 120, pp. 714–720, Mar. 2016.

[217] S. Cho, S. Shin, and S. Choi, "Haptic texture rendering using random fractal surface," in *2017 14th International Conference on Ubiquitous Robots and Ambient Intelligence (URAI)*, pp. 290–292, June 2017.

[218] M. Abdullah, M. Kim, W. Hassan, Y. Kuroda, and S. Jeon, "HapticDrone: An encountered-type kinesthetic haptic interface with controllable force feedback: Example of stiffness

and weight rendering," in *2018 IEEE Haptics Symposium (HAPTICS)*, pp. 334–339, Mar. 2018.

[219] S. Chaudhury and S. Chaudhuri, "Volume preserving haptic pottery," in *2014 IEEE Haptics Symposium (HAPTICS)*, pp. 129–134, Feb. 2014.

[220] S. B. Kang and K. Ikeuchi, "Toward automatic robot instruction from perception-recognizing a grasp from observation," *IEEE Transactions on Robotics and Automation*, vol. 9, pp. 432–443, Aug. 1993.

[221] R. Adams, M. Moreyra, and B. Hannaford, "Stability and Performance of Haptic Displays: Theory and Experiments," in *Proceedings of the ASME Winter Annual Meeting Haptics Workshop*, (Anaheim, CA), 1998.

[222] R. J. Adams and B. Hannaford, "Control law design for haptic interfaces to virtual reality," *IEEE Transactions on Control Systems Technology*, vol. 10, pp. 3–13, Jan. 2002.

[223] C. Pacchierotti, V. Magdanz, M. Medina-Sanchez, O. G. Schmidt, D. Prattichizzo, and S. Misra, "Intuitive control of self-propelled microjets with haptic feedback," *Journal of Micro-Bio Robotics*, vol. 10, pp. 37–53, Oct. 2015.

[224] M. Lopez, E. Castillo, G. Garcia, and A. Bashir, "Delta robot: Inverse, direct, and intermediate Jacobians," *Proceedings of the Institution of Mechanical Engineers, Part C: Journal of Mechanical Engineering Science*, vol. 220, pp. 103–109, Jan. 2006.

[225] D. Prattichizzo, C. Pacchierotti, and G. Rosati, "Cutaneous Force Feedback as a Sensory Subtraction Technique in Haptics," *IEEE Transactions on Haptics*, vol. 5, no. 4, pp. 289–300, 2012.

[226] C. Pacchierotti, "Peg-in-Hole in Simulated and Real Scenarios," in *Cutaneous Haptic Feedback in Robotic Teleoperation*, Springer Series on Touch and Haptic Systems, pp. 37–58, Springer International Publishing, 2016.

[227] C. Pacchierotti, M. Abayazid, S. Misra, and D. Prattichizzo, "Teleoperation of Steerable Flexible Needles by Combining Kinesthetic and Vibratory Feedback," *IEEE Transactions on Haptics*, vol. 7, pp. 551–556, Oct. 2014.

[228] L. Meli, C. Pacchierotti, and D. Prattichizzo, "Sensory Subtraction in Robot-Assisted Surgery: Fingertip Skin Deformation Feedback to Ensure Safety and Improve Transparency in Bimanual Haptic Interaction," *IEEE Transactions on Biomedical Engineering*, vol. 61, pp. 1318–1327, Apr. 2014.

[229] J. E. Speich and M. Goldfarb, "Implementation of loop-shaping compensators to increase the transparency bandwidth of a scaled telemanipulation system," in *Proceedings 2002*

IEEE International Conference on Robotics and Automation (Cat. No.02CH37292), vol. 3, pp. 2886–2893, 2002.

[230] R. Lozano, B. Brogliato, O. Egeland, and B. Maschke, *Dissipative systems analysis and control*.
Springer Verlag, 2000.

[231] G. Niemeyer and J.-J. E. Slotine, "Telemanipulation with Time Delays," *The International Journal of Robotics Research*, vol. 23, pp. 873–890, Sept. 2004.

[232] J.-H. Ryu, Y. S. Kim, and B. Hannaford, "Sampled- and continuous-time passivity and stability of virtual environments," *IEEE Transactions on Robotics*, vol. 20, pp. 772–776, Aug. 2004.

[233] J.-H. Ryu, C. Preusche, B. Hannaford, and G. Hirzinger, "Time domain passivity control with reference energy following," *IEEE Transactions on Control Systems Technology*, vol. 13, pp. 737–742, Sept. 2005.

[234] N. Tsunashima and S. Katsura, "Bilateral control based on human model for haptic communication," in *2010 11th IEEE International Workshop on Advanced Motion Control (AMC)*, pp. 319–324, Mar. 2010.

[235] S. E. Salcudean, N. M. Wong, and R. L. Hollis, "Design and control of a force-reflecting teleoperation system with magnetically levitated master and wrist," *IEEE Transactions on Robotics and Automation*, vol. 11, pp. 844–858, Dec. 1995.

[236] C. Secchi, S. Stramigioli, and C. Fantuzzi, "Transparency in Port-Hamiltonian-Based Telemanipulation," *IEEE Transactions on Robotics*, vol. 24, pp. 903–910, Aug. 2008.

[237] M. Franken, S. Misra, and S. Stramigioli, "Improved transparency in energy-based bilateral telemanipulation," *Mechatronics*, vol. 22, pp. 45–54, Feb. 2012.

[238] J. G. W. Wildenbeest, D. A. Abbink, and J. F. Schorsch, "Haptic transparency increases the generalizability of motor learning during telemanipulation," in *2013 World Haptics Conference (WHC)*, pp. 707–712, Apr. 2013.

[239] T. Hulin, C. Preusche, and G. Hirzinger, "Stability boundary for haptic rendering: Influence of human operator," in *2008 IEEE/RSJ International Conference on Intelligent Robots and Systems*, pp. 3483–3488, Sept. 2008.

[240] G. D. Gersem and H. V. Brussel, "Influence of force disturbances on transparency in bilateral telemanipulation of soft environments," in *IEEE International Conference on Robotics and Automation, 2004. Proceedings. ICRA '04. 2004*, vol. 2, pp. 1227–1232 Vol.2, Apr. 2004.

[241] A. Dietrich, X. Wu, K. Bussmann, C. Ott, A. Albu-Schaffer, and S. Stramigioli, "Passive Hierarchical Impedance Control Via Energy Tanks," *IEEE Robotics and Automation Letters*, vol. 2, pp. 522–529, Apr. 2017.

[242] W. R. Ferrell, "Delayed Force Feedback," *Human Factors*, vol. 8, pp. 449–455, Oct. 1966.

[243] J. E. Speich, K. Fite, and M. Goldfarb, "A method for simultaneously increasing transparency and stability robustness in bilateral telemanipulation," in *Proceedings 2000 ICRA. Millennium Conference. IEEE International Conference on Robotics and Automation. Symposia Proceedings (Cat. No.00CH37065)*, vol. 3, pp. 2671–2676 vol.3, Apr. 2000.

[244] J. L. Pinto Rebelo, F. C. T. Van der Helm, A. Schiele, TU Delft: Mechanical, Maritime and Materials Engineering: BioMechanical Engineering, and TU Delft, Delft University of Technology, *Robust and Transparent Multi-Degree-of-Freedom Bilateral Teleoperation with Time-Delay*.
PhD thesis, Technische Universiteit Delft, May 2015.

[245] J. Colgate, P. Grafing, M. Stanley, and G. Schenkel, "Implementation of stiff virtual walls in force-reflecting interfaces," in *, 1993 IEEE Virtual Reality Annual International Symposium, 1993*, pp. 202–208, Sept. 1993.

[246] A. M. Niknejad, *"Analysis, Simulation, and Applications of Passive Devices on Conductive Substrates"*.
PhD Thesis, Dept. EECC., California Univ., 2000.

[247] L. Marton, J. Esclusa, P. Haller, and T. Vajda, "Passive bilateral teleoperation with bounded control signals," in *2013 11th IEEE International Conference on Industrial Informatics (INDIN)*, pp. 337–342, July 2013.

[248] B. E. Miller, J. E. Colgate, and R. A. Freeman, "On the role of dissipation in haptic systems," *IEEE Transactions on Robotics*, vol. 20, pp. 768–771, Aug. 2004.

[249] K. Kosuge, J. Ishikawa, K. Furuta, and M. Sakai, "Control of single-master multi-slave manipulator system using VIM," in *, IEEE International Conference on Robotics and Automation Proceedings*, pp. 1172–1177 vol.2, May 1990.

[250] A. A. Goldenberg, "On the bilateral control of master-slave teleperators," *Robotersysteme*, vol. 7, pp. 91–99, 1991.

[251] R. Tao and M. Tavakoli, "Multilateral haptic system stability analysis: The effect of activity or passivity of terminations via a series-shunt approach," in *2014 IEEE Haptics Symposium (HAPTICS)*, pp. 203–208, Feb. 2014.

[252] P. Shull and G. Niemeyer, "Force and Position Scaling Limits for Stability in Force Reflecting Teleoperation," *Proceedings of the ASME Dynamic Systems and Control Conference*, pp. 607–614, Jan. 2008.

[253] X. Xu, C. Schuwerk, B. Cizmeci, and E. Steinbach, "Energy Prediction for Teleoperation Systems That Combine the Time Domain Passivity Approach with Perceptual Deadband-Based Haptic Data Reduction," *IEEE Transactions on Haptics*, vol. 9, pp. 560–573, Oct. 2016.

[254] P. Robuffo Giordano, A. Franchi, C. Secchi, and H. H. Bulthoff, "A passivity-based decentralized strategy for generalized connectivity maintenance," *The International Journal of Robotics Research*, vol. 32, pp. 299–323, Mar. 2013.

[255] J. E. Colgate and G. G. Schenkel, "Passivity of a class of sampled-data systems: Application to haptic interfaces," *Journal of Robotic Systems*, vol. 14, pp. 37–47, Jan. 1997.

[256] R. Akmeliawati and Mareels, Iven, "Flight control systems using passivity-based control - Disturbance rejection and robustness analysis," in *Guidance, Navigation, and Control Conference and Exhibit*, (Portland, OR, U.S.A.), American Institute of Aeronautics and Astronautics, Aug. 1999.

[257] B. Miller, J. Colgate, and R. Freeman, "Guaranteed stability of haptic systems with nonlinear virtual environments," *IEEE Transactions on Robotics and Automation*, vol. 16, pp. 712–719, Dec. 2000.

[258] S. Leeraphan, T. Maneewarn, and D. Laowattana, "Stable adaptive bilateral control of transparent teleoperation through time-varying delay," in *IEEE/RSJ International Conference on Intelligent Robots and Systems*, vol. 3, pp. 2979–2984 vol.3, Sept. 2002.

[259] R. Ortega and E. Garcia-Canseco, "Interconnection and Damping Assignment Passivity-Based Control: A Survey," *European Journal of Control*, vol. 10, no. 5, pp. 432–450, 2004.

[260] D. W. Weir and J. E. Colgate, "Stability of Haptic Displays," in *Haptic Rendering: Foundations, Algorithms, and Applications*, pp. 123–156, Ming C. Lin, Miguel Otaduy, Eds.CRC Press, 2008.

[261] B. Ydstie, "Process Control: The Passive Systems Approach (Bao, K. and Lee. P.L.; 2007)[Book Shelf]," *IEEE Control Systems*, vol. 30, pp. 78–80, Feb. 2010.

[262] I. Desai, A. Gupta, and D. Chakraborty, "Transparency enhancement of haptic interface using model matching approach," in *2016 Indian Control Conference (ICC)*, pp. 399–404, Jan. 2016.

[263] S. V. Velanas and C. S. Tzafestas, "Human telehaptic perception of stiffness using an adaptive impedance reflection bilateral teleoperation control scheme," in *19th International Symposium in Robot and Human Interactive Communication*, pp. 21–26, Sept. 2010.

[264] H. Li and K. Kawashima, "Bilateral teleoperation with delayed force feedback using time domain passivity controller," *Robotics and Computer-Integrated Manufacturing*, vol. 37, pp. 188–196, Feb. 2016.

[265] F. Ferraguti, C. Secchi, and C. Fantuzzi, "A tank-based approach to impedance control with variable stiffness," in *2013 IEEE International Conference on Robotics and Automation (ICRA)*, pp. 4948–4953, May 2013.

[266] C. Secchi, S. Stramigioli, and C. Fantuzzi, *Control of Interactive Robotic Interfaces: A Port-Hamiltonian Approach*.
Springer Tracts in Advanced Robotics, Berlin Heidelberg: Springer-Verlag, 2007.

[267] M. Franken, B. Willaert, S. Misra, and S. Stramigioli, "Bilateral telemanipulation: Improving the complementarity of the frequency- and time-domain passivity approaches," in *2011 IEEE International Conference on Robotics and Automation*, pp. 2104–2110, May 2011.

[268] M. Franken, S. Misra, and S. Stramigioli, "Friction compensation in energy-based bilateral telemanipulation," in *2010 IEEE/RSJ International Conference on Intelligent Robots and Systems*, pp. 5264–5269, Oct. 2010.

[269] M. Quigley, K. Conley, B. Gerkey, J. Faust, T. Foote, J. Leibs, R. Wheeler, and A. Ng, "ROS: an open-source Robot Operating System," in *Open-source software workshop of the Int. Conf. on Robotics and Automation*, (Kobe, Japan), IEEE, 2009.

[270] E. Tosello, R. Bortoletto, S. Michieletto, E. Pagello, and E. Menegatti, "An Integrated System to approach the Programming of Humanoid Robotics," in *4th International Workshop "Teaching Robotics & Teaching with Robotics" & 5th International Conference "Robotics in Education" (2014)*, (Padova(Italy)), Dimitris Alimisis, Grzegorz Granosik, Michele Moro, July 2014.

[271] R. Kikuuwe, N. Takesue, A. Sano, H. Mochiyama, and H. Fujimoto, "Fixed-step friction simulation: from classical Coulomb model to modern continuous models," in *2005 IEEE/RSJ International Conference on Intelligent Robots and Systems*, pp. 1009–1016, Aug. 2005.

[272] Y. F. Liu, J. Li, Z. M. Zhang, X. H. Hu, and W. J. Zhang, "Experimental comparison of five friction models on the same test-bed of the micro stick-slip motion system," *Mechanical Sciences*, vol. 6, pp. 15–28, Mar. 2015.

[273] J. Chen, C. Du, and Z. Jiang, "A Universal and Configurable Simulator for Distributed Systems," in *2018 2nd IEEE Advanced Information Management,Communicates,Electronic and Automation Control Conference (IMCEC)*, pp. 900–904, May 2018.

[274] B. Fry, *Computational Information Design*.
PhD Thesis, Massachusetts Institute of Technology, Boston, Massachusetts, USA, 2004.

[275] C. C. E. Reas, *Behavioral kinetic sculpture*.
Thesis, Massachusetts Institute of Technology, 2001.

[276] C. Reas and B. Fry, "Processing: programming for the media arts," *AI & SOCIETY*, vol. 20, pp. 526–538, May 2006.

[277] C. Reas, B. Fry, and J. Maeda, *Processing: A Programming Handbook for Visual Designers and Artists*.
Cambridge, Mass: The MIT Press, Aug. 2007.

[278] B. Fry, *Visualizing Data: Exploring and Explaining Data with the Processing Environment*.
Sebastopol, CA: O'Reilly Media, edition: 1 ed., Dec. 2007.

[279] D. Shiffman, *Learning Processing: A Beginner's Guide to Programming Images, Animation, and Interaction*.
Amsterdam ; Boston: Morgan Kaufmann, 2008.

[280] J. Noble, *Programming Interactivity: A Designer's Guide to Processing, Arduino, and openFrameworks*.
Beijing ; Sebastopol, CA: O'Reilly Media, second edition ed., Feb. 2012.

[281] C. Reas and B. Fry, *Getting Started with Processing: A Hands-On Introduction to Making Interactive Graphics*.
Place of publication not identified: Maker Media, Inc, 2 edition ed., Sept. 2015.